In presenting the dissertation as a partial fulfillment of the requirements for an advanced degree from the Georgia Institute of Technology, I agree that the Library of the Institute shall make it available for inspection and circulation in accordance with its regulations governing materials of this type. I agree that permission to copy from, or to publish from, this dissertation may be granted by the professor under whose direction it was written, or, in his absence, by the Dean of the Graduate Division when such copying or publication is solely for scholarly purposes and does not involve potential financial gain. It is understood that any copying from, or publication of, this dissertation which involves potential financial gain will not be allowed without written permission.

7/25/68

A STUDY OF ELECTROANALYTICAL METHODS EMPLOYING POTENTIAL STEP PERTURBATION AND THE INVESTIGATION OF THE KINETIC PARAMETERS OF THE POLAROGRAPHIC REDUCTION OF HYDRATED ZINC IONS IN POTASSIUM NITRATE

A THESIS

Presented to

The Faculty of the Division of Graduate

Studies and Research

by

John Anderson Liddle

In Partial Fulfillment

of the Requirements for the Degree

Doctor of Philosophy

in the School of Chemistry

Georgia Institute of Technology

March, 1972

A STUDY OF ELECTROANALYTICAL METHODS EMPLOYING POTENTIAL STEP PERTURBATION AND THE INVESTIGATION OF THE KINETIC PARAMETERS OF THE POLAROGRAPHIC REDUCTION OF HYDRATED ZINC IONS IN POTASSIUM NITRATE

Approved:

Chairman

Date approved by Chairman: 14 March 72

ACKNOWLEDGMENTS

I wish to thank my preceptor, Dr. P. E. Sturrock, for his guidance, inspiration, and friendship, shown throughout the research work and the preparation of this manuscript. The unselfish contributions of his time, energy, and knowledge were an invaluable asset in this endeavor. Dr. H. Flaschka and Dr. Frank O'Brien are also thanked for their generous assistance in preparation of this manuscript.

I am especially grateful to my wife, Glenda, for her patience, support, and for her assistance in the preparation of this manuscript.

TABLE OF CONTENTS

LIST OF TABLES

LIST OF ILLUSTRATIONS

SUMMARY

Contamination of water with heavy metals is an ecological problem facing contemporary society. Heavy metals in water can be harmful to aquatic life and, if present at a sufficient level, can endanger humans. In this study the application of square-wave polarography to the analysis of heavy metals in water was investigated. An instrument capable of performing square-wave polarography and other potential step techniques was designed and built to implement this study.

It was found that the sensitivity of the instrument is such that Pb^{2+} and Cd^{2+} can be analyzed down to a lower concentration limit of about 10^{-7} F. Sb^{3+}, As^{3+}, Cu^{2+}, Ni^{2+}, and Zn^{2+} can be analyzed down to a limit of approximately 10^{-6} F. In addition, Co^{2+} was analyzed down to approximately 10^{-6} F.

Chronocoulometry, selective for the detection of adsorption of electroactive species, was employed to determine possible adsorption of reactants or products in the electron exchange reactions of the cadmium ethylene bis (oxyethylenenitrilo) N, N, N^{1}, N^{1} tetraacetic acid (EGTA) complexes and the chromium (III) Tris (BiPyridine) complex. No adsorption of electroactive species was detected in the cadmium-EGTA system. Surface excess values of 1.1×10^{-10} moles cm^{-2} for the reactants and 1.9×10^{-10} moles cm^{-2} for the reduction products were obtained for the chromium (III) Tris (BiPyridine) complex. The percentages of electrode surface covered by adsorption of reactants and products were calculated.

Kinetic parameters of the electrode reaction of hydrated zinc ions with a supporting electrolyte of potassium nitrate were studied by potential step methods. Both large (Tafel Plots) and small step techniques were used. Apparent exchange current densities and transfer coefficients were found to be highly dependent on the concentration of the supporting electrolyte. It was observed that the cathodic and anodic exchange current densities were not equal and the sum of the two transfer coefficients did not equal unity. It is postulated that the zinc reduction is <u>via</u> a two step reaction, with the $Zn^{2+} + e \rightleftarrows Zn^{+}$ rate determining at moderately high ionic strengths.

Reaction orders of one were determined for both zinc (II) in solution and zinc metal in the amalgam electrode.

CHAPTER I

INTRODUCTION

The purpose of this study was to evaluate the application of square-wave and pulse polarography to the analysis of heavy metals in an aqueous medium and to investigate the kinetics of the Zn(II)/Zn(Hg) charge transfer in potassium nitrate solutions.

Electrochemical Instrumentation

Electrochemical instrumentation has advanced rapidly in the last two decades. Heyrovsky's first polarograph was hardly more than a galvanometer to monitor the current and a battery to supply the required potential to a chemical cell, point by point. With the appearance of Sputnik I in 1957 and the ensuing space race, the developments in the field of electronics have been astronomical in scope. The quality of available electrochemical instruments has improved greatly, but still workers in the field are faced with the necessity to tailor design and build instruments to meet the precise requirements of their research.

The present work requires a highly flexible, multipurpose instrument capable of performing classical dc, Tast, square-wave, and differential pulse polarography. In addition, chronocoulometry capability was needed for electrode kinetics and adsorption studies. An instrument with the desired characteristics was not available commercially; therefore, it was necessary to design and build one.

Plug-in type operational amplifiers are utilized in the potentiostat and current monitoring circuitry. The instrument's functional configuration is selected by front panel controls. For example, one can change from Tast to square-wave polarography by the simple repositioning of two switches. All time parameters, such as drop life, pulse width, etc., that are required by pulse related techniques, are variable and may be adjusted for maximum sensitivity for each of the analytical techniques. A unique positive feedback system was especially designed for the instrument and is employed to compensate for the internal resistance (see page 59) of the system. This increases the rise time of the potentiostat and thereby decreases the time required to charge or discharge the double-layer. A complete description of the instrument is given in Chapter III.

The flexibility of the time parameters and the highly effective positive feedback system makes the instrument a very useful tool in study of electrode kinetics. Fast electrode charge-transfer reactions can be studied by chronocoulometry and potential step techniques. The electrode kinetic parameters and reaction mechanism for the Zn(II)/Zn(Hg) system were determined by potential step technique. These data are given in Chapter VI.

Application of Electroanalytical Techniques

Contaminating the water systems of the world with trace amounts of heavy metals is a mounting problem in today's industrial economy. Aquatic life is often severely damaged or totally eradicated by the presence of these impurities.

Analytical techniques are needed that allow the rapid and accurate

determination of a variety of metals in an aqueous medium. Poole (1) investigated the use of phase selective ac polarography for the analysis of water for trace concentrations of heavy metal ions. A study was undertaken to evaluate square-wave and rapid sweep square-wave polarography as analytical tools in the measurement of heavy metal ions in an aqueous medium. Results of this study are given in Chapter IV.

Electrokinetics of Zinc

Upon first observation the mechanism of the oxidation-reduction reaction of zinc at a mercury electrode appears to be simple. Yet it has been the subject of many studies. Various mechanisms have been proposed for the reaction. Heyrovsky (2) has proposed that Zn^{2+} is reduced to Zn^{+}, and then by dismutation, elemental zinc is obtained. Others (3,4) have proposed a two step reaction involving two one-electron transfers. A third group of workers (5,6,7) disagree with the two step mechanism and postulate a simple one step reaction.

The aim of this study was to gain more information about the detailed mechanism of the $Zn^{2+}/Zn(Hg)$ exchange in potassium nitrate solutions *via* potential step techniques. The ionic strength dependency of the exchange currents and transfer coefficients was studied. These results are given in Chapter VI.

CHAPTER II

EXPERIMENTAL METHODS

Potentiostatic Methods

Potential Step Methods

Theory. The potential step method is a relaxation technique in which the potential of the electrode under investigation is changed from its equilibrium potential to a potential where a net faradaic current is obtained by a step function of time. The kinetic parameters are then obtained by analyzing the resulting transient current as a function of time. The method has been developed by Gerischer and Vielstich (8) and, with the advent of fast electronic potentiostats, was extensively used to study fast electrode processes. Delahay (9), at a later date, gave a theoretical treatment of the technique based on the standard energies of the reactants and products. The theory for a single step electrode reaction will first be discussed, then theory will be expanded to a two step reaction.

Consider the simple electrode charge transfer for which the overall reaction is

$$Ox + ne \rightleftarrows Red \qquad (2\text{-}1)$$

At equilibrium potential, E_e, the net faradaic current is zero. The equilibrium is dynamic with the cathodic current equal to the anodic current. The current flowing per unit area in either direction at E_e is

defined as the exchange current density, i^o. At $E = E_e$, an expression for the net faradaic may be written as follows

$$i = i^o\{[(C_o/C_o^o)\exp - (\alpha nf\eta)] - (C_r/C_r^o)\exp(1-\alpha)nf\eta\} \qquad (2\text{-}2)$$

where i^o is the exchange current density for the relative bulk concentrations, C^o's. C_o and C_r are the concentrations of the oxidized and reduced forms, respectively, of the electroactive species at the electrode surface; n, is the number of electrons involved in the reaction, and f is defined as

$$f = F/RT \qquad (2\text{-}3)$$

where F, R, and T are Faraday's constant, gas constant, and absolute temperature, respectively. α is the transfer coefficient, and η is the charge-transfer overvoltage and is given by

$$\eta = (E - E_e) \qquad (2\text{-}4)$$

The ratios C_o/C_o^o and C_r/C_r^o as functions of time must be determined for each particular set of experimental conditions. During the cathodic electrolysis, C_o will decrease due to the consumption of Ox, and C_r will increase. The reverse occurs during the anodic electrolysis. Quantitative treatment of the i-t relation is based on, first, the assumption that mass-transport of the reactants is solely by semi-infinite linear diffusion, and secondly, the application of Fick's first and second laws of diffusion. By applying the above assumption and Fick's laws to equation (2-2), the function will be transformed into a set of differential

equations. In order to solve these equations, certain initial and boundary conditions must be defined. For the potential step technique, these are (10)

$$C_o = C_o^o \text{ and } C_r = C_r^o \text{ at } x \geq 0 \text{ and } t = 0 \tag{2-5a}$$

$$C_o \rightarrow C_o^o \text{ and } C_o \rightarrow C_r^o \text{ for } x \rightarrow \infty \text{ and } t \geq 0 \tag{2-5b}$$

$$i = nf(\partial C_o/\partial x) \text{ at } x = 0 \text{ and } t > 0 \tag{2-5c}$$

$$D_o(\partial C_o/\partial x) + D_r(\partial C_r/\partial x) = 0 \text{ at } x = 0 \text{ and } t > 0 \tag{2-5d}$$

where x is the distance from the electrode surface, t is the time elapsed since the application of the potential step.

The expression for the current density i (obtained by using Laplace transforms to solve the differential equations) is

$$i = i^o[\exp - (\alpha nf\eta) - \exp(1-\alpha)nf\eta] \exp y^2 \operatorname{erfc} y \tag{2-6}$$

where y is defined as

$$y = \lambda t^{\frac{1}{2}} \tag{2-7}$$

and λ is given by

$$\lambda = (i^o/nF)[\exp - (\alpha nf\eta)/(C_o^o D_o^{\frac{1}{2}}) + \exp(1-\alpha)nf\eta/(C_r^o D_r^{\frac{1}{2}})] \tag{2-8}$$

where t is time in seconds, and D_o and D_r are the diffusion coefficients for the oxidized and reduced forms, respectively, in cm^2/sec.

The two terms within the brackets of equation (2-6) are independent of t and, therefore, their contribution to the current-time function is constant. The $\exp y^2 \operatorname{erfc} y$ factors correct the current density for the formation of a concentration gradient at the electrode surface and define the transfer of current control from reaction kinetics to mass-transport.

The chronoamperometric equation for the current density may be expressed as

$$i = i_o \exp y^2 \operatorname{erfc} y \tag{2-9}$$

where i_o is the current at t=0 and is given by

$$i_o = i^o(\exp - (\alpha n f \eta) - \exp(1-\alpha) n f \eta) \tag{2-10}$$

The dependency of $\exp y^2 \operatorname{erfc} y$ on the value of y is shown in Figure 1. The function

$$f(y) = \exp y^2 \operatorname{erfc} y \tag{2-11}$$

decreases constantly with increase in time, indicating that concentration polarization becomes more pronounced with time. At t=0, f(y)=1, and the current is controlled solely by the kinetics of the electrode reaction. The current density, i, contains appreciable kinetic information only at sufficiently short time.

Direct measurement of i_o is precluded by limitations of the instruments and by the double-layer charging current which was ignored in the preceding derivation. The faradaic current, i, and the double-layer charging current are additive. The charging current, i_c, is very high

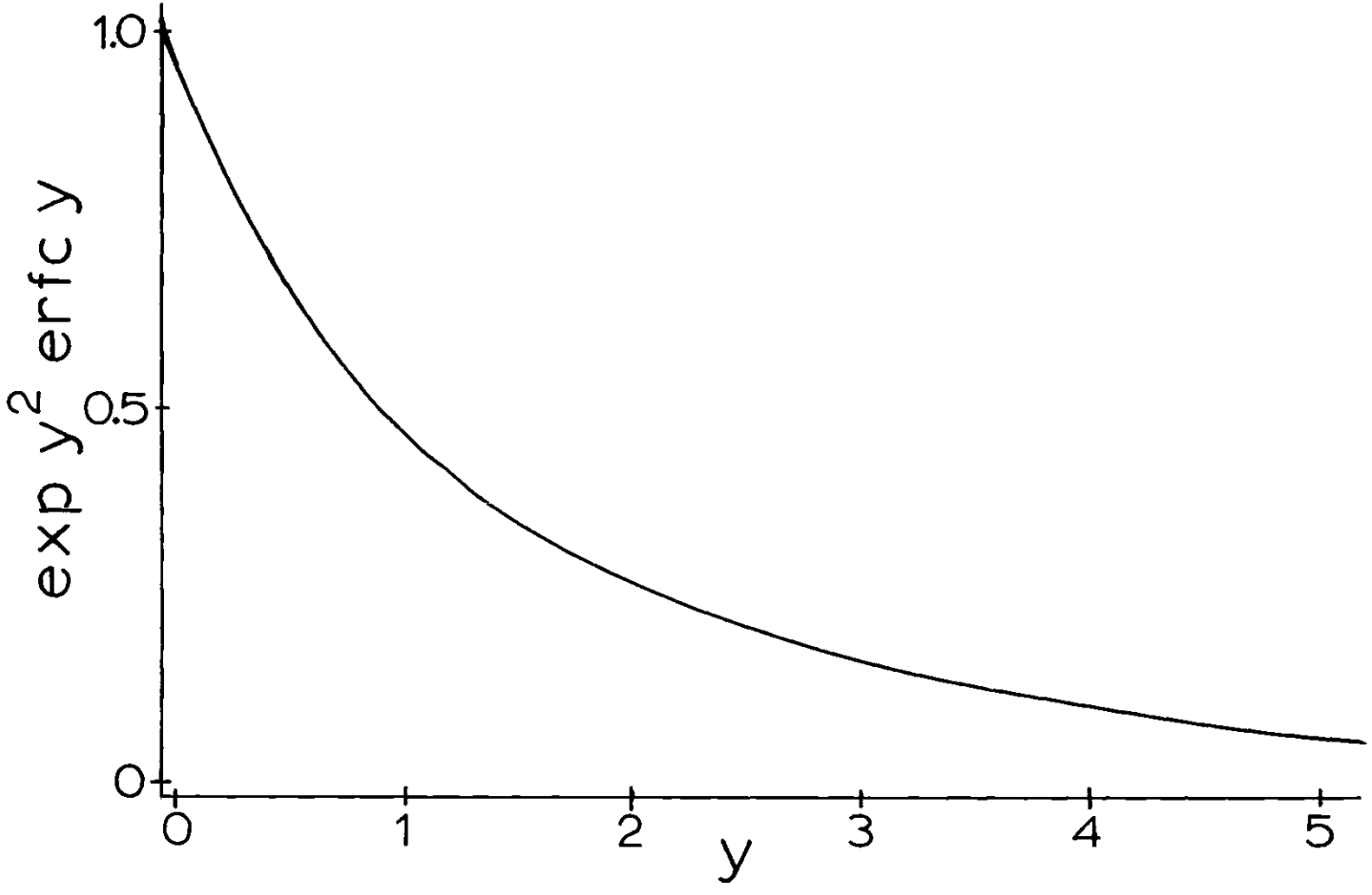

Figure 1. The Function exp y^2 erfc y Versus Its Argument y

initially, but decays more rapidly than does i. The rate of decay of the current required to charge the double layer depends on the resistance-capacitance time constant of the system. A typical value of this constant for a carefully designed system is ten microseconds.

The term erfc y can be expanded for any argument as follows (10)

$$\text{erfc } y = 1 - 2/\pi^{\frac{1}{2}}[y - (y^3/3.1!) + y^5/5.2!) + \cdots] \qquad (2\text{-}12)$$

For small values of y, f(y) simplifies to

$$\exp y^2 \text{ erfc } y \simeq 1 - 2y/\pi^{\frac{1}{2}} = 1 - (2\lambda t^{\frac{1}{2}}/\pi^{\frac{1}{2}}) \qquad (2\text{-}13)$$

Under these conditions the current density may be expressed as

$$i = i_o[1 - 2\lambda(t/\pi)^{\frac{1}{2}}] \qquad (2\text{-}14)$$

and a plot of i versus $t^{\frac{1}{2}}$ should be linear and have an intercept at $t^{\frac{1}{2}} = 0$ of i_o.

The values of i derived for equation (2-14) will differ from those generated by equation (2-9) by one percent or less only if (11)

$$y \leqq 0.1 \qquad (2\text{-}15)$$

This also implies, according to equation (2-14), that the condition

$$i/i_o \geqq 0.9 \qquad (2\text{-}16)$$

must be met in order for the extrapolation to $t^{\frac{1}{2}} = 0$ to be valid (11,12).

The criterion set by equation (2-16) is very difficult to meet experimentally. Oldham and Osteryoung (11) have developed two methods of obviating this difficulty; these methods also measure the amount of kinetic information contained in the data.

In the first technique, tangents are drawn to the curve of the current density versus square root time at ordinate value i, and extrapolated to $t^{\frac{1}{2}}=0$ to obtain i_x. An equation for the tangent can be obtained by differentiation of equation (2-9) with respect to y and evaluating the differential equation at $t^{\frac{1}{2}}=0$. This gives

$$i_x/i_o = (1 - 2\lambda^2 t)i/i_o + 2(t/\pi)^{\frac{1}{2}} \qquad (2\text{-}17)$$

Equations (2-9) and (2-17) define the unique relationship between the two ratios i_x/i_o and i/i_x. Figure 2 includes a working curve of this relationship. The i/i_x ratio is determined experimentally and the value i_x/i_o is obtained from the graph, then i_o is calculated. As i/i_x decreases to zero, the kinetic content of the data eventually vanishes.

The second Oldham-Osteryound method utilizes the i-t function and thereby obviates the necessity of transposing the data into an i versus $t^{\frac{1}{2}}$ relationship. The equation for a tangent drawn to the curve of i versus t may be obtained by differentiation of equation (2-9) with respect to y^2 and evaluation at t=0. This yields

$$i_y/i_o = (1 - \lambda^2 t)i/i_o + (t/\pi)^{\frac{1}{2}} \qquad (2\text{-}18)$$

where t and i are the coordinates of the point at which the tangent is

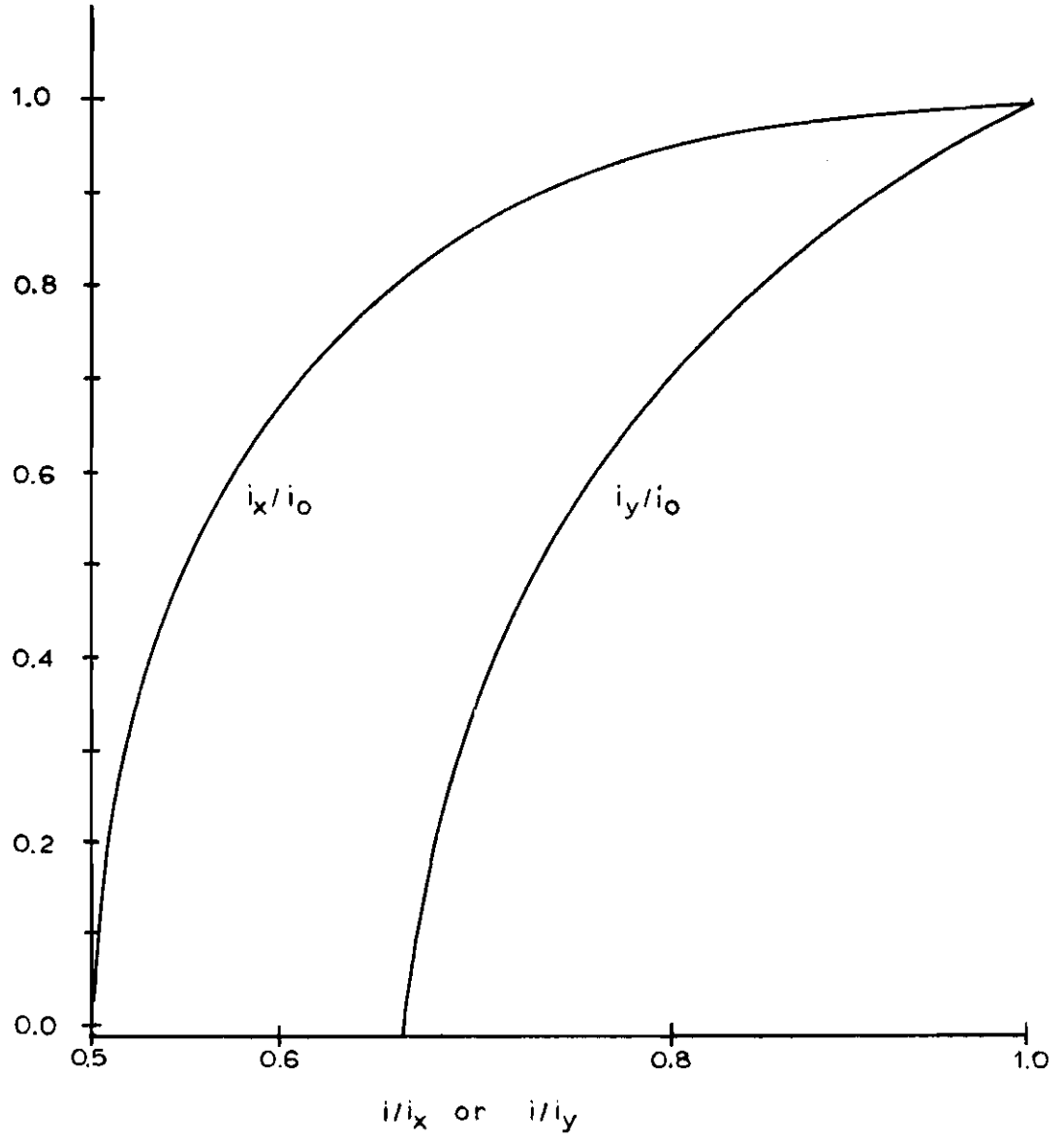

Figure 2. Working Curves for Potential Step Extrapolations

drawn. The $i_y/i_o - i/i_y$ relationship is shown graphically in Figure 2. The values of i and i_y are determined experimentally, and i_o is then calculated with the help of the working curve.

To determine the kinetic parameters, i^o and α, from the i_o data, equation (2-10) is used. Butler (13) pointed out that when $|\eta| \ll 1/\alpha nf$ [or $|\eta| \ll 1/(1-\alpha)nf$] the exponential factors in equation (2-10) can be linearized. The current-overvoltage characteristic is reduced to

$$i = i^o nf\eta \tag{2-19}$$

Vetter (14,15) recognized equation (2-19) to be in the form of Ohm's law and defined the so called "charge-transfer resistance"

$$(-\partial\eta/\partial i)_{i\to 0} = 1/nfi^o \tag{2-20}$$

At high overvoltages, $|\eta| \gg 1/\alpha nf$ [or $|\eta| \gg (1/(1-\alpha)nf$], one of the exponential terms in equation (2-18) can be dropped. In logarithm form the i versus η relationship would then be

$$\ln i = \ln i^o - \alpha nf\eta \text{ (cathodic process)} \tag{2-21a}$$

$$\ln i = \ln i^o + (1-\alpha)nf\eta \text{ (anodic process)} \tag{2-21b}$$

These are the equations of the familiar Tafel lines (16) at high overvoltage. Equations (2-21a) and (2-21b) hold when the overvoltage exceeds at least 0.1 volt. The two Tafel lines ($\ln i$ versus η) at high overvoltage intersect at the point having i^o as ordinate and $\eta=0$ as abscissa.

The slope of the cathodic Tafel line yields α and that of the anodic line gives $1-\alpha$.

Vetter (17) extended the foregoing treatment to processes involving two consecutive steps.

Consider the overall electrode reaction consisting of two one-electron charge transfer reactions involving soluble species

$$Ox + e \rightleftarrows X \tag{2-22a}$$

$$X + e \rightleftarrows Red \tag{2-22b}$$

Each of the reactions in equation (2-22) is characterized by its own transfer coefficient, α_a or α_b, and by its own exchange current density, i_a^o or i_b^o. The current-overvoltage function for the overall reaction can be derived by applying equation (2-10) to each separately and recognizing that each step accounts for one half of the total faradaic current. This leads to (18)

$$i = 2\,\frac{\exp - (\alpha_a+\alpha_b)f\eta - \exp(2-\alpha_a-\alpha_b)f\eta}{(1/i_b^o)\exp(1-\alpha_a)f\eta - (1/i_a^o)\exp - (\alpha_b f\eta)} \tag{2-23}$$

For the reduction depicted in equation (2-22), there exist three possible conditions that may characterize the kinetics of this reaction. First, the reaction may consist of two one-electron charge transfers with mixed kinetic control between the two steps. In the second and third cases, the reaction consists of two steps with either the first or second step completely controlling the kinetics. Characterization of an electrode reaction, such as in equation (2-22), can be made by evaluation of experi-

mental potential step data in terms of equation (2-23).

For the condition where large cathodic or anodic overvoltages exist, equation (2-23) can be reduced to the logarithmic Tafel relationship. In cases where the overall reaction is a two step charge transfer with mixed kinetic control and at large cathodic overvoltages, equation (2-23) becomes

$$i = 2i_a^o \left[\exp - (\alpha_a f\eta)\right] \tag{2-24}$$

or

$$\ln i = \ln 2i_a^o - \alpha_a f\eta \tag{2-25}$$

The Tafel plots at large cathodic overvoltage have a slope of $-\alpha_a f$ and yield $2i_a^o$ by extrapolation to $\eta=0$. Using the same reasoning, Tafel plots at large anodic overvoltages yield $(1-\alpha_b)$ and $2i_b^o$ for slope and intercept, respectively. The sum of α_a and $(1-\alpha_b)$ generally is not unity because the transfer coefficients for the two steps are normally different in value.

If $i_a^o \rightarrow \infty$, i.e., the second step completely controls the kinetics of the reaction, equation (2-23) reduces to

$$i = 2i_b^o \left[\exp - (1+\alpha_b) f\eta - \exp(1-\alpha_b) f\eta\right] \tag{2-26}$$

For large cathodic overvoltages, equation (2-26) becomes

$$i = 2i_b^o \left[\exp - (1+\alpha_b) f\eta\right] \tag{2-27}$$

and for large anodic overvoltages

$$i = 2i_b^o \left[\exp(1-\alpha_b)f\eta\right] \qquad (2\text{-}28)$$

Tafel plots of the functions in equations (2-27) and (2-28) have slopes of $-(1+\alpha_b)f$ and $(1-\alpha_b)f$ and extrapolation of both Tafel curves to $\eta=0$ yields $2i_b^o$. Conversely, for $i_b^o \rightarrow \infty$, Tafel plots yield slopes of $-\alpha_a f$ and $(2-\alpha_a)f$ and an intercept at $\eta=0$ of $2i_a^o$. A summary of the three cases is presented in Table 1.

The equation for the "charge-transfer resistance" at low overvoltages (cf. eq. (2-20)) was derived by Vetter as

$$-\left(\partial\eta/\partial i\right)_{i\rightarrow 0} = (1/4f)(1/i_a^o + 1/i_b^o) \qquad (2\text{-}29)$$

Equation (2-29) provided a means of verifying the values of i_a^o and i_b^o determined from the Tafel plots.

Experimental Techniques. The equipment used in the present study consisted of the locally built instrument, square root of time generator (Chapter IV), and a Tektronix Type 564 Storage Oscilloscope equipped with a Type 3B4 Time Base, a Type 3A6 Dual-Trace Vertical Amplifier, and a C12A camera. The electrode system consisted of a dropping zinc amalgam electrode as the working electrode, a locally fabricated saturated calomel electrode as reference, and a platinum wire as the auxiliary electrode.

The zinc amalgam was stored in an all glass system and under a positive pressure nitrogen blanket to prevent air oxidation. The nitrogen

Table 1. Summary of Consecutive Step Reaction Kinetics

Type of Control	Polarity	Theoretical Equations	Intercept	Slope
Mixed control	Cathodic	$\ln i = \ln 2i_a^o - \alpha_a f\eta$	$2i_a^o$	$-\alpha_a f$
	Anodic	$\ln i = \ln 2i_b^o - (1-\alpha_b)f\eta$	$2i_b^o$	$(1-\alpha_b)f$
First step controls	Cathodic	$\ln i = \ln 2i_a^o - \alpha_a f$	$2i_a^o$	$-\alpha_a f$
	Anodic	$\ln i = \ln 2i_a^o - (2-\alpha_a)f\eta$	$2i_a^o$	$(2-\alpha_a)f$
Second step controls	Cathodic	$\ln i = \ln 2i_b^o - (1+\alpha_b)f\eta$	$2i_b^o$	$(1+\alpha_b)f$
	Anodic	$\ln i = \ln 2i_b^o + (1-\alpha_b)f\eta$	$2i_b^o$	$(1-\alpha_b)f$

was passed over hot copper metal turnings to remove all oxygen. The area of the zinc amalgam electrode was determined for each particular time delay, column height, and glass capillary used in the experiments. The technique employed to measure the area will be discussed in Chapter IV.

A test solution containing zinc ions and supporting electrolyte was placed in the electrolysis cell and purged with nitrogen. Nitrogen was allowed to flow over the test solution constantly during the experiment to exclude all air from the electrolysis cell.

The potential of the working electrode was set to E_e, and at a selected time in the drop life a potential step was applied to the electrode. The positive feedback was adjusted to optimum capacitance current decay without causing "ringing" (i.e., instability of the potentiostat). The square root of time generator was used to drive the horizontal axis of the oscilloscope and was triggered simultaneously with the application of the potential step to the summing point of the control amplifier. The $i - t^{\frac{1}{2}}$ relationship was displayed and stored by the oscilloscope. Photographs of the traces at various overvoltages were made and analyzed for kinetic information.

Chronocoulometry

Theory. Chronocoulometry is a relaxation technique in which the potential is the perturbed parameter, and the resulting current is monitored as a coulomb-time function. The potential is stepped from a value at which no faradaic current flows to one at which the current is controlled by semi-infinite linear diffusion. A single-step chronocoulometric technique has been developed and used by many workers (19,20,21,

22,23) to study kinetics of fast electrode reactions and the adsorption of reactants or products. Anson (19) extended the theory to a double-step technique for the accurate study of adsorbed reactants or products, and his theories are used in this study.

When there is no adsorption of reactant and the applied step is such that the faradaic current is controlled by semi-infinite diffusion, the charge-time relationship can be derived from the integrated Cottrell equation (22)

$$Q = \frac{2nFAC(Dt)^{\frac{1}{2}}}{\pi^{\frac{1}{2}}} + Q_{dl} \qquad (2\text{-}30)$$

where Q is the total amount of charge in coulombs that has passed in time, t, since the application of the potential step; A is the area of the electrode; C and D are the concentration and diffusion coefficients of the reactants, respectively; n and F are the number of electrons involved in the reaction and Faraday's constant, respectively; and Q_{dl} is the number of coulombs required to charge the double-layer capacitance when the potential is changed. A plot of Q versus $t^{\frac{1}{2}}$ is linear with an intercept on the Q axis at $t^{\frac{1}{2}}=0$ equal to Q_{dl}.

If adsorption of reactants occurs, an additional term must be included in equation (2-30)

$$Q = \frac{2nFAC(Dt)^{\frac{1}{2}}}{\pi^{\frac{1}{2}}} + Q_{dl} + nFA\Gamma \qquad (2\text{-}31)$$

where Γ is the surface excess of reactant in moles per square centimeter.

A Q versus $t^{\frac{1}{2}}$ plot has a Q axis intercept of $(Q_{dl}+nAF\Gamma)$ and Γ can thereby be ascertained if Q_{dl} is known.

The difficulty with the single step technique is the accurate determination of Q_{dl}. A value is normally obtained from a blank experiment and assumed to be constant when the faradaic processes are involved. One way of solving the problem is to eliminate any net double-layer charging by performing a double potential step technique so that the electrode ends up back at its initial potential. The charge in the double layer will then be the same as it was at the beginning of the experiment, and no value for Q_{dl} is needed.

Consider the typical completely reversible electrode reaction

$$O + ne \rightleftarrows R \qquad (2\text{-}32)$$

with a half wave potential of $E_{\frac{1}{2}}$. Initially, the concentration of O at the electrode surface is equal to the bulk concentration C_o, and the concentration of R is zero; the potential, E_1, is such that no faradaic current flows. The potential is then stepped cathodically to a new potential, E_2, where the current is diffusion controlled, and the concentration of O at the electrode surface drops to zero. At some later time, τ, the potential is stepped back to E_1 and the reaction is reversed with the rate controlled by the diffusion of R back to the electrode. A typical charge-time curve is shown in Figure 3.

For times less than τ, the charge-time function is given by equation (2-30). For times greater than τ, it is given by (19)

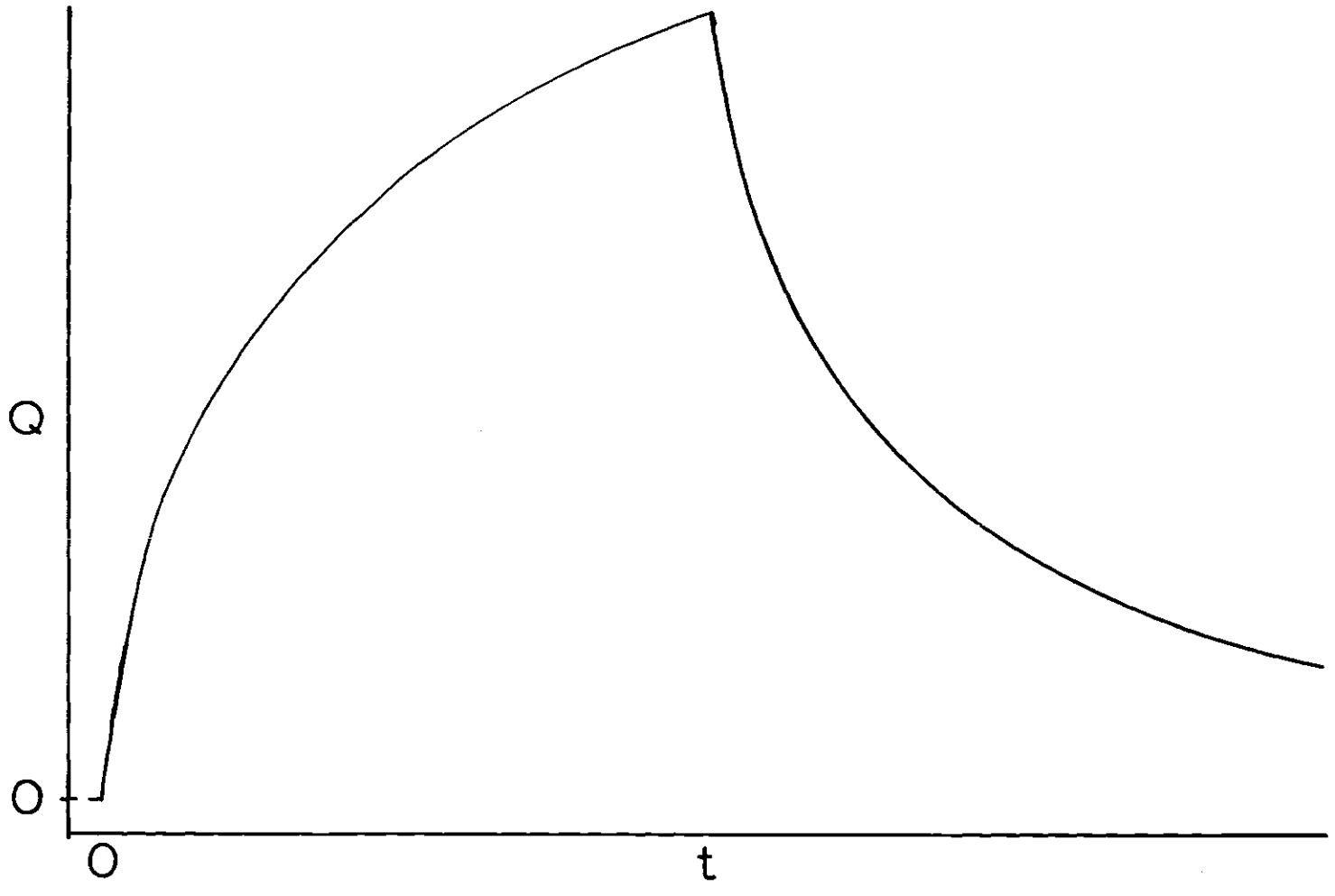

Figure 3. Theoretical Double-Step Chronocoulometric Trace

$$Q_{(t > \tau)} = [(2nFAD^{\frac{1}{2}})/\pi^{\frac{1}{2}}][t^{\frac{1}{2}} - (t-\tau)^{\frac{1}{2}}] \qquad (2\text{-}33)$$

and there is no term for the charging of the double layer. A curve of $Q_{(t > \tau)}$ versus $[t^{\frac{1}{2}} - (t-\tau)^{\frac{1}{2}}]$ will pass through the origin if neither O nor R is specifically adsorbed.

If the coulombs that flow after τ are measured with respect to the charge at τ, Q_τ, then a new charge-time function is obtained. Q_A, the coulombs that flow following the second potential step, is given by

$$Q_A = Q_\tau - Q_{(t > \tau)} \qquad (2\text{-}34)$$

where Q is

$$Q_\tau = (2nFACD^{\frac{1}{2}}\tau^{\frac{1}{2}})/\pi^{\frac{1}{2}} + Q_{dl} \qquad (2\text{-}35)$$

Combining equations (2-33) and (2-35), it follows that

$$Q_A = [(2nFACD^{\frac{1}{2}})/\pi^{\frac{1}{2}}][\tau^{\frac{1}{2}} + (t-\tau)^{\frac{1}{2}} - t^{\frac{1}{2}}] + Q_{dl} \qquad (2\text{-}36)$$

From a plot of Q versus $t^{\frac{1}{2}}$ and on the same graph, Q_A versus $[\tau^{\frac{1}{2}} + (t-\tau)^{\frac{1}{2}} - t^{\frac{1}{2}}] = \theta$, the degree of adsorption of species can be determined. The value of Q or $-Q_A$ at $f(t) = 0$ is a measure of the degree of adsorption present plus the Q_{dl} factor.

There are four possible situations of species adsorption: (1) no adsorption of O or R; (2) O adsorbed but R is not; (3) O not adsorbed but R adsorbed; and (4) O and R both adsorbed. In each case the graphs should be linear and information about the adsorption is obtained from the values

of Q's at f(t) = 0.

For case one (no adsorption), $|Q|$ and $|Q_A|$ at f(t) = 0, should be the same and equal to Q_{dl}. For case two, at f(t) = 0, Q will be larger than Q_A, and the difference will be proportional to Γ_o (the surface excess of the oxidized form). The reverse is true for the third case with Γ_a being calculated from $Q - |Q_A|$. In the case of adsorption of O and R, both intercepts of the f(t) = 0 line will be larger than Q_{dl}. The Q values may be equal or different. For an evaluation of the degree of adsorption, Q_{dl} must be determined independently by another technique.

Experimental Techniques. Instrumentation was identical to that used for potential step techniques except that a Beckman 39016 hanging drop electrode was used as the working electrode instead of the zinc amalgam electrode.

Logic to control the integrator is obtained from the timing system of the polarograph. This logic activates the integrator simultaneously with the application of the square-wave to the summing point of the control amplifier. The oscilloscope is triggered approximately ten microseconds previous to the integrator being turned on.

The maximum length of an integration was arbitrarily set at 100 milliseconds to avoid possible spherical diffusion. This value is well below the maximum allowable time of two seconds, as calculated from Shain's theoretical equations (24). The cathodic and anodic chronocoulograms are displayed and stored by the oscilloscope. Photographs are made and analyzed for adsorption information.

Voltammetry Techniques

Residual Current

The total observed current in an electrochemical experiment results from two different processes at the electrode. There are faradaic currents which result from the transfer of electrons across the electrode-solution interface, and a capacitance current which flows due to the capacitive characteristics exhibited by the electrode-solution interface. This "non-faradaic" current is required anytime the potential or the area of this "pseudo-capacitor" is changed. Since the potential during a drop life is almost constant, the capacitance current obtained in dc polarography is primarily a result of changes in the area of the electrode.

The polarity of the capacitance current will depend on the potential of the working electrode with respect to the point of zero charge. At the potential of the point of zero charge, E_{max}, there is no excess of anions or cations in the layer of solution in immediate contact with the electrode. This means that there is no separation of charges, and no expenditure of energy is required; therefore, no current will flow into charging the double layer. At potentials more positive than E_{max}, a negative (anodic) current is required to charge the double layer while at potentials more negative than E_{max}, a positive (cathodic) current is required for double-layer charging.

The total faradaic current will be the sum of the currents from all electrochemical reactions that occur at the electrode's surface. In addition to the current coming from the reaction of the species under

study, there may be small amounts of faradaic current obtained from trace impurities, such as oxygen or copper, from the distilled water in the solution. The sum of these undesirable faradaic currents and the capacitance current, discussed in the preceding paragraph, is known as the residual or background current.

The separation of the residual current from the desired faradaic current has long been the limiting factor in the sensitivity of polarographic techniques. Various polarographic methods have been developed to effect this separation. Two basic characteristics of the currents are used: (1) current-time characteristics and (2) phase-shift characteristics. The techniques described in the following pages employ the current-time relationships for the separation of the various currents.

Tast or Current-Sampled dc Polarography

Theory. The equation for the instantaneous diffusion limited current was originally derived by Ilkovic (25), who assumed semi-infinite linear diffusion rather than spherical diffusion. The so-called Ilkovic equation can be written in the form

$$i_d = 708nD^{\frac{1}{2}}Cm^{\frac{2}{3}}t^{\frac{1}{6}} \qquad (2\text{-}37)$$

where n is the number of electrons transferred per atom, D is the diffusion coefficient of the reactant in solution in units of $cm^2\ sec^{-1}$, C is the concentration of the reactant in mmoles per liter, m is the weight of mercury in mg per sec flowing from the capillary, and t is any instant of time, in sec, during the drop life. Using the above units, the current, i_d, will have units of μA.

The equation for the instantaneous capacitance current during the drop life, as derived by Bresle (26) is

$$i_c = 0.00569\ K\ (E_{max}-E)m^{-\frac{2}{3}}t^{-\frac{1}{3}} \qquad (2\text{-}38)$$

where K is the integral capacitance of the double layer per unit area, E is the potential of the DME with respect to the reference electrode, E_{max} and t have the same meanings as in the preceding section.

Considering equations (2-37) and (2-38), it is seen that the faradaic current increases with time by a factor of $t^{\frac{1}{6}}$, while the capacitance current decreases according to $t^{-\frac{1}{3}}$. If the total instantaneous current $(i_d + i_c)$ is measured very near the end of drop life, the maximum separation of the two currents is obtained, i.e., i_d/i_c is a maximum at the end of the drop life. Figure 4 shows the relation between i_d/i_c and time during the drop life for a typical solution. The contributions to the total residual current made by the electrode reactions of impurities are not included. This omission does not affect the basic conclusions reached in this discussion.

In addition to the greater separation of currents at the end of the drop life, there is another important factor to consider. The error in the experimentally determined i_d/i_c caused by an error in the time of measurement is a minimum near the end of the drop life; because the rate of change in current flows with respect to time decreases during the drop life.

The technique of measuring the cell current only near the end of

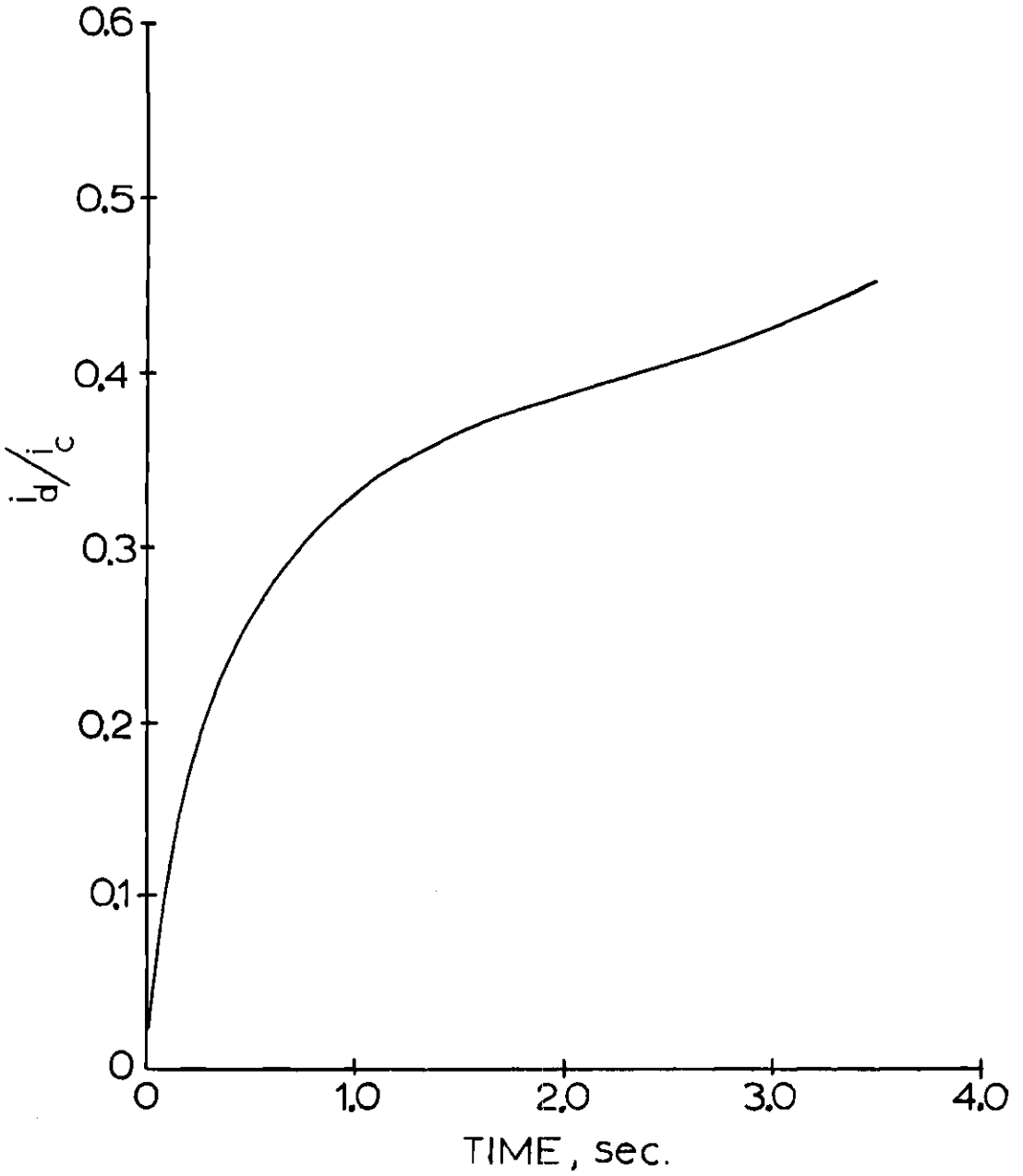

Figure 4. Ratio of Diffusion Current to Capacitance Current as a Function of Time

the drop life is known as Tast polarography. The method was first used by Kane (27) and later by Mark and Reilley (28). Sturrock (29) suggested that, to evaluate the improvement that is achieved by using Tast instead of normal dc polarography, the basic concepts of the two methods must be compared. Direct current polarography is based on the measurement of the average current during the drop life, while Tast measures the instantaneous current at a point in time very near the end of the drop life.

Integration of equation (2-36) over the drop life yields the total microcoulombs per drop, and dividing this results by the drop life, t, in seconds gives the average diffusion current, $\bar{i}_d$, during the drop life

$$\bar{i}_d = 1/t \int_o^t i_f dt = 607nD^{\frac{1}{2}}m\ t \qquad (2\text{-}39)$$

A comparison of equations (2-37) and (2-39) shows that

$$\bar{i}_d = 607/708\ i_d = 0.847\ i_d \qquad (2\text{-}40)$$

To obtain the average capacitance current, $\bar{i}_c$, the total quantity of electricity required to charge the double layer is divided by the drop life, t,

$$\bar{i}_c = q/t = (1/t)KA_t(E_{max}-E) \qquad (2\text{-}41)$$

where A_t is the area in cm^2 at time, t. The value of A_t can be expressed in terms of the parameters m and t. The volume, V_t, of the drop is given by

$$V_t = 4/3\ r_t^3 = 10^{-3}\ mt/d_{Hg}$$

where d_{Hg} is the density of mercury. One can now write

$$A_t = 4\pi r_t^2 = 0.00853 m^{\frac{2}{3}} t^{-\frac{1}{3}} \tag{2-43}$$

and

$$\bar{i}_c = 0.00853 K (E_{max} - E) m^{\frac{2}{3}} t^{-\frac{1}{3}} \tag{2-44}$$

A comparison of equations (2-38) and (2-44) gives

$$\bar{i}_c = 0.00853/0.00569 \; i_c = 1.50 \; i_c \tag{2-45}$$

The factor 0.00569 in equation (2-38) is obtained by differentiation of the equation for the charge on the electrode with respect to the drop age, t,

$$dq/dt = i_c = K(E_{max} - E) \; dA/dt \tag{2-46}$$

where

$$dA/dt = 0.00852 \; m^{\frac{2}{3}} \; (2/3) t^{-\frac{1}{3}} \tag{2-47}$$

Combining equations (2-40) and (2-45) yields

$$\bar{i}_d/\bar{i}_c = \frac{0.847}{1.50} \frac{i_d}{i_c} = 0.565 \; i_d/i_c \tag{2-48}$$

Equation (2-48) indicates an approximate twofold gain in current separation by the Tast technique as compared to normal dc polarography. This is far below the tenfold increase indicated by Mark and Reilley (28).

The major advantage of Tast polarography is the removal of drop action in the current readout. This facilitates the measurement of the

diffusion limited currents and also the use of current off-set techniques in the quantitation of minor constituents that are reduced at more negative potential than a major component.

Square-Wave Polarography

Theory. The effectiveness of square-wave polarography in the separation of capacitance and faradaic currents was first described by Barker and Jenkins (30). The technique utilizes the time dependency function of the two currents to effect the separation.

In square-wave polarography, a small continuous square-wave voltage is superimposed on the slowly changing polarizing potential which is applied to the electrodes of a polarographic cell. The resulting alternating component of the cell current is measured shortly before each change in potential of the square wave, and an output voltage proportional to this alternating component is obtained.

For a reversible electrode reaction such as,

$$O + ne \rightleftarrows R \tag{2-49}$$

when only O is initially present, and R is soluble in either the aqueous or mercury phase, the amplitude of the faradaic alternating component of the cell current density is given by (32)

$$i = \pm (n^2F^2/RT)C_o\Delta E[P/(1+P)^2](D_o/\pi\tau)^{\frac{1}{2}}\sum_{m=o}^{\infty}(-1)^m[1/(m+\beta)^{\frac{1}{2}}] \tag{2-50}$$

where

$$\beta = t/\tau \qquad (0 < t < \tau) \tag{2-51}$$

and

$$P = \exp(E-E_{\frac{1}{2}})\ nf \qquad (2\text{-}52)$$

In equation (2-52), E is the average potential of the mercury drop during its drop life, and $E_{\frac{1}{2}}$ is the half wave potential of the redox couple. ΔE is the peak to peak amplitude of the square-wave voltage. The parameter, t, is the elapsed time (sec) since the last charge in the square-wave polarity, and τ is the half-wave length (sec) of the square-wave signal. C_o and D_o are the bulk concentration (moles cm^{-3}) and diffusion coefficient ($cm^2\ sec^{-1}$) of O, respectively. F, N, R, T, and f have the same meanings as in the previous section.

For a given experiment, all parameters in equation (2-50) except P are kept constant. Equation (2-50) shows that the faradaic current density is at a maximum when P is a minimum, and P will be a minimum when $E = E_{\frac{1}{2}} = E_s$, where E_s is the so-called summit potential. It is also seen that the current is proportional to the bulk concentration of O, and the current peak will be symmetrical about the half-wave potential. By setting equation (2-50) equal to one half of the maximum current and solving for $(E-E_{\frac{1}{2}})$, it is found that, at 25°C, $(E-E_{\frac{1}{2}})$ equals 45.2 and 22.6 mv for n=1 and n=2, respectively (i.e., the width at half-height of the waves is 90.4 mv for n=1 and 45 mv for n=2).

The capacitance component of the cell current is given by

$$i_c = \pm\ (\Delta E/R)\exp(-t/RC) \qquad (2\text{-}53)$$

where ΔE and t have the same meaning as above. R^* is the solution resistance, and C^* is the double-layer capacitance. The plus or minus sign holds for charging or discharging, respectively. Comparing equations (2-50) and (2-53), it is seen that the double-layer charging current is proportional to $\exp(-t/RC)$ and the faradaic current is approximately proportional to $t^{-\frac{1}{2}}$. This means the greater the value of t, the more effectively the currents are separated.

Typical values for R and C are 50 ohms and 2×10^{-7} farads, respectively. The time delays used for most square-wave polarography analysis ranged from 0.3 to 1.4 msec. Substituting into equation (2-53) the values for R, C, and the shortest time delay and calculating i_c, it is seen that, even for the 0.3 msec time delay, the capacitance current has decayed to approximately 1×10^{-11} percent of the initial value.

Differential Pulse Polarography

Theory. There are three basic types of pulse polarography. The one common characteristic of the techniques is that only one potential pulse is applied to each mercury drop near the end of its life. The major differences in the three methods consist of variations in the initial potential and current monitoring techniques. The three types are normal pulse, derivative pulse, and differential pulse polarography.

In normal pulse polarography, a potential step is applied to the mercury electrode near the end of its life, with the drop being held at the initial potential during its growth period. A slightly higher pulse

*R and C were previously used as symbols for the reduced form of an electroactive species and to denote concentration of a species. They are employed again because the term "RC constant" is universally known and understood.

is applied to each succeeding drop. The current is sampled during the latter part of the pulse life, and a voltage proportional to this current is amplified and presented to the recorder until the next current sample is taken.

In derivative pulse polarography, the potential pulse applied to the electrochemical cell is identical to that used in normal pulse polarography. In both cases, potential pulses of increasing heights are applied to each successive mercury drop. The cell currents for the two techniques are thus exactly the same, and the only differences are in the way in which the current signals are processed.

In normal pulse polarography, the current is measured and a proportional voltage is applied to the recorder for each drop. In derivative pulse, the sampled current from a particular drop is not immediately amplified and presented to the recorder. Instead, a differential amplifier compares the current from two successive drops and generates a voltage proportional to the difference between the two currents. From derivative pulse polarography, curves are obtained that are the derivative of the normal pulse polarograms, and the electrode reaction of each reversible species will produce a Gaussian shape peak.

In differential pulse polarography, a linearly increasing ramp is applied to the working electrode and a fixed height pulse is superimposed upon this ramp near the end of the life of each drop. The currents are sampled just before the end of the two-half cycles of the square wave pulse. A voltage proportional to the difference of these two cell currents is amplified and applied to the recorder. The current readout is very

similar to that obtained by the derivative pulse method.

Experimental Techniques

The locally fabricated instrument described in Chapter III was used for all voltammetry experiments. All polarograms were recorded with a Hewlett-Packard 7005B X-Y recorder. The timers in the timing systems were calibrated using a Tektronix Type 564 Storage Oscilloscope which had a Type 3B4 Time Base, and a Type 3A6 Dual-Trace Vertical Amplifier. A Tektronix Type 184 Time-Mark Generator was used as a time standard for all calibrations.

The electrode system consisted of a DME as the working electrode, a Beckman 39170 fiber-junction calomel electrode as reference, and the counter electrode was a short length of platinum wire.

Test solutions of known concentrations of various cations were prepared. The solutions were purged and then blanketed with dry nitrogen to remove oxygen from the electrolysis cell. The various time and potential parameters controls were set according to the electrochemical technique being performed. Variables such as positive feedback, sampling delay, and sampling gate width were set using the Tektronix oscilloscope to monitor the current readout.

CHAPTER III

DESCRIPTION OF INSTRUMENT

General Description

The instrument was designed to function as a multipurpose polarograph, so that its operational characteristics can easily be changed from one polarographic technique to another. It was built around a fast, three electrode potentiostat that was constructed using operational amplifiers. All amplifiers were chosen for gain, high-gain band width product, and stability, consistent with the instrument's design.

The overall concept of the instrument is not novel. Many of the circuits described have appeared in chemical publications and/or manufacturer's literature. The circuits are included here to show the exact configuration and component values used in the instrument. Where a specific reference is known it will be acknowledged, but many of the circuits have never been properly acknowledged in the literature. A detailed description of the operation is given for all circuits that have been designed explicitly for this instrument.

The instrument consists of two main chassis; (1) the timing chassis which contains the power supplies, and timers needed for potential step techniques; (2) potentiostat and current monitoring chassis. The two chassis are mounted in a large instrument cabinet, and all interchassis connections are made on the back panels using shielded leads. Analog

signals and digital timing logic are carried through miniature coaxial cables, the shields of which are carefully grounded in order to eliminate all ground loops. All major controls are mounted on the front panels; other controls less often used are mounted on the rear panels.

Commercial instrumentation such as the oscilloscope, recorder, and digital voltmeter are connected to the instrument using front panel mounted BNC connectors and coaxial cables. The cable shields were carefully grounded only to the instrument to prevent ground loops.

Each major part of the system (cell cage, instrument cabin, recorder, etc.) was individually grounded to a laboratory instrument grounding system. An one-quarter inch wide copper mesh grounding lead was used for this purpose. The major parts were also isolated from the laboratory's ac power ground to remove possible ground loops.

Timing Chassis

General Description of Timing System

The timing system consists of ten printed circuit boards. Five of these boards are delay timers which control the five time functions required by potential step techniques. The timer boards are basically identical and may be used interchangeably with only slight modifications. Mounted on the other five circuit boards are: (1) power supplies for the timing system, (2) the controls for the solenoid used to dislodge the mercury electrode drop, (3) square-wave output controls, and, (4) logic circuits for the two track and hold modules. A block diagram of the timing system is shown in Figure 5.

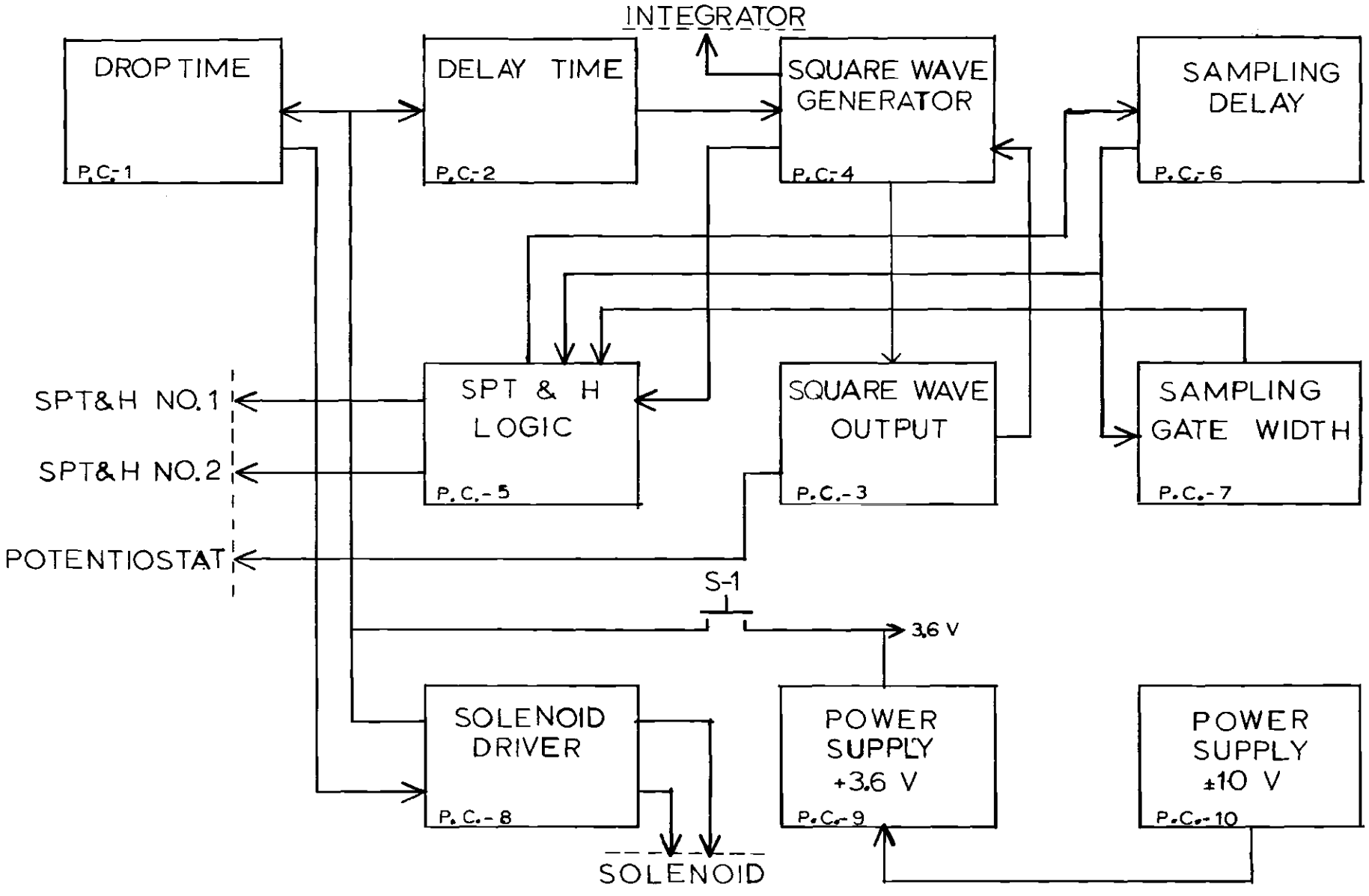

Figure 5. Block Diagram of the Timing Chassis

The operation of the timing system can be understood by studying the chronological sequence of events during the life of a drop. A detailed description of the circuitry and performance characteristics of each board will not be made at this point. Only the major inputs and outputs of the circuit boards will be considered in the present discussion.

For the purpose of this discussion, assume that the technique being performed is differential pulse polarography. As will be seen, all circuits in the timing system are used in this technique.

The timing cycle is initiated by depressing switch S-1, shown in Figure 5, which applies + 3.6 volt simultaneously to the drop time timer (PC-1) and the delay time timer (PC-2). This positive voltage starts the unijunction oscillators, (see page 39) in these timing circuits.

The delay time is the time between the start of the drop and the application of the perturbation signal to the electrolysis cell. The delay time is therefore always less than the drop time. The two timers are normally set so that the perturbation signal is applied 90 percent into the drop life. When this point in the drop life is reached, the delay time timer generates pulse which is applied to the square-wave generator (PC-4), starting its unijunction oscillator.

The circuitry on PC-4 generates two square-wave functions (one the reverse of the other). One of the square-wave signals is used in the development of logic for the current integrator; the other square-wave function is simultaneously applied to a splitter-amplifier and square-wave cycle counter on PC-3 and to the track and hold logic circuits of PC-5.

Before the square-wave function from PC-4 is applied to the summing

point of the potentiostat, the magnitude of the step function must be increased and two square-wave signals that are in phase but of opposite polarity must be developed. The splitter-amplifier circuit on PC-3 performs both operations.

A square-wave counter on PC-3 controls the number of square-wave cycles that will be applied to the working electrode during the life of one drop. The number of cycles can be any power of two from zero to four, or the counter can be used in a continuous mode, where a continuous square-wave signal is applied to the working electrode during the entire life of a drop. At the end of the desired number of square-waves, a pulse is generated by the counter and applied to PC-4 (square-wave generator) stopping its unijunction oscillator. In the differential pulse technique the counter is set for one square-wave cycle per drop life.

Also located on PC-3 is the square-wave follower, the output of which is fed through a resistor to the summing point of the potentiostat. The follower, a Philbrick SQ-10a operational amplifier, is used to isolate the square-wave generator circuit and to reduce loading on the splitter-amplifier circuits so that the controls have a linear response.

PC-5 controls the logic for the sampling delay timer (PC-6), sampling gate width timer (PC-7), and the Track and Hold modules in the current measuring circuits. A square-wave function from PC-4 is used to generate these logic signals. Each time the potential is stepped, the logic circuit on PC-5 starts the sampling delay timer on PC-6. After a predetermined length of time this timer will generate a pulse, which starts the sample gate width timer. The pulse is also used by PC-5 for Track and Hold modules logic. The input gate to one of the Track and Hold units

is opened at this point, and the cell current is monitored. The timing circuit on PC-7 will determine how long the sample gate is open. After a set period of time, the sample gate width timer generates a pulse, which is used by PC-5 to close the Track and Hold unit input gate.

The next sequential event is the termination of the drop life. This occurs when the drop time timer on PC-1 has counted the preset number of cycles of its unijunction oscillator. A pulse is generated and applied to the solenoid control, PC-8. The pulse causes this circuit to actuate the solenoid which dislodges the mercury drop. The solenoid control circuit also generates a slightly delayed pulse that is applied to PC-1 and PC-2, which in turn starts a new complete cycle of the timing system.

Timer Circuit (PC-1, 2, 4, and 7)

A detailed schematic of the timer circuit is given in Figure 6. The heart of this circuit is the unijunction transistor oscillator, and the wave-length of the output signal of this oscillator is used as the basic unit of time. By changing the wave-length (which is the reciprocal of the frequency) of this oscillator *via* changes of the resistance-capacitance (RC) constant, any length of time from a few tenths of a microsecond to several seconds can be measured accurately. A knowledge of the functional characteristics of the unijunction transistor is required to fully understand the operations of the timing circuit.

The unijunction transistor (UJT) is a three-terminal device with only one p-n junction. The stability of its characteristic parameters makes it ideal for timing circuit applications. Figure 7 shows the schematic circuit symbol and nomenclature, and Figure 8 shows a simplified

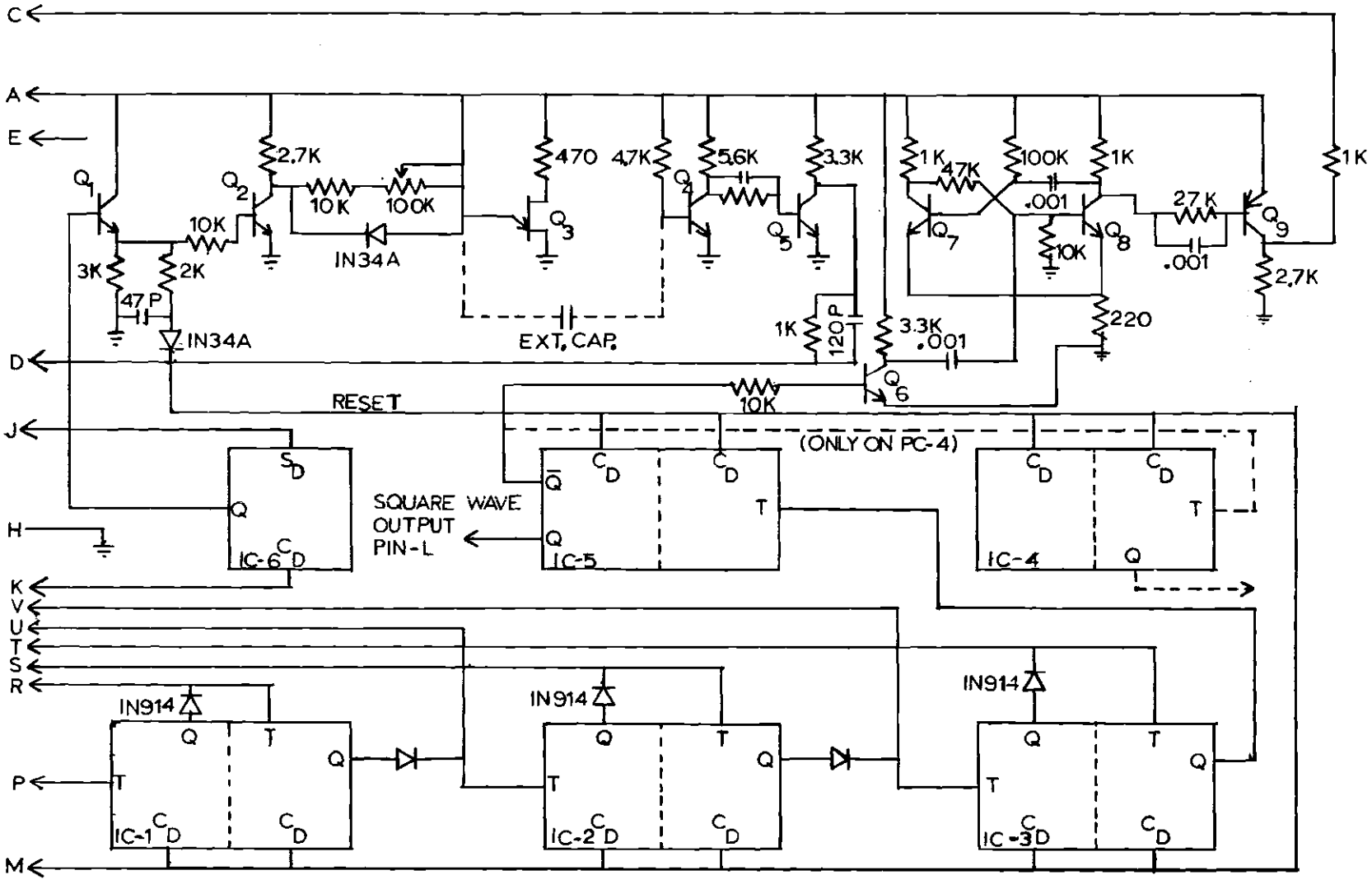

Figure 6. Detailed Schematic of the Timer Circuit

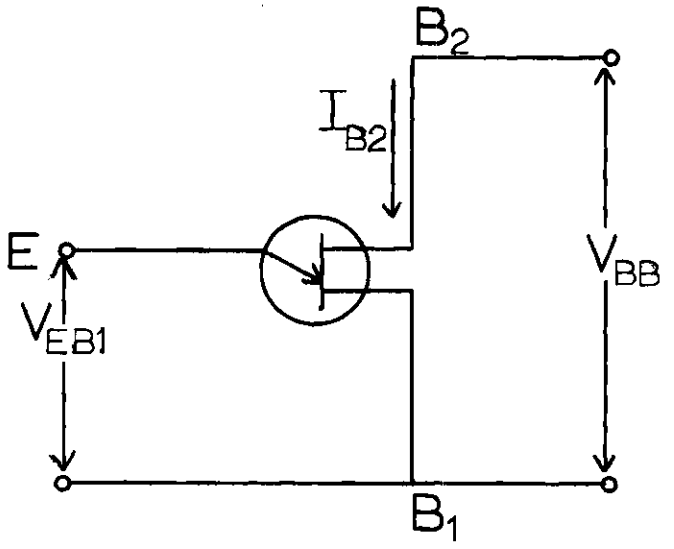

Figure 7. Unijunction Transistor Circuit Symbol and Nomenclature

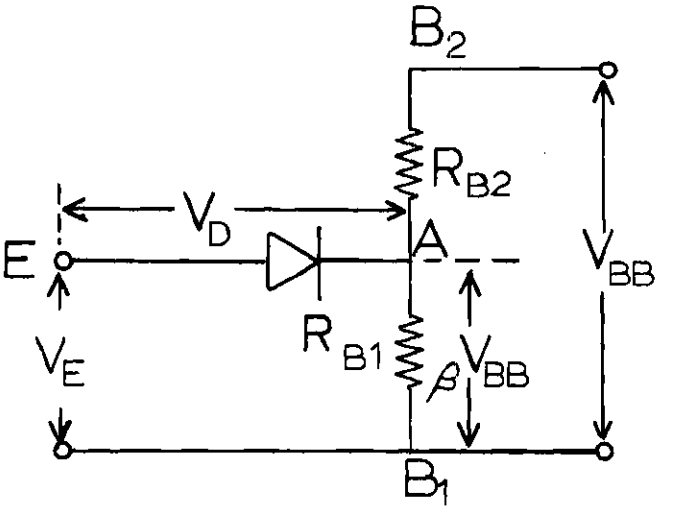

Figure 8. Simplified Equivalent Circuit of a Unijunction Transistor

equivalent circuit (32).

In the normal use of a UJT a positive voltage, V_{BB}, is connected across B_2 to B_1. The resistance of the n-type semi-conductor acts as a voltage divider, R_{B_1} and R_{B_2}, to establish a potential βV_{BB}, at the emitter contact; where β is the fraction of the applied voltage, V_{BB}, between the emitter contact and B_1. As long as the externally applied emitter potential is more negative than the sum of βV_{BB} and the forward voltage drop, V_D, of the p-n junction, the emitter junction is reverse-biased and virtually no current will flow in the emitter circuit. If the emitter potential is made more positive than the sum $\beta V_{BB} + V_D$, the emitter junction is forward-biased and current will begin to flow from the emitter to B_1. The emitter-B_1 junction then has the low resistance characteristic of a forward-biased diode. The sum of $\beta V_{BB} + V_D$ is known as the peak-point voltage and is a very stable characteristic of a given UJT. The increased current in the n-type silicon effectively decreases the value of R_{B_1}. This decreases the fraction, β, which causes a further increase in emitter current, and a lower effective resistance for R_{B_1}. This cyclic effect will continue until the emitter voltage is equal to V_D, and the junction no longer conducts.

The other major type of component in the timer circuit is the binary flip-flop. The J-K master-slave flip-flops used in the instrument consist of two cross-coupled gated memory circuits; one to hold the output state and the other to hold the input data present at the beginning of the timing pulse for later transfer to the output memory. In the J-K configuration, the binary outputs of the slave flip-flop are connected to

the input of the master flip-flop to obtain a toggle operation. J-K flip-flops can then be used as electronic counters by connecting them in series.

Under normal initial conditions, the control flip-flop (IN-C of Figure 6) has a high level at the Q output, which also appears at the emitter of Q_1. This positive voltage is applied to the C_d pins of the counter flip-flops, holding all Q outputs at the "0" (low) level. The positive voltage at the emitter of Q_1 also saturates Q_2 thus preventing the unijunction oscillator, Q_3, from running. The positive voltage at the Q output of the IC-5 counter flip-flop saturates Q_8.

When a positive voltage or trigger pulse is applied to C_d of the control flip-flop, IC-6, the outputs change state. The Q output drops to the "low" level. This lowers the emitter voltage of Q_1 to approximately zero volts, turning off Q_2. This allows the timing capacitor of the unijunction oscillator to be charged through the fixed 10K resistor and the 100K twenty turn Helipot potentiometer until the peak-point voltage of the unijunction transistor is reached. The time in seconds required to obtain the peak-point voltage is equal to the capacitance (in farads) times the resistance (in ohms). This R-C constant thus controls the frequency of the oscillator. Coarse frequency control is obtained by varying the capacitance and fine control is obtained via the 100K potentiometer. In this way any frequency from 10 Hz to 1 MHz can be selectively achieved.

When the peak-point voltage is reached, the unijunction transistor will begin to conduct, and as a consequence discharges the timing capacitor. This charging and discharging of the capacitor will appear as a saw

tooth signal on the base of Q_4. The resulting collector voltage of Q_4 is a positive-going pulse, which is inverted by Q_5. The negative pulse is then applied, by means of an external switch, to a selected point in the chain of counter flip-flops. The unijunction oscillator will freerun until the control flip-flop, IC-6, changes state, which occurs if a positive voltage is applied to the S_D input of the flip-flop.

Motorola MC790P dual J-K master-slave flip-flops are used in the cycle counters. The set and clear inputs are grounded. In this configuration the flip-flop will change states only when a negative going transit is detected at the T (time) input. By connecting the flip-flops in series, the oscillator frequency is divided by $2^{(n-1)}$, where n is the number of flip-flops used.

When the final flip-flop in IC-5 toggles, Q_8 is turned off, generating a positive spike which triggers the ten microsecond one-shot multivibrator. The negative, ten microsecond pulse generated by this multivibrator is inverted by Q_9 and applied to pin C of the board as the timed delay output.

The Q outputs of the two flip-flops in IC-5 are used as the source of square-wave functions on PC-4. On the other timer boards these outputs are not used.

Track and Hold Logic (PC-5)

Figure 9 shows a detailed schematic of the Track and Hold modules' logic circuits located on PC-5. The logic circuits use binary inverters, NAND gates and J-K master-slave flip-flops to develop the required plus and minus volt logic signal. To understand the logic circuit, it must first be

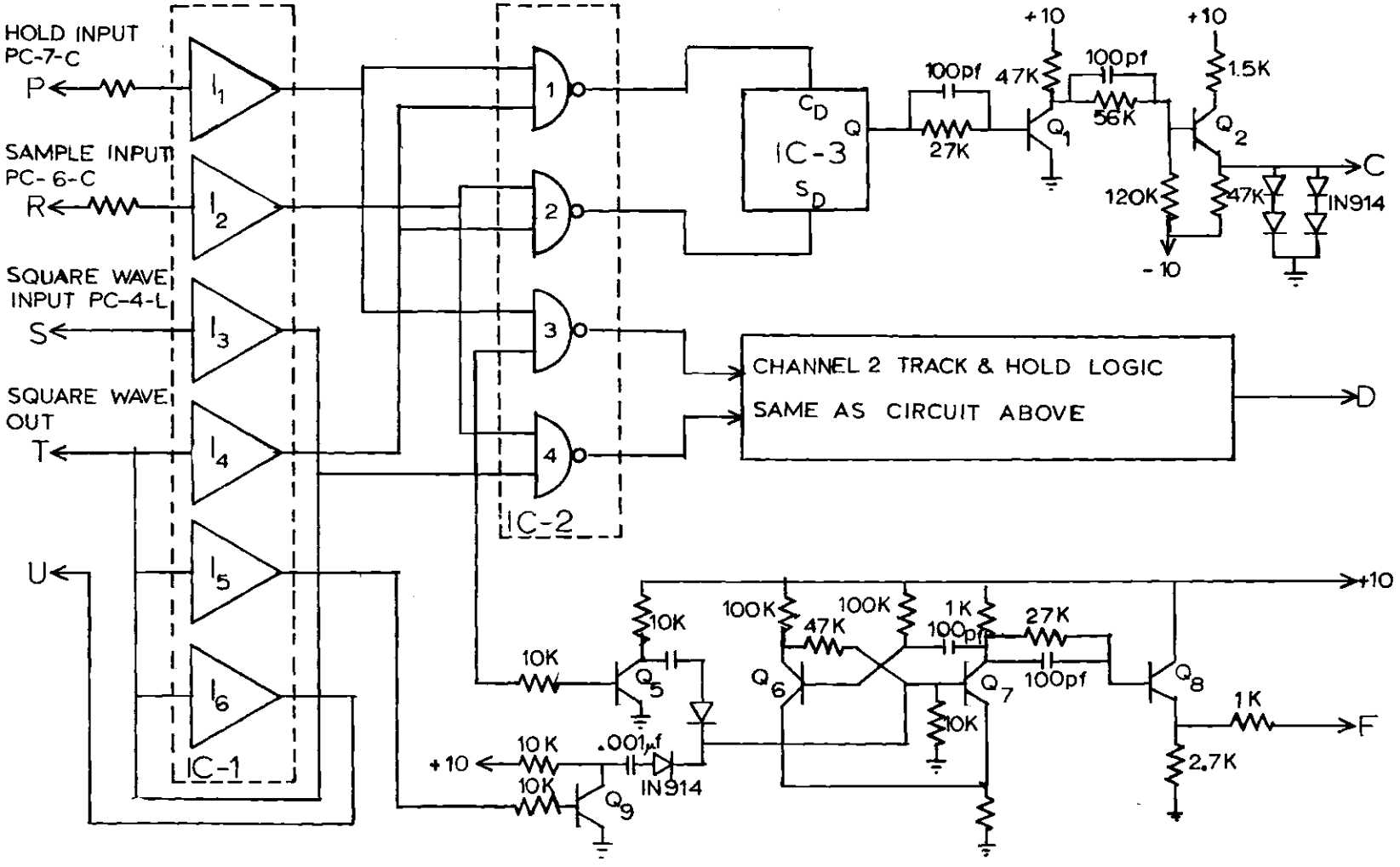

Figure 9. Detailed Schematic of the Track and Hold Logic Circuit

recalled that with the NAND gate the output is "high" (3.6 volt) if any input is "low" (0 volts) and the output is "low" only when all inputs are "high" or unused.

Also important is a knowledge of the operational characteristics of a flip-flop in the configuration shown in Figure 9. A positive pulse at the C_d input causes the Q output to be "low," and a positive pulse at S_d input causes a "high" voltage level at the Q output. Once toggled to a given state, the bistable circuit remains in that state until another command is sensed. A positive voltage applied to S_d overrides any command given to the C_d input.

The square-wave function, from PC-4 is applied to the hexa-inverter integrated circuit (IC-1). The first inverter output is applied to the inputs of three other inverters. This makes available to the logic circuitry square-wave functions which are in phase but of opposite polarity. The inputs and outputs of the three integrated circuit packages are shown chronologically in Figure 10 for one full square-wave cycle.

The rise times of the binary circuits are very short in comparison to the various time parameters, and therefore may be omitted from consideration. The parameter t_0 is the time when the initial potential step is applied to IC-1. While t_1 is the timed delay pulse from the sampling delay timer. This pulse opens the designated (either channel 1 or 2) Track and Hold gate. Time t_2 is the time delay pulse from the sampling gate width timer. This pulse closes the designated Track and Hold gate. At time t_3 the square-wave is stepped back to zero potential. Times t_4, t_5, and t_6 have the same functions as t_1, t_2, and t_0 respectively, but for the second half of the cycle.

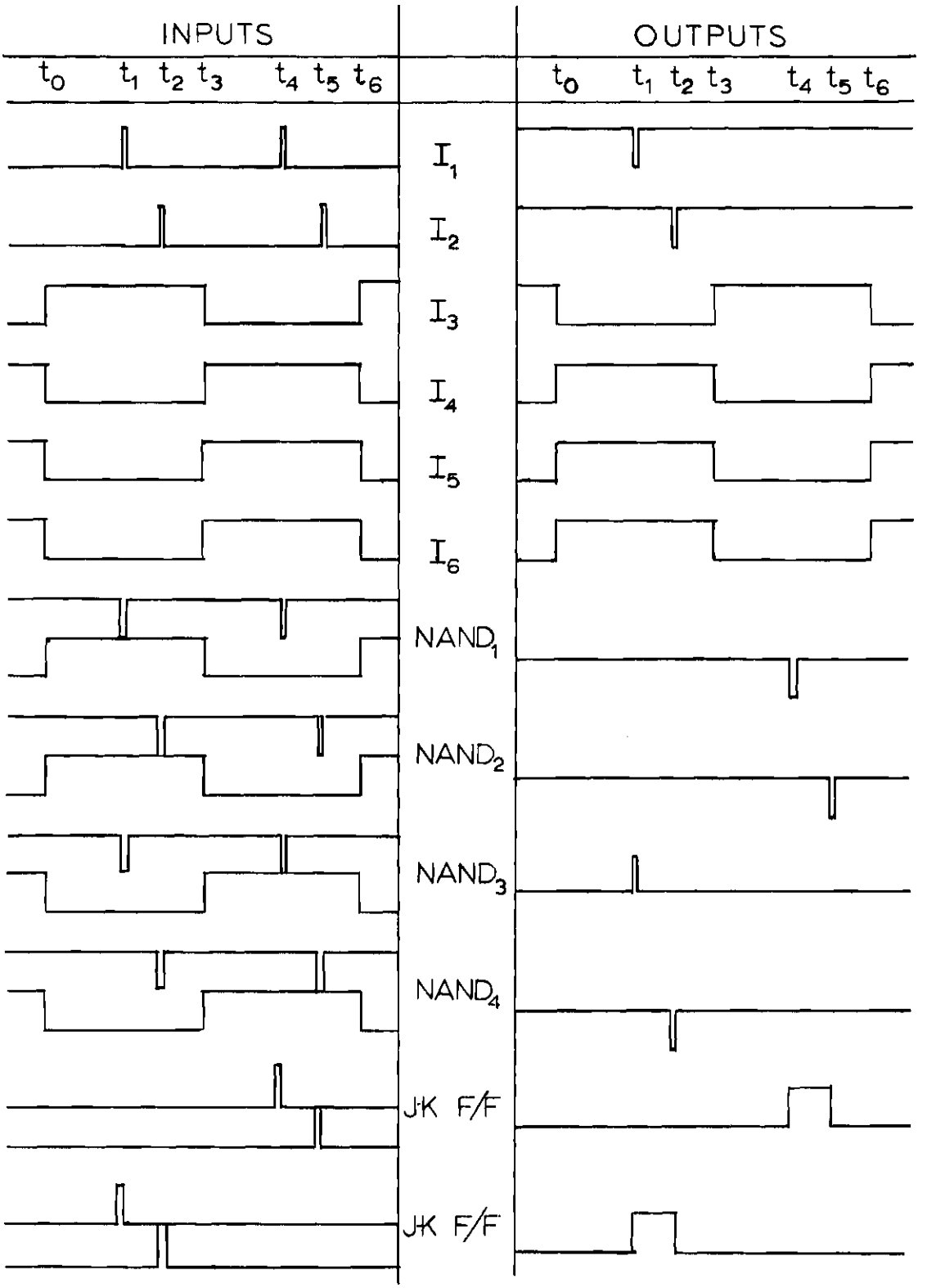

Figure 10. Chronological Sequence of Events in the Track and Hold Logic

The output of the J-K flip-flop, IC-3, is inverted by Q_1, and then amplified and centered about zero potential by Q_2. The emitter voltage of Q_2 is reduced to the desired plus or minus one volt logic signal by the "forward resistance" of the IN914 diodes.

Square-Wave Splitter-Amplifier, Cycle Counter, and Follower Amplifier (PC-3)

Figure 11 is a schematic drawing of the circuitry on PC-3. The splitter-amplifier circuit takes the square-wave signal generated on PC-4 and produces two square-wave signals, which are in phase but of opposite polarity. The final outputs voltages of the system are controlled by two carbon 2K twenty-turn Helipot potentiometers. These potentiometers are normally set for a one volt step function output at pin D (positive) and pin C (negative).

Either the positive or negative output of the splitter-amplifier is applied to the top of a voltage divider which is used to control the magnitude of the square-wave imposed on the working electrode. In the original design of the instrument a 100K ten-turn wire-wound potentiometer was used as the voltage divider. It was later discovered that when a fast potential step transit was applied to this potentiometer, inductance effects caused undesirable spikes on the square-wave signal. To obviate this problem, the ten-turn wire-wound potentiometer was replaced with a system of fixed-carbon resistors, which allows the control of the square-wave amplitude from 0 to 1000 mv in 1 mv steps.

The output of the voltage divider is applied to the follower amplifier input. The follower is a unit-gain amplifier network used to isolate the square-wave generator from the potentiostat. The follower's output

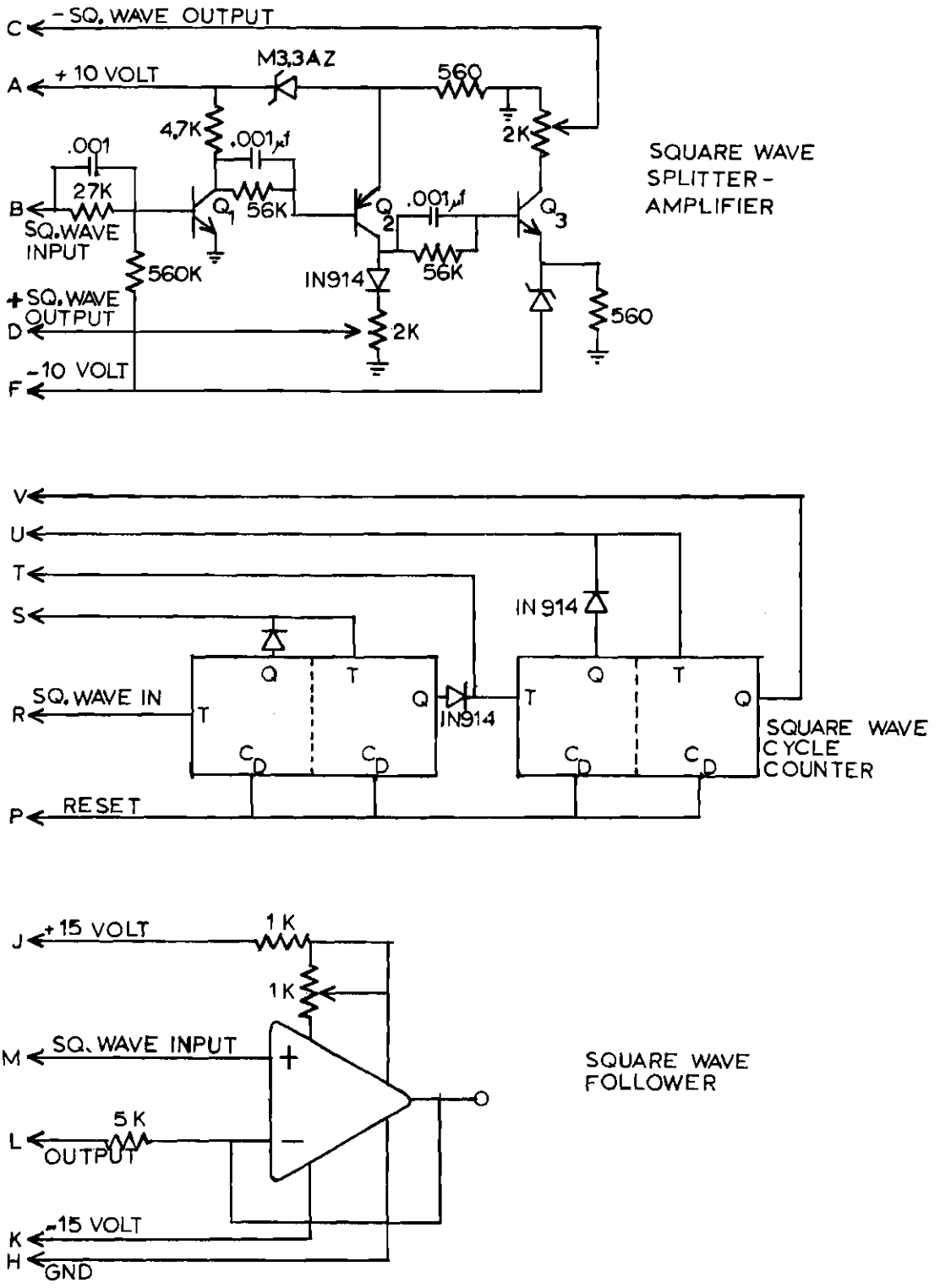

Figure 11. Detailed Schematic of the Square-Wave Splitter-Amplifier, Cycle Counter, and Follower

is applied through a 5K precision resistor to the summing point of the potentiostat.

The J-K flip-flops in the cycle counter are in the same configuration as those in the various timers. The number of square-waves used during the life of a mercury drop is determined by the point of entry into the chain of flip-flops. When the Q output of the last flip-flops goes "high," the resulting positive voltage is applied to the square-wave generator, stopping its unijunction oscillator.

Solenoid Driver and Restart Trigger (PC-8)

As discussed in Chapter II, the drop life must be carefully controlled in potential step techniques. It is a known fact that the surface tension and therefore the drop life is dependent on the potential imposed on the drop. By mechanically controlling the dislodgment, constant drop lifes can be maintained throughout the entire potential scan. If the flow of mercury is constant, the surface area of the electrode will be constant for a given point in time of the drop life, regardless of the potential imposed on the drop. Figure 12 shows the schematic of the solenoid driver and the master restart trigger generator.

The timed delay pulse from the drop time timer, PC-1, is applied to pin D of PC-8. This pulse triggers a variable width monostable oscillator. The output of this oscillator has two functions. First, it starts a 10 microsecond monostable oscillator that will generate a 9 volt positive pulse at the collector of transistor Q_8. This pulse is the restart trigger that is applied to PC-1, and PC-2 to begin a new timing cycle. Second, it activates the variable width monostable oscillator of

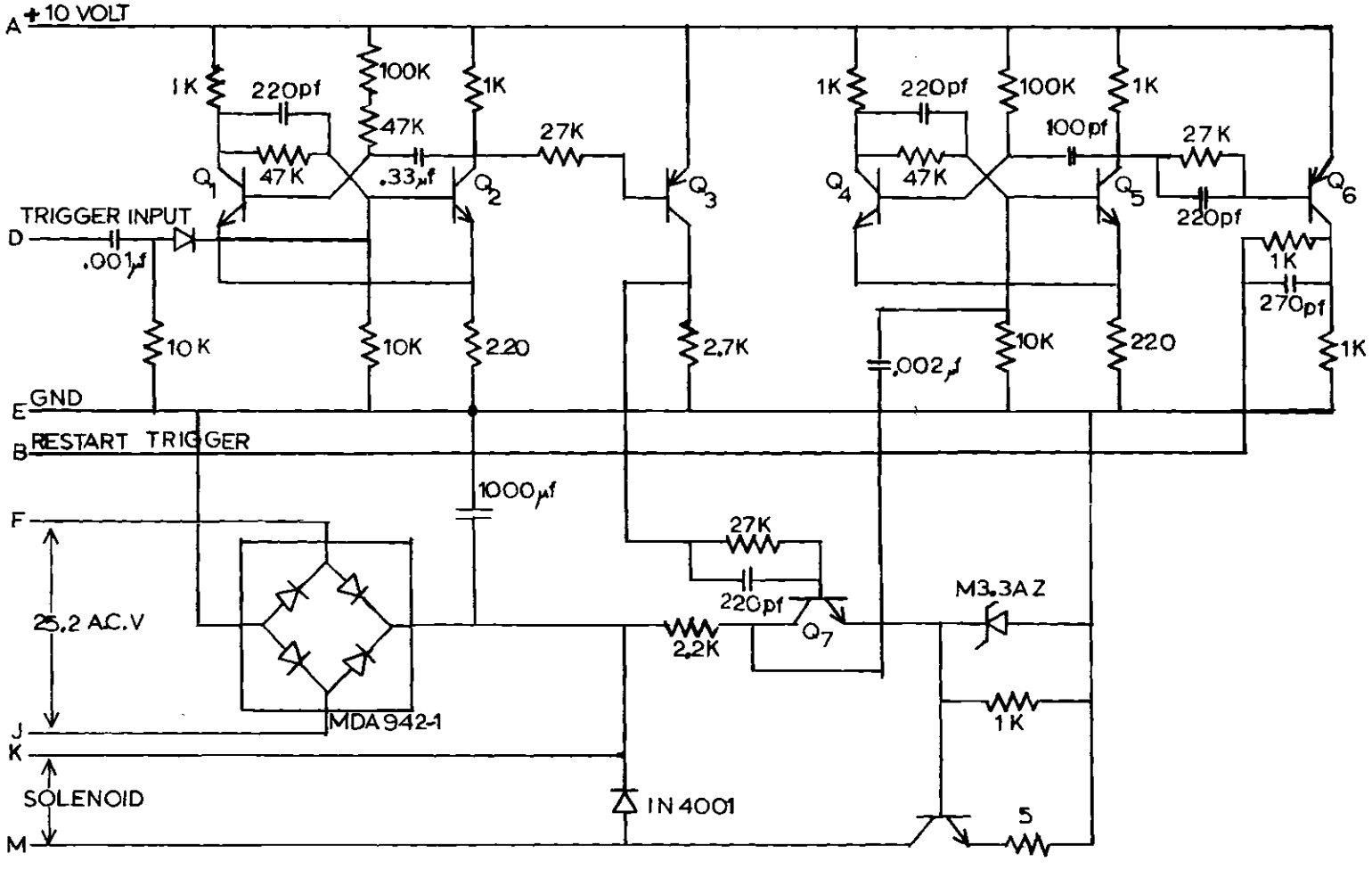

Figure 12. Detailed Schematic of the Solenoid Driver and Restart Trigger

the solenoid used to dislodge the mercury drop. The length of time for which the solenoid remains activated is controlled by the 100K ten-turn Helipot potentiometer in the variable width oscillator circuit. The solenoid dislodges the drop by slightly tapping the glass capillary electrode.

The circuitry for the timing chassis + 3.6 volts, PC-10, and ± 10 volts, PC-9, power supplies are not novel in concept and are given in Appendix II. It should be noted that the 8.4 vdc required to operate relays used in zeroing the instrument's operational amplifiers is obtained from PC-10.

Potential and Current Monitoring Chassis

Figure 13 shows a block diagram of the potentiostat and current monitoring circuits, which consist of five major functional sections. On the following pages detailed descriptions of the circuit and performance characteristics of the individual sections are given.

Power for all operational amplifiers is supplied by a Philbrick Model PR-300 regulated dual power supply which is mounted on the timing chassis. Model PR-300 is a compound unit made of two tracking regulated power supplies which provide 300 milliamperes at ± 15 vdc with respect to common. It also provides 115 vac for photochoppers and 6.3 vac for demodulators. The two ac voltage signals are in phase as required by chopper stabilized operational amplifiers.

All operational amplifiers power leads (ac, dc, and grounds) are wired parallel to one another. All ac power leads are carefully shielded to reduce 60 cycle noise. To reduce spikes and noise on the dc power, each amplifier has a 40 microfarad capacitor connected from its plus and

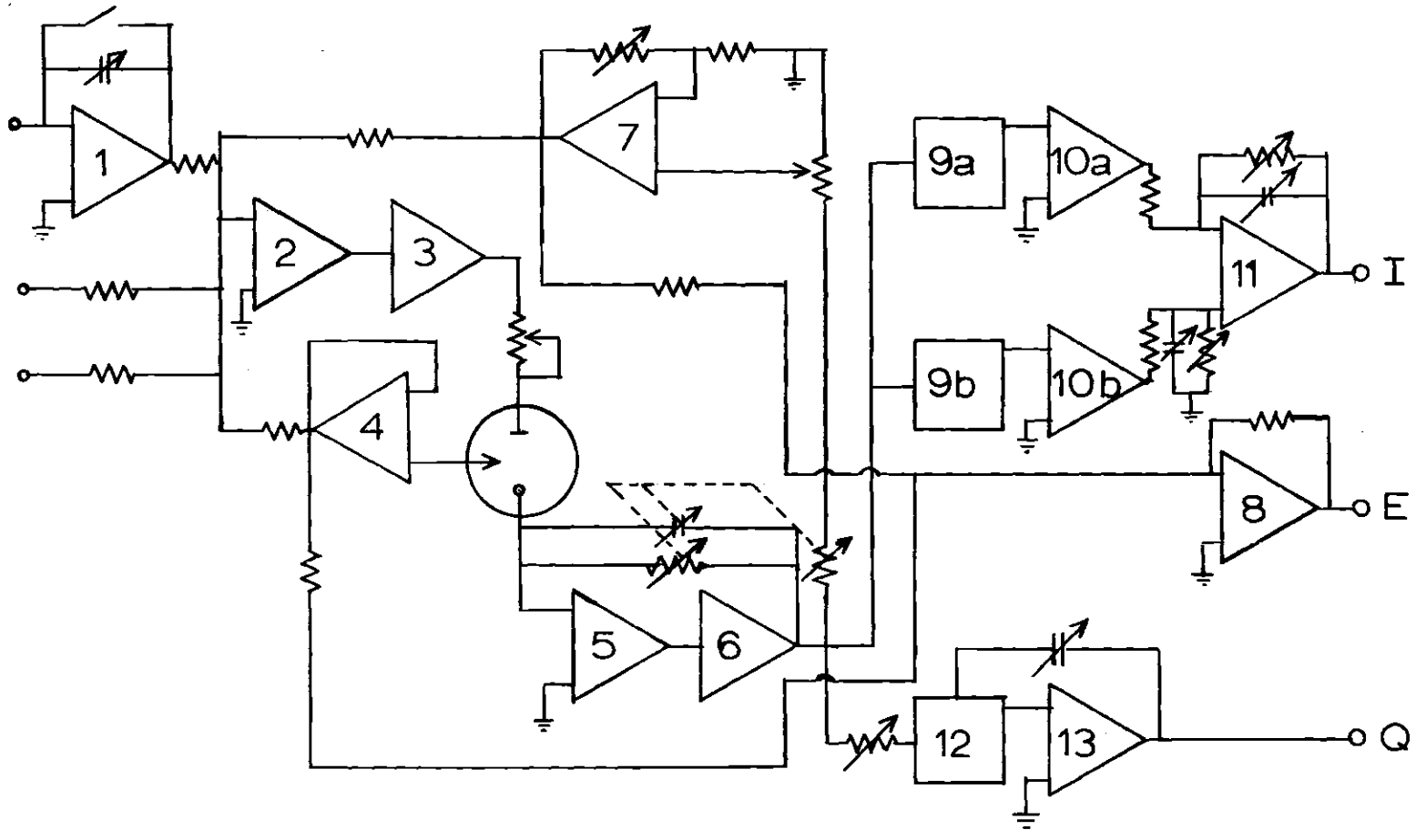

Figure 13. Block Diagram of the Potentiostat and Current Monitoring Chassis

minus 15 dc terminals to the power common terminal.

Potential Functions

This section of the instrument contains the various function inputs that may be imposed on the summing point of the potentiostat. There are three internally generated potential inputs: (1) initial potential; (2) dc ramp; and, (3) square-wave.

The initial potential and dc ramp generator are shown in Figures 14 and 15, respectively. Potentiometer P_1, is used to set the range of the initial potential to $\pm$ 1.0 volts. P_2, is a 500 ohm 10-turn Helipot potentiometer that allows a continuously variable initial potential to be imposed on the summing point.

The heart of the dc ramp generator is the Philbrick Model SP65AHP operational amplifier, A_1. The SP65AHP is a high-gain photoelectric chopper stabilized amplifier, which has a unity gain bandwidth response (open loop) of 20 MHz and a 2.2 mA output current capability at $\pm$ 10 volt (33). The scan rate of the ramp generator is controlled by switch S_2, and potentiometer P_3. Using P_3 the fastest scan rate is normally set at 50 mv/sec, then by S_1 the scan rate can be reduced in a 1-2-5 stepping sequence to 1mv/sec as the lowest rate.

Potentiostat

Figure 16 shows the potentiostat used in the instrument. The potentiostat is a conventional three-electrode design (34-37). The control amplifier, A_2, and the follower amplifier, A_4, are Philbrick Model SP65AHP and P25AH operational amplifier, respectively. A_3, is a Burr-Brown Model 1634A power booster amplifier which operates in cascade with the Philbrick

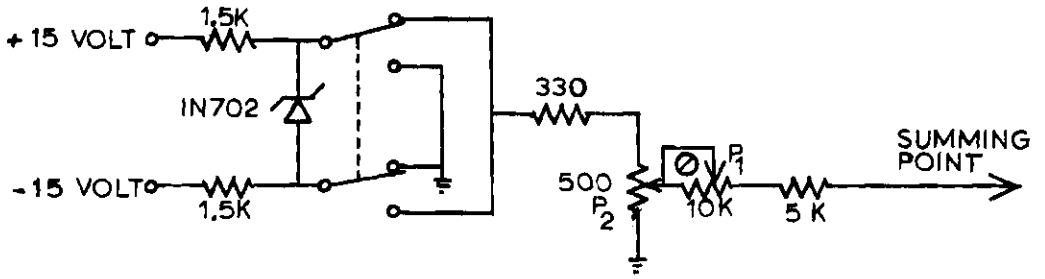

Figure 14. Schematic of the Initial Potential Circuit

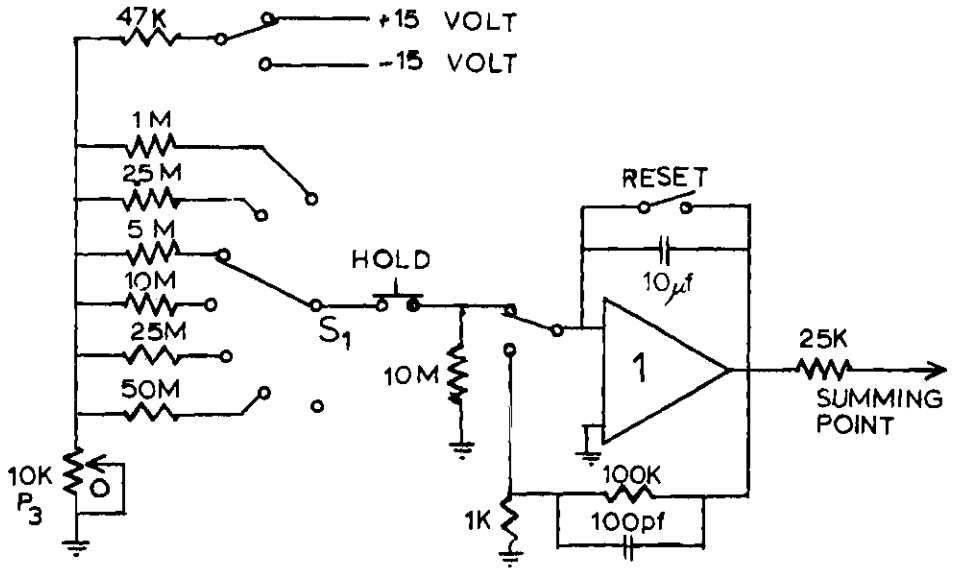

Figure 15. Schematic of the Linear Ramp Generator

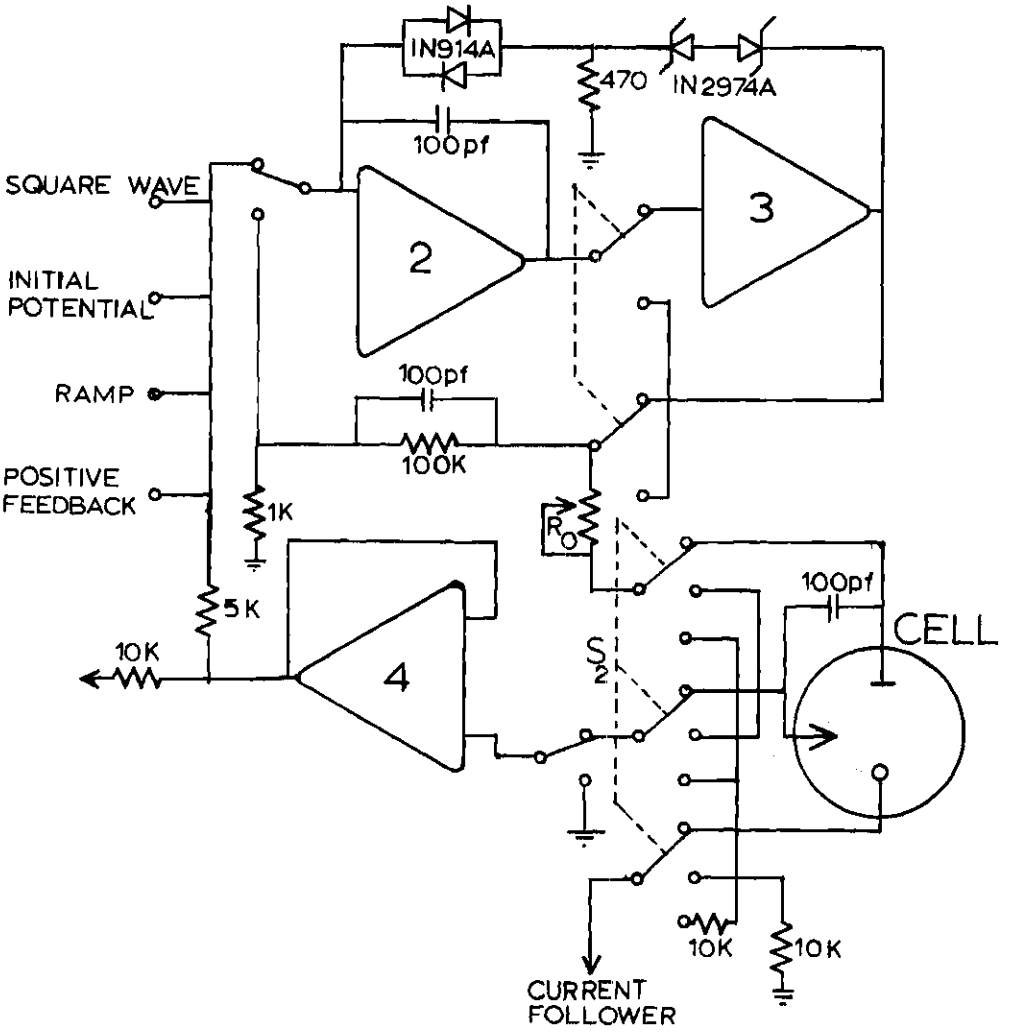

Figure 16. Potentiostat Circuit

SP65AHP to increase its output capability to 500 mA at ± 10 volts. The 1634A is designed to provide high power efficiency with low quiescent current drain, and full output power can be obtained without appreciable distortion at frequencies up to 50 KHz/sec.

The three-pole, three-position switch, S_2, allows the switching of the potentiostat from the chemical cell to a dummy cell (10K, 1 percent resistor) for calibration. Position two of S_2 is "stand-by," and is used to maintain continuity of the negative feedback loop when the chemical cell is removed from the circuit.

A_8 is a Philbrick Model SP65AHP amplifier and controls the potential readout of the instrument. This summing amplifier corrects the potential readout for the positive feedback component. Its output indicates the true effective (IR drop component removed) potential imposed on the working electrode.

Current Follower

A detailed schematic of the current follower is shown in Figure 17. Amplifiers A_5 and A_8 are Philbrick Model SP65AHP and Burr-Brown Model 1634A, respectively.

The Burr-Brown 1634A power booster amplifier is again used to increase the current capability of the instrument. The booster amplifiers in both the potentiostat and current follower circuits may be electrically removed from the systems by two toggle switches located on the back panel of the instrument. The capability of using an internal or an external power supply for the two booster amplifiers is also designed into the instrument. A Burr-Brown Model 506/26 dual regulated ± 15 volt power supply

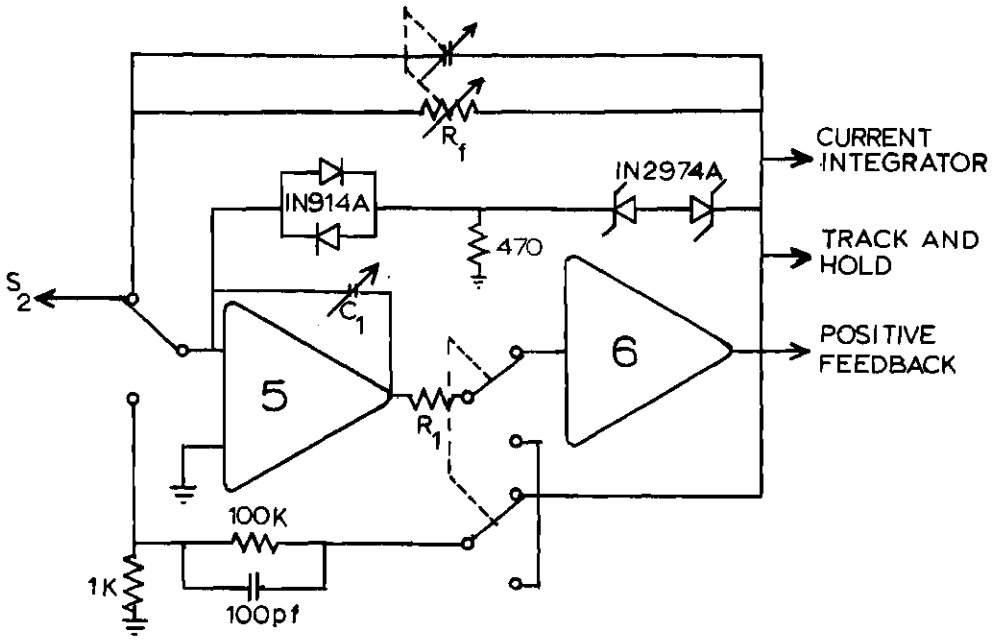

Figure 17. Schematic of the Current Follower Circuit

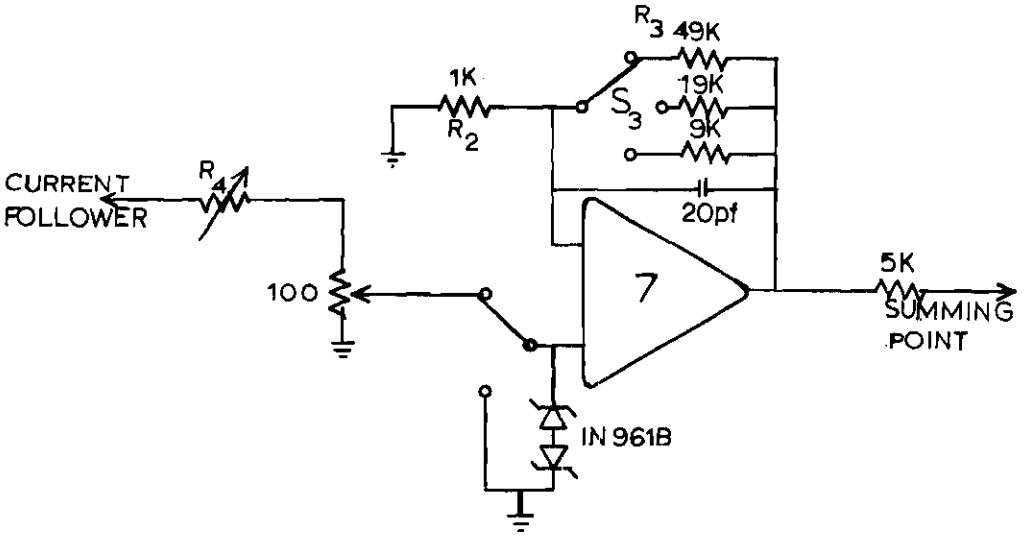

Figure 18. Positive Feedback System

is used as the external power source.

Two current measuring modes were considered for use in the instrument, current follower and voltage follower configurations. Initially it was thought the voltage follower mode would be the more stable one, but a study by Brown (35) showed this not to be true. In fact, the added impedance of the resistor to ground in the voltage follower configuration actually decreased the stability slightly. Another point of consideration is the fact that in the voltage follower mode the working electrode is not held at ground potential.

The output of the current follower is a precise function of its input current, i.e.

$$e_o = - i_{in} R_f \qquad (3\text{-}1)$$

where e_o is the output voltage, i_{in} is the input current, and R_f is the resistance of the negative feedback loop. R_f in the instrument may be varied from one hundred ohm to one megohm in decade steps.

Capacitor, C_1, and resistor, R_1, were found to be necessary to improve the stability of the system with boosters in the circuit. C_1 is a variable capacitor (90-200 picofarad) and is used to fine tailor the negative feedback capacitance of the current follower amplifier. R_1 is an one hundred ohm resistor used to prevent capacitance coupling between the two amplifiers.

Compensation of IR Drop (Positive Feedback Loop)

The decomposition voltage, E_d, is in essence the applied voltage required to initiate electrolysis. In order to advance electrolysis at

a reasonable rate, an additional voltage is required to overcome the electrical resistance within the cell system. With a total current flow, I, the voltage required in excess over the decomposition voltage is given E = IR. This voltage is called the "IR drop" of the system. The applied voltage, E_{app}, required to perform an electrolysis with a current flow of I, is given by $E_{app} = E_d + IR$.

In Chapter II it was shown that in potential step techniques it is very important to have the cell resistance, R, as low as possible. The rate of decay of the capacitance current is highly dependent on R. The cell resistance can be divided into two components: (1) internal resistance, R_i; (2) external resistance, R_e. R_i results from the load resistor, the capillary resistance of the DME and the solution resistance between the reference electrode and the DME (38). R_e is the resistance of the bulk of the solution between the auxilliary electrode and the working electrode.

The external and internal resistance of the IR drop are compensated for separately. R_e is virtually eliminated by the use of the three electrode system, and R_i is compensated for by a positive feedback loop in the potentiostat. A discussion of the R_i compensation is given below.

The load resistor and capillary resistance are constant, but the solution resistance changes as the surface area of the mercury drop increases. Nemec (39) has shown that the potential loss between a reference electrode and a spherical microelectrode is

$$E_u = \frac{1}{4\pi rk} \frac{x}{x - r} = IR_u \qquad (3\text{-}2)$$

where I is the cell current, r the drop radius, x the distance between the electrodes, and k the specific conductance of the solution. Placing the two electrodes very close together (making x small) will reduce R_u, but to effect a 50 percent reduction in R_u, x must equal r. A normal value for r is of the order of 0.5 mm and to reproducibly place the electrodes this close is very difficult (38,40).

The internal resistance may be electrically compensated for by the use of a positive feedback system. Such a system feeds back a portion of the current signal to the control amplifier through the summing resistor network. A potential, which is proportional to the cell current, is additionally applied to the control amplifier to effectively compensate for the ohmic potential losses of the system.

A detailed schematic of the positive feedback system used in the instrument is shown in Figure 18. In order to maintain the correct proportionality between the cell current and the positive feedback voltage, the controls for the current follower gain and the positive feedback are ganged together. The voltage divider, R_1, allows the division of the feedback voltage into one hundred equal parts. The divider is constructed from two rotary switches and fixed one percent carbon resistors. The total effective resistance of the voltage divider is one hundred ohms.

A_7 is a Philbrick Model P85AH operational amplifier in a follower-with-gain configuration. The response of this amplifier circuit is

$$e_o = \left(1 + \frac{R_3}{R_2}\right) e_{in} \qquad (3\text{-}3)$$

where e_o and e_{in} are the voltage output and input, respectively. Positions a, b, and c of switch, S_3, will give rise to gains of ten, twenty, and fifty, respectively. The values of the resistors R_4 were chosen so that each step of the voltage divider equals to one, two, or five ohms of compensation, depending on the gain setting of the follower. The follower-with-gain amplifier is "broadbanded" by omitting the tailoring capacitors and using a small 20 picofarad capacitor in the feedback loop.

Track and Hold Modules and Current Readout

Figure 19 shows a detailed schematic of the track and hold and current readout amplifier circuits. T/H_{9a} and T/H_{9b} are Philbrick Model SPT+H Track and Hold Modulators. Amplifiers A_{10a} and A_{10b} are Philbrick Model SP65AHP, and amplifier A_{11} is a Philbrick Model P85AU.

The track and hold modules are non-inverting, unit gain, gated amplifiers used to shift the circuit from the track mode to the hold mode or vice versa. An internal gated amplifier is used as a current amplifier, increasing the speed of tracking by providing more current to charge the memory capacitor. The external amplifiers, A_{10a} and A_{10b}, are coupled to the SPT+H units in such a way that they act as inverting, unit gain, integrator amplifiers. The SPT+H - SP65AHP combination will, upon a first command, track and assume the value of the current follower output, and will, on a second command, remember the value of the current follower output at the time of the latter command and hold this value for an extended period of time. The required command signals for the two track and hold modules are developed by the circuits on PC-5 on the timing chassis. Each track and hold unit, along with its coupled amplifier, is used to monitor the current during one half of the square-wave cycle.

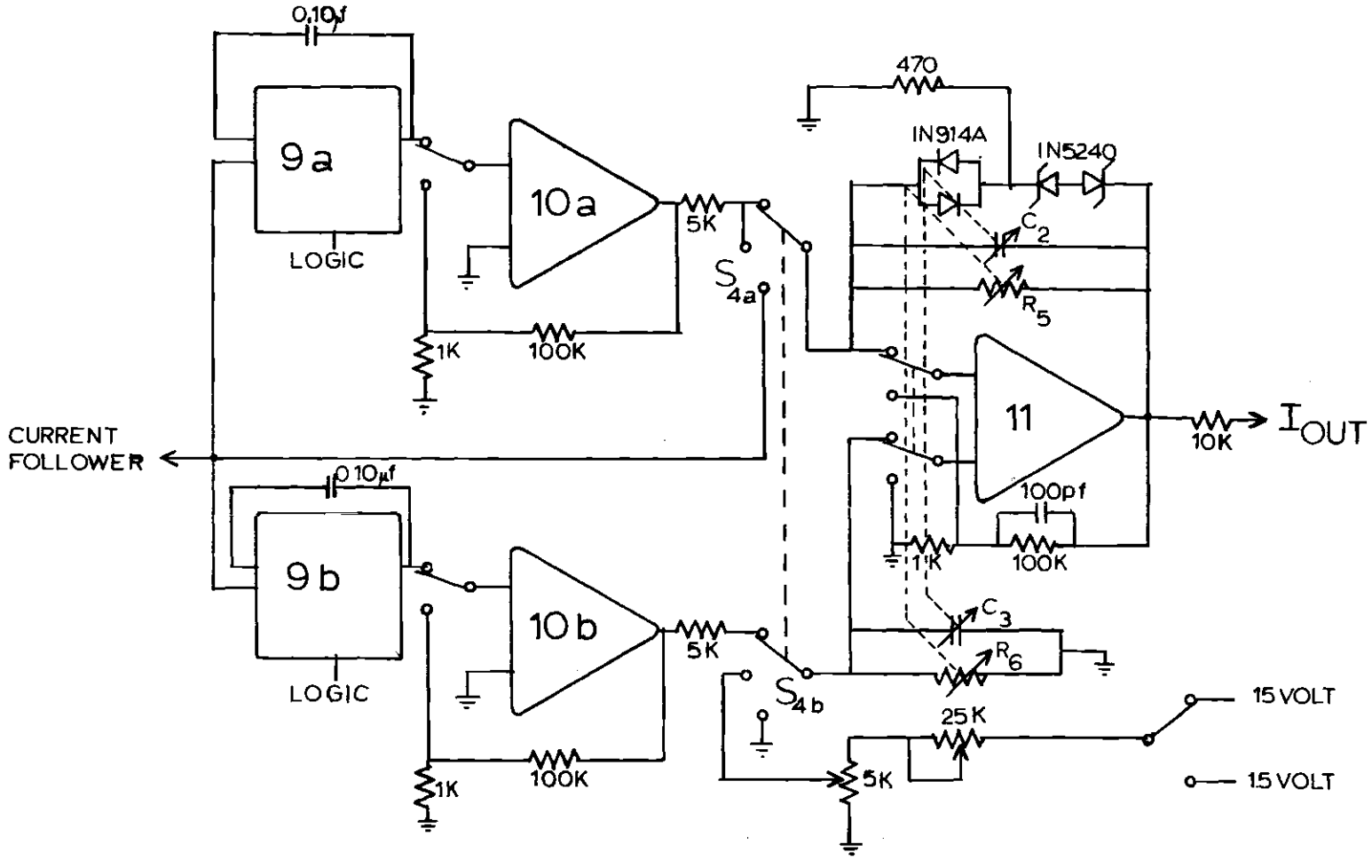

Figure 19. Schematic of the Track and Hold Modules and the Current Output Amplifier

The slew rate of the SPT-H as received from Philbrick was too great (0.5 volts per microsecond). The units were tracking the high frequency noise and their outputs were instantaneous current values instead of the desired average current for the time the sample gates were open. To minimize this effect, the units were slightly modified internally to allow the addition of an external capacitor, which increased the integrator's RC constant without changing the unit gain characteristic, and had the effect of averaging out the noise component of the signal. The best value for the external capacitor, C_1, was found to be 0.01 microfarad, which gives the track and hold modules a RC constant of 1.0×10^{-4} seconds.

The current readout amplifier, A_{11}, may function either as a difference amplifier or as an inverting voltage amplifier. The type of configuration used depends on the electrochemical technique that is employed. With S_4 in position a, the amplifier response will be proportional to the algebraic difference of the two track and hold modules' outputs. If S_4 is in position b, A_{11} will compare the output of one track and hold unit to a constant voltage source (current off-set mode). In position c, both track and hold modules are removed from the circuit and the current readout amplifier monitors the output of the current follower amplifier.

The gain of the current readout amplifier is determined by the variable resistors, R_5 and R_6. The gain may be varied from one to twenty thousand in a 1-2-4 sequence. The filter capacitors, C_2 and C_3, may be varied from zero to ten microfarads in a 1-2-5 sequence.

Current Integrator

A detailed schematic of the current integrator system is shown in

Figure 20. A_{13} is a Philbrick Model SP656P amplifier in a basic integrator configuration. G_1 is a Philbrick Model SPG-1 current gates module.

The Philbrick SP656P amplifier is a high gain, chopper-stabilized operational amplifier, with a current output capability of 20 mA. This is almost a tenfold increase over the rated current capability of the SP65AHP. This large output current capability makes the SP656P ideal for use in an integrator circuit.

The operation of the integrator is controlled by the SPG-1. The SPG-1 consists of two diode-bridges and a complementary pushpull driver, designed to be used with operational amplifiers. In response to a logic signal, the driver "enables" one diode-bridge and simultaneously "inhibits" the other. Reversing the polarity of the logic reverses the states of the two bridges. By connecting the SPG-1 so that one diode-bridge is parallel to the feedback capacitor, C_4, and the other is in the input of the amplifier, the operational functions of the integrator circuit can be controlled.

The output voltage of the integrator will be

$$e_o = - 1/RC \int_o^t e_{in} dt \qquad (3\text{-}4)$$

where e_{in} is the output voltage of the current follower. R_7 can be either 1K or 10K ohm, and C_4 can be 0.2, 0.5, or 1.0 microfarads. Taking into consideration Ohm's law and that one amp of current will charge a one farad capacitor to one volt in one second, the total charge (in coulombs) can be calculated for any time (t) from the output voltage (e_o).

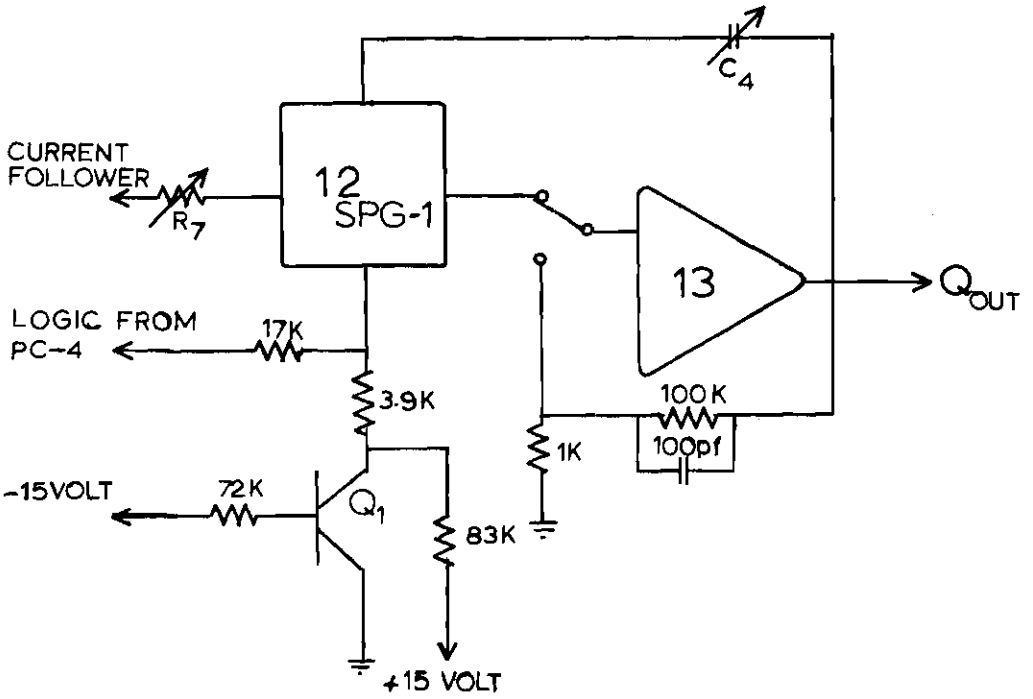

Figure 20. Current Integrator Circuit

The logic signal that controls the SPG-1 gating system is obtained from PC-4 on the timing chassis. Q_1 and the related resistors are used to obtain the correct polarity and voltage level of the signal.

The overall configuration of the current monitoring circuits depends on the electrochemical technique being performed. For example, in techniques such as square-wave or pulse polarography, the current follower, both track and hold systems, and the current readout amplifiers, must be used. But in electrode kinetic studies, such as potential step technique, only the current follower is needed. The change from one configuration to another can be made with controls mounted on the front panel of the instrument. Changing two or three switch positions allows any function of the instrument to be selected.

CHAPTER IV

EQUIPMENT, INSTRUMENTATION, AND CHEMICALS

Electrodes and Cell

Mercury working electrodes were used in all polarographic and kinetics work. A dropping mercury, a hanging mercury drop, and a dropping zinc amalgam electrode were used.

The dropping mercury electrode (DME) was constructed of 6 mm Pyrex glass tubing, a Pyrex reservoir, and Tygon tubing. The glass tubing was affixed to a meter stick so that the mercury head could be measured. Approximately two cm from the bottom of the glass a platinum wire was introduced through the wall of the tubing for electrical connection. One half of a Sargent 2-4 second polarographic capillary was used. The capillary was rinsed with distilled water prior to interruption of mercury flow and was stored in air between experiments.

The hanging drop mercury electrode (HDME) was a Beckman Model 39016 electrode. Area calibrations showed the micrometer dial values to be within 0.05 mm^2 of the measured values.

A dropping zinc amalgam electrode was constructed of Pyrex glass. The all-glass construction was used to reduce air oxidation of the zinc amalgam. The electrode consisted of a 150 ml reservoir atop a jacketed glass column approximately 20 cm in length. Below the column was a 2 mm stopcock, a through-glass platinum electrical connection, and a standard external 10/30 glass joint. A 2 cm glass tubing, which had a diameter

slightly larger than a polarographic capillary, was fused to an internal 10/30 glass joint. One half of a Sargent 2-4 second capillary was then sealed into the 2 cm glass tubing with Varno cement. The arrangement allowed replacement of the capillary without exposing all of the amalgam to the atmosphere.

The amalgam electrode was readied for use by adding amalgam to the upper portion and attaching the capillary assembly filled with pure mercury. A vacuum pump was then used to remove most of the air from the amalgam. The contents of the reservoir were protected by a covering of Nujol and a blanket of purified nitrogen. The tip of the capillary was maintained below the surface of a zinc amalgam pool in a 100 ml beaker. Above the amalgam pool in the beaker was distilled water that was constantly purged with purified nitrogen. In this way air oxidation of the amalgam in the capillary was avoided and the electrode was stable and flowed freely for an extended period of time.

To determine the flow rate of the dropping mercury and dropping amalgam electrodes, the following technique was used. Three hundred drops of mercury (amalgam) were collected at a potential close to the PZC in a solution representative of those used in the polarographic studies and the elapsed time was measured. The collected mercury was washed with distilled water, then dried with reagent grade acetone and weighed. The flow rate, M, in grams per second, was obtained from the equation

$$M = \frac{w}{t} \qquad (4\text{-}1)$$

where w is the weight of mercury collected in grams and t is the time.

Assuming sphericity and negligible contact area, the surface area at any time, t, in the drop life was then calculated from

$$A = (3V)^{\frac{2}{3}} (4\pi)^{\frac{1}{4}} \qquad (4\text{-}2)$$

where V is the volume in cubic centimeters, given by

$$V = \frac{mt}{d_{Hg}} \qquad (4\text{-}3)$$

and d_{Hg} is the density of mercury in gm/ml. The Beckman hanging mercury drop electrode was calibrated by collecting twenty drops, that according to the micrometer dial contained 1 μl each. The mercury collected was washed, dried, and weighed. The volume per drop was then calculated using this weight and the density of mercury.

The counter electrode consisted of a platinum wire, approximately 1.5 cm long, sealed in a glass tube inside of which electrical connection was made with the lead from the polarograph.

The reference electrode employed for most of the work was made according to Figure 21. The saturated calomel electrode was employed together with a saturated potassium chloride agar salt bridge junction. These electrodes were trouble-free and reproducible throughout the investigation. The small electrode solution interface area facilitated placement of the electrode close to the working electrode.

The cell consisted of a 100 ml spoutless Berzelius beaker, capped with a Beckman 101253 beaker cap. A medium porosity gas dispersion tube was used to disperse the nitrogen during deaeration.

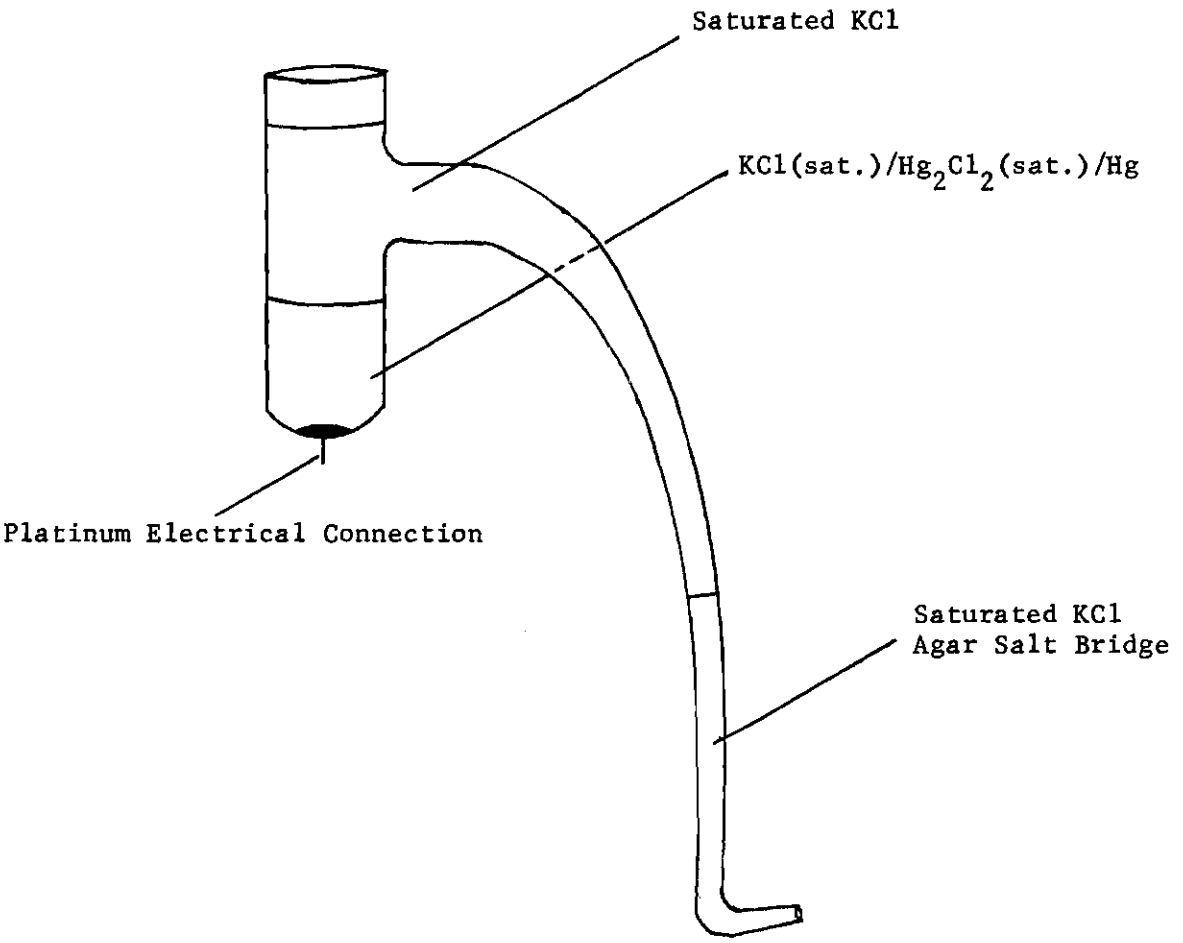

Figure 21. Diagram of the Saturated Calomel Reference Electrode Used

Faradaic Cage

To shield the electrolytic cell system from picking up electromagnetic radiation noise, a faradaic cage was locally fabricated. The cage was made from a large medicine cabinet. All glass panels were replaced with aluminum panels, and the shelves were cut out to allow room for the mercury columns. The cage was grounded to the laboratory instrument system by a one quarter inch copper mesh grounding lead. Leads connecting the electrolyte cell electrodes to the polarograph were isolated from the cage and were made with shielded conductor. These shields were grounded only on the instrument end to remove possible ground loops.

Square Root of Time Generator

In potential step techniques the kinetically controlled faradaic current is a function of the square root of time (cf. Eq. 2-14). Normally, current versus time data is experimentally obtained and the data is then replotted as current versus square root of time. This is very time consuming and reduces accuracy and precision of the final results. To obviate the problem a square root of time generator was designed and built in the electronics shop of the School of Chemistry.

The $t^{\frac{1}{2}}$ generator is used to drive the horizontal axis of the oscilloscope. Current versus square root of time data is displayed and stored by the oscilloscope. The data may then be photographed and the i/i_x ratio determined directly from the photograph (cf. Eq. 2-17).

The block diagram in Figure 22 illustrates the basic design of the $t^{\frac{1}{2}}$ generator. In normal operation a trigger from the polarograph

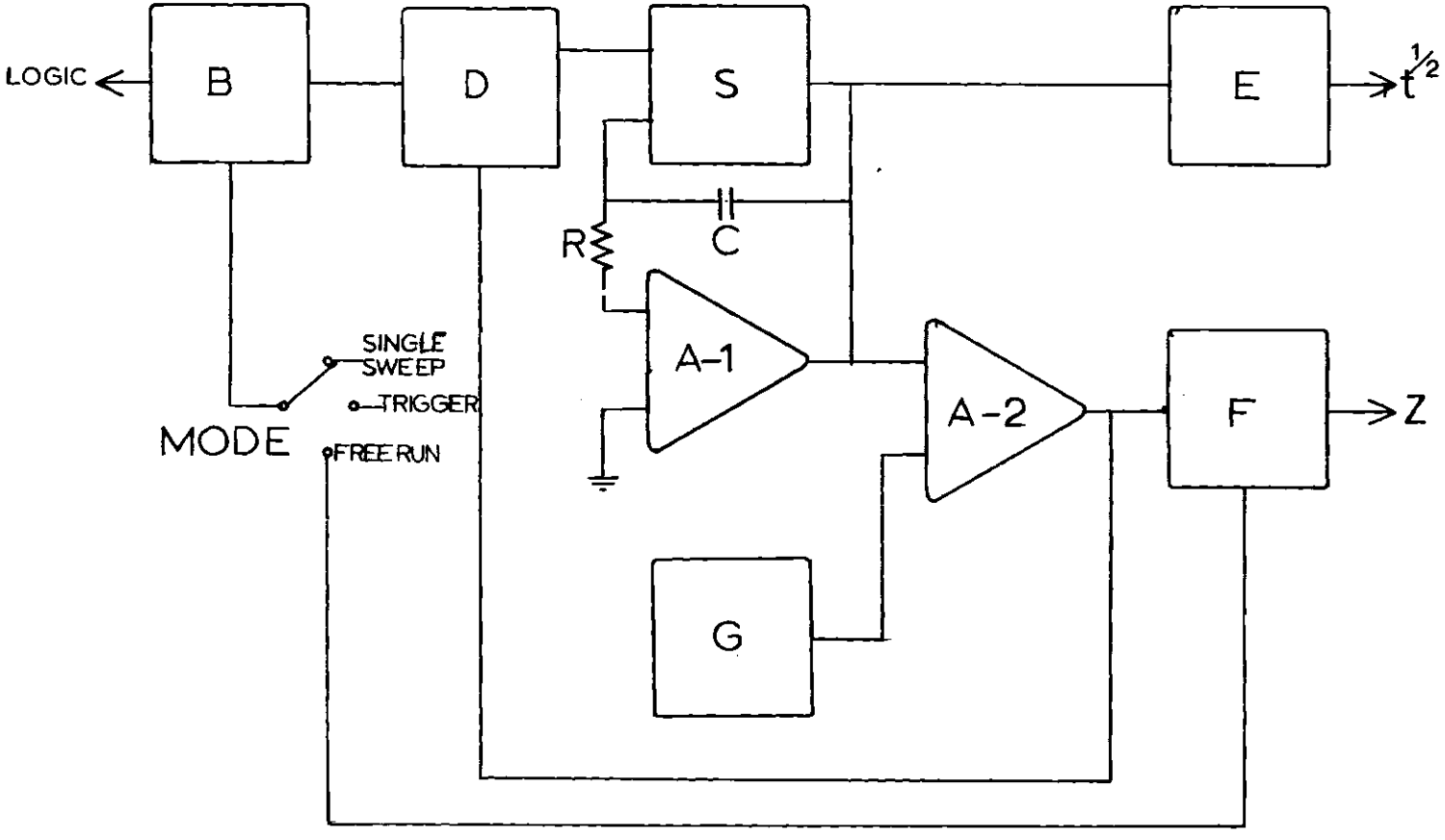

Figure 22. Block Diagram of Square Root of Time Generator

timing system initiates a pulse from the Schmidtt trigger amplifier, B, which is applied to the sweep control flip-flop, D. D is a current mode (non-saturating) flip-flop with buffered outputs. The outputs of D control the FET reset switch, S, and are also a gated current source for the sweep generator, A-1. When the FET switch is off and a constant current from D is applied to the integrator, the output of A-1 increases at a linear rate. The sweep rate is determined by the value of R and C. The output of A-1 is applied to the comparator, A-2, and the Square Rooter, E. A-1 and A-2 are Fairchild Model A715C operational amplifiers.

The comparator, A-2 controls the upper limit of the sweep generator. When the output of A-1 reaches the absolute value of the constant voltage source, G, A-2 generates a pulse that is applied to D and a delay monostable, F. D then turns off the charging current and closes the FET switch, discharging the integrator capacitor.

F has two functions: it develops and controls the "Z" axis output and also generates the recycle trigger which is applied to B when the instrument is in the free run mode.

The linear ramp output of A-1 is also applied to the Square Rooter, E, this is a Burr-Brown Model 4126/15C square root generator. This module takes the square root of the input voltage. Its output is given by

$$E_o = [10E_{in}]^{\frac{1}{2}} \qquad (4\text{-}4)$$

where $+ 3mv < E_{in} < + 10mv$. The $f(t^{\frac{1}{2}})$ output of E is used to drive the horizontal axis of the oscilloscope.

The intensity of the trace on the oscilloscope is controlled by the "Z" axis output of F. The Type 3B4 Time-Base used for the horizontal axis amplifier was modified to allow external control of the trace intensity. The "Z" axis signal greatly reduces the trace intensity during the time period between experiments and prevents the burning of spots in the fluorescent screen of the cathode ray tube while the sweep is static.

Commercial Equipment

A Hewlett-Packard 7005B X-Y recorder was used for the recording of all polarograms.

A Tektronix 564 Storage Oscilloscope was employed for the recording of current-time curves, current-square-root of time curves, and chronocoulometry. A 3A6 Dual-Trace plug-in amplifier was used in the vertical axis and 3B4 plug-in Time Base was used for the horizontal axis. The 3B4 has calibrated sweep rates from 5 seconds to 200 nanoseconds per division. Periodic recalibration of the Time Base amplifier was performed. A Tektronix Type 184 Time-Mark Generator served as a time standard. A Tektronix C-12A oscilloscope camera with a Polaroid back was employed to photograph traces.

A Keithley Instrument Model 160 Digital Multimeter was used to monitor potential outputs, to measure equilibrium potential and to calibrate initial potential, and square-wave amplitude controls.

Chemicals

Potassium Nitrate

A 2.0 F stock solution was prepared from Fisher Chemical Company

reagent grade potassium nitrate and diluted as needed.

Potassium Chloride

J. T. Baker Analyzed reagent grade potassium chloride was used.

Zinc Nitrate

J. T. Baker Analyzed reagent grade zinc nitrate was used. Zinc amalgam for the amalgam electrodes was prepared by electrolytically reducing a quantity of Zn ions into a known volume of mercury. Trace impurities in the Zn nitrate solution were removed before making the amalgam by electrolyzing the solution at 0.8 volt versus SCE for 24 hours on a stirred mercury pool. The zinc concentration in the amalgam was determined from the polarographic anodic diffusion current found with the dropping amalgam electrode. The diffusion coefficient of Zn (0) in the amalgam was assumed to be equal to that of the aquo zinc ion.

Water

Doubly-deionized water was used for polarography work; distilled water for all kinetic or adsorption work.

Nitrogen

American Cryogenics Company purified dry nitrogen was utilized for purifying all systems. The nitrogen was passed over hot copper turnings to remove traces of oxygen.

Mercury

Bethlehem Instruments triple-distilled pure mercury was used.

Agar

Agar salt bridges were prepared from Difco Laboratories agar according to Meites (ref. 10, Chapter I) by dissolving 4 grams in 90 grams

of water, heating gently until solution was affected, and adding 30 grams of potassium chloride. The reference electrode side arms were filled with an agar plug by placing them in the solution and allowing it to cool.

CHAPTER V

VOLTAMMETRY EXPERIMENTAL RESULTS

The primary objective of the work presented in this chapter was the evaluation of the various modes of operation of the instrument described in Chapter III. The applicability of Tast, differential pulse, and square-wave polarography to the analysis of metal ions in aqueous media was investigated. This study was not designed to be an exhaustive investigation; therefore, the work was limited only to the more commonly occurring cations. Results from single and multicomponent samples will be given.

To evaluate the coulometry mode of operation, experiments using double-step chronocoulometry for the study of specific adsorption were performed. The system of known, as well as unknown, adsorption characteristics was investigated.

Tast or Current-Sampled DC Polarography

Classical (direct current) polarography is usually limited in the analysis of single component systems to solutions having concentrations of the reducible species of 1×10^{-5} F or greater. In multicomponent systems the limitation is even more severe due to the additive characteristic of diffusion currents. The ratios of concentrations and the order of the reduction potential of the reactants are both very important. For example, the current from the reduction of cadmium in small concentrations is almost impossible to measure in the presence of the current

from the reduction of lead at high concentration.

Mark and Reilley (41) reported that, by using Tast polarography, the lower quantitative limit could be reduced to 10^{-6} F, which is a tenfold improvement over dc polarography, for both single and multicomponent systems. In Chapter II, however, it was shown that theoretically only a twofold improvement should be expected. In a study to compare the two techniques, lead and cadmium cations were used as the reducible species. The electrolytic reaction of the two ions is reversible and their $E_{\frac{1}{2}}$ values are well separated.

Solutions containing various concentrations of either lead ions (Pb^{2+}) or cadmium ions (Cd^{2+}) were analyzed by both dc and Tast polarography. Potassium nitrate (1.0 F) was used as supporting electrolyte in all tests. The lower practical limit for quantitative determinations by dc polarography for both lead and cadmium was approximately 1×10^{-5} M. Diffusion limited currents of 0.10 to 0.15 μA were obtained from 1×10^{-5} F concentration solutions of both cations. The electrode area (A_{max}) was 2.4×10^{-2} cm^2. Accurate measurement of the diffusion currents was severely limited by the drop action on the current output and the high slope of the residual current component of the polarograms.

The diffusion limited currents measured by Tast polarography were equal, within experimental error, to those obtained by dc polarography. However, due to the removal of the drop action from the current output and the reduction in the slope of the residual current, the diffusion limited currents could be measured with reasonable accuracy at lower levels of concentrations. The lower quantitative limit for both lead and cadmium was approximately 5×10^{-6} F.

In the study of multicomponent systems, solutions 1×10^{-3} F in lead with 1×10^{-4} F cadmium and 1×10^{-4} F in lead with 1×10^{-5} F cadmium were analyzed by both techniques. Classical dc polarograms obtained with the first solution had well defined waves for both lead and cadmium. The lead and cadmium diffusion limited currents were 7.5 and 0.72 μA, respectively ($A_{max} = 2.4 \times 10^{-2}$ cm^2). However, by using Tast polarography and the current offset capability built into the instrument, the cadmium wave was amplified to give nearly a full scale readout on the recorder. The 0.72 μA was amplified to approximately 600 mv readout with less than 20 mv peak to peak noise.

The solution of 1×10^{-4} F lead and 1×10^{-5} F cadmium gave well defined lead waves by both techniques, but an accurate measurement of the cadmium by either method was virtually impossible. Diffusion limited currents for the lead of 0.84 and 0.80 μA were obtained by dc and Tast polarography, respectively. The values of the diffusion currents for cadmium were approximately 0.1 μA , but accurate measurements were prevented by the low signal to noise ratios. A_{max} was 2.4×10^{-2} cm^2 and the sample delay time for Tast polarograms was 90 percent of t_{max}.

Square-Wave Polarography

A large number of variations of classical dc polarographic techniques has been developed over the years. Among these procedures is square-wave polarography. Barker (30) and Milner (42) were among the first to study the analytical applications of this technique. Lower detection limits of 4×10^{-8} F for reversibly reduced species and 1×10^{-6} F for irreversibly reduced species have been reported (30).

The work presented in this section is an evaluation of the square-wave polarography mode of operation of our instrument. Results obtained from both normal and rapid sweep square-wave polarography are reported. All summit potential (E_s) are measured with reference to the saturated calomel electrode (S.C.E.).

Considering the similarity of the effects of irreversibility on ac and square-wave polarography, the supporting electrolyte found to be most effective for each particular metal ion by Poole (43) in his work with phase selective ac polarography was employed in the analysis of most metal ions. No extensive work was undertaken to find supporting electrolytes with improved characteristics.

In all square-wave and pulse polarographic analysis performed in this series of studies, the potential step function was always a negative stepping function, i.e., the square-wave input to the summing point of the control amplifier always steps from zero potential to some negative potential value and then back to zero potential.

Single Component Systems

Each metal will be presented in alphabetical order with the conditions for the analysis of the metals being given. It was found that the sensitivity of the square-wave mode of operation was such that Cd^{+2} and Pb^{+2} ions can be analyzed down to a lower concentration limit of about 10^{-7} F. Cations that can be analyzed down to a limit of approximately 10^{-6} F are Sb^{+3}, As^{+3}, and Zn^{+2}. In addition, Co^{+2} and Ni^{+2} are detected down to a lower limit of about 10^{-6} F. The results obtained are summarized in Table 2.

Table 2. Summary of Results Obtained from the Analysis of Metal Ions by Square-Wave Polarography

Metal Ion	Supporting Electrolyte	Approximate Detection Limit	Summit Potential
Sb^{3+}	0.5 F HCl_5	5×10^{-7} F (0.06 ppm)	-0.15 volts
As^{3+}	0.1 F H_2SO_4	5×10^{-6} F (0.10 ppm)	-0.69 volts
Cd^{2+}	1 F KNO_3	1×10^{-7} F (0.01 ppm)	-0.59 volts
Co^{2+}	1 F NH_4Cl- 1 F NH_4OH	2×10^{-5} F (1.1 ppm)	-1.30 volts
Cu^{2+}	1 F KNO_3	5×10^{-6} F (0.32 ppm)	0.03 volts
Pb^{2+}	1 F KCl	1×10^{-7} F (0.02 ppm)	-0.45 volts
Ni^{2+}	1 F KSCN	5×10^{-6} F (0.30 ppm)	-0.70 volts
Zn^{2+}	0.01 F KCl	1×10^{-6} F (0.07 ppm)	-1.00 volts

Antimony. A detection limit of about 5×10^{-7} is obtained for the analysis of antimony in the +3 oxidation state utilizing 0.5 F hydrochloric acid as the supporting electrolyte. The summit potential, E_s, is -0.15 volt and the width at half-height is about 35 mv, which corresponds to the three electron reduction reaction of the species $SbCl_4^-$ to elemental antimony.

Using 0.1 F nitric or sulfuric acid media, the sensitivity is reduced to about 1×10^{-5} F. This is in agreement with the fact that the reduction of SbO^+ does not proceed reversibly in a non-complexing acid medium (44). A summit potential of -0.30 volt is obtained for both nitric and sulfuric acid.

Arsenic. The analysis of arsenic with a 0.1 F sulfuric acid solution as supporting electrolyte was investigated. A broad wave (width at half-height is 40 mv), with a summit potential of -0.69 volt is obtained. The lower detection limit is about 5×10^{-6} F. No analyses were made with hydrochloric acid as supporting electrolyte.

A 25 mv, 250 Hz, square-wave function was used in all analyses of arsenic. The sample delay time was 1.4 msec, and the sample gate width was 0.4 msec. Due to the high slew rate of the track and hold units (a point discussed in Chapter III), the effective sample delay time was approximately 1.8 msec.

Cadmium. The cadmium cation possesses very favorable polarographic characteristics, reversibly reduced to the metal in a wide variety of supporting electrolytes. In a 1 F potassium nitrate solution, a detection limit of about 1×10^{-7} F and a summit potential of -0.59 volt are obtained. The width at half-height of the wave is 45 mv, which corresponds to a two

electron reduction.

A 30 mv, 500 Hz, square-wave function was used. Sample delay time and sample gate width were 0.31 and 0.10 msec, respectively. The very short sample delay time was made possible by the careful optimization of the positive feedback. This insures the decay of the double-layer capacitance current to a negligible amount in 40 to 50 microseconds.

Cobalt. A well defined wave is obtained from the reduction of hexamminocobalt (II) ion, $Co(NH_3)_6^{2+}$, in a supporting electrolyte 0.8 F in ammonium chloride and 0.8 F in ammonia. A lower detection limit of 2×10^{-5} F and a summit potential of -1.3 volts are obtained. The width at half-height is 110 mv, which is very broad for a two electron change of Co^{2+} to elemental cobalt.

The square-wave amplitude was 20 mv and the half-wave length was 2 msec (250 Hz). Sample delay time and sample gate width were 1.4 and 0.4 msec, respectively.

Copper. In a noncomplexing medium, such as potassium nitrate, the copper (II) ion is reversibly reduced to the elemental copper. A wave with a width at half-height of 45 mv (a two electron reduction) and a summit potential of +0.03 volt are obtained. The lower detection limit is approximately 5×10^{-6} F, but the lower quantitative limit is only about 1×10^{-5} F due to the anodic dissolution of mercury occurring immediately before the reduction wave of copper.

Square-wave amplitude and time parameters were the same as those used in the arsenic study.

Lead. Lead, like cadmium, possesses very favorable polarographic characteristics. Lead (II) reduces reversibly to the elemental state in a

wide variety of supporting electrolytes. The detection limit in supporting electrolytes, such as potassium nitrate, potassium chloride, and hydrochloric acid, are all about the same, 1×10^{-7}. The summit potential varies from -0.39 volt in 1.0 F potassium nitrate to -0.45 volt in 1 F hydrochloric acid. The sensitivity is slightly reduced when an alkali metal hydroxide is used as supporting electrolyte.

When working at low concentrations, such as 10^{-7} F or less, trace contamination of reagents becomes an increasingly important problem. Trace amounts of lead are known to often occur in many reagent grade salts commonly used as supporting electrolytes. For example, a 1 F potassium nitrate solution prepared with reagent grade material as received from J. T. Baker Company had a lead concentration of about 5×10^{-7} F (see Figure 24). The trace contaminates (lead, cadmium, etc.) were removed from the supporting electrolyte solutions by electrolytic prereduction. Electrolysis times of approximately forty-eight hours were normally required to sufficiently reduce the lead and cadmium content.

An additional problem encountered in the analysis of lead by square-wave polarography is the occurrence of a low, broad wave at -0.1 to -0.5 volt in many electrolyte media. Lead (II) reduction wave appears as a shoulder on this broad wave. The uncertainty of the base line raises the lower quantitative limit of the lead analysis. Using a supporting electrolyte solution 0.5 F in sodium perchlorate and 0.005 F in sodium fluoride effectively reduced the magnitude of the low, broad wave. Trace amounts of oxygen in the nitrogen used to purge the sample solutions increase the magnitude of this broad wave. Oxygen was removed by passing the nitrogen over hot copper turnings.

Nickel. The thiocyanate complex of nickel (11) ion formed in a 1 F potassium thiocyanate solution is reduced to elemental nickel at a summit potential of -0.70 volt. The width at half-height was 70 mv and the detention limit was about 5×10^{-6} F.

A supporting electrolyte solution of 0.8 F ammonium chloride - 0.8 F ammonia gave a well defined, symmetrical wave with a summit potential of -1.07 volts. The width at half-height increased over the thiocyanate system to 130 mv; indicating a decrease in the reversibility of the reduction reaction. A detection limit of about 10^{-5} F was found for the ammoniacal medium. The square-wave function magnitude and time parameters were identical to those used for the cobalt analysis.

Zinc. The square-wave polarographic reduction of the zinc (II) to the metal was investigated in potassium chloride and potassium nitrate media. Results in both electrolytes were about the same, with the best sensitivity being obtained using 0.01 F concentration of either salts. Symmetrical waves were obtained with summit potential of -0.995 volt, and a detection limit of 1×10^{-6} F zinc (II).

The square-wave function magnitude was 40 mv, with a sample delay time of 1.4 msec, and a sample gate width of 0.4 msec.

Concentration of the supporting electrolyte was found to have a very significant effect on the reversibility of the wave. Figure 23 shows this effect. The width at half-height remained almost constant (60 to 67 mv) over the 0.01 F to 1.0 F concentration range of supporting electrolyte. The shape of the polarographic wave changes from a symmetrical to a slightly asymmetrical wave as the electrolyte concentration is increased. An extensive study of the electrode reaction kinetics of zinc in potassium

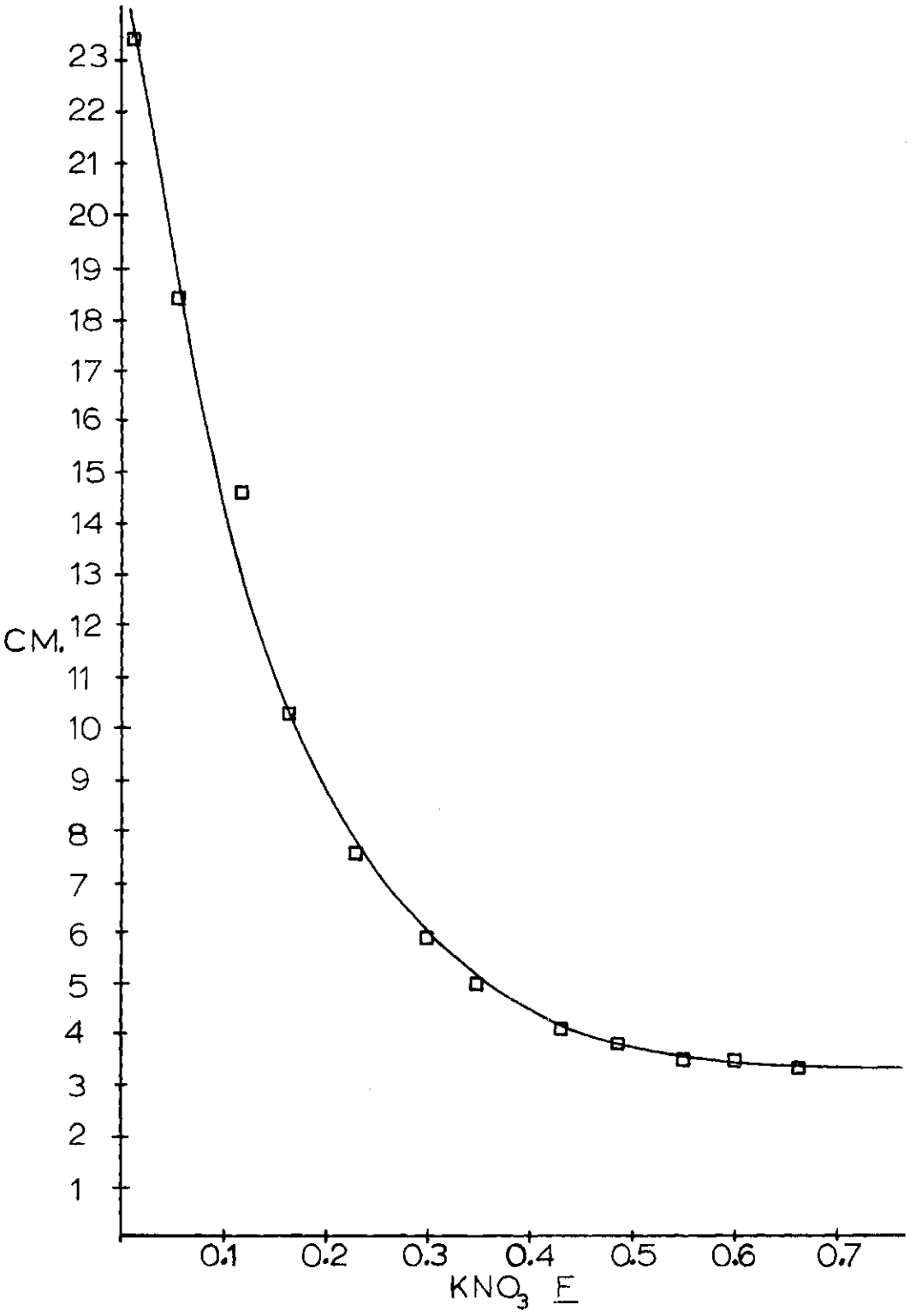

Figure 23. Wave Height Versus Concentration of the Supporting Electrolyte. Solution 1 x 10^{-4} F in Zn (II).

nitrate medium is presented in Chapter VI.

Multicomponent Systems

Lead and Cadmium. The divalent ions of these elements are reversibly reduced and do not normally interfere with each other polarographically. The work involving these two metal ions demonstrates the use of square-wave polarography in the analysis of a minor species in the presence of a relatively large amount of substance that is reduced at a more positive potential.

In a 1 F solution of potassium nitrate, cadmium ion, even at 1×10^{-6} F, gives a well-defined square-wave polarogram with a summit potential of -0.59 volt. Solutions with a cadmium ion concentration of 1×10^{-8} F and 1×10^{-6} F, 1×10^{-5} F, and 1×10^{-4} F in lead ions (E_s = -0.39 volt) were prepared and analyzed for cadmium. The magnitude of the cadmium wave was identical in all cases. With the concentration ratio of lead to cadmium at 100 to 1, the cadmium appears as a shoulder on the larger lead wave, but it can still be measured with reasonable accuracy.

Copper and Cadmium. In a 1 F solution of potassium nitrate, the summit potentials of these substances are widely separated, E_s = +0.03 volt for copper and -0.59 volt for cadmium, and both give well defined square-wave polarograms. Solutions containing a constant 1×10^{-3} F copper (II) ion and 1×10^{-4} F, 1×10^{-5} F, and 1×10^{-6} F cadmium ions were prepared and the cadmium determined. Even at a 1000 to 1 (Cu^{2+} to Cd^{2+}) ratio the cadmium ion wave was sufficiently separated to allow easy evaluation.

A 40 mv, 250 Hz square-wave function was used in the copper-cadmium study.

Nickel and Cobalt. A 1 F ammonium chloride - 1 F ammonia solution is suitable for the simultaneous determination of these two substances. The summit potentials are -1.07 and -1.3 volts for nickel and cobalt, respectively.

Although the summit potentials of nickel and cobalt are separated by approximately 0.2 volt, there is considerable interference between the two waves. Both cations exhibit some irreversibility in their reduction, leading to broad, slightly asymmetric waves. With the nickel (II) ion present at 1×10^{-4} F, the lower detection limit of cobalt is only about 5×10^{-5} F.

Lead, Cadmium, Thallium, and Indium. The summit potentials of these four metal ions in 0.1 F and 1.0 F potassium chloride solutions are summarized in Table 3.

Table 3. Summit Potential of Lead, Thallium, Cadmium, and Indium in 0.1 F and 1.0 F Potassium Chloride

	Summit Potentials (volts)	
	0.1 F KCl	1.0 F KCl
Lead	0.38	0.44
Thallium	0.46	0.44
Cadmium	0.57	0.60
Indium	0.56	0.56

It is obvious that, in a supporting electrolyte, 1.0 F in potassium chloride, neither lead and thallium nor cadmium and indium are separated.

In a 0.1 F potassium chloride, however, the lead and thallium waves are separated enough to allow the detection of either ion in the presence of the other, so long as their concentrations are about equal. Cadmium and indium remain unseparated in 0.1 F potassium chloride solution.

Rapid-Sweep Square-Wave Polarography

This technique is a modification of normal square-wave polarography in which a hanging drop mercury electrode is used in lieu of the usual dropping mercury electrode. In addition, the linear ramp is scanned rapidly (0.01 to 0.02 volt per second) over the desired potential range. Potential versus current is recorded in the usual polarographic way. Primary advantages of this method are the speed of analysis and the elimination of the drop action in the current readout.

The sensitivity of rapid-sweep square-wave polarography for many cations is better than that of normal square-wave techniques. Shown in Figure 24 is an illustration of the use of the rapid-sweep technique in the determination of cadmium ion at very low concentrations. It is seen that cadmium at 1.5×10^{-7} F can be measured easily. A plot of the maximum current versus concentrations for the four solutions is shown in Figure 25 and yields a straight line that passes through the origin. The wave for lead in Figure 24 resulted from lead impurities (approximately 5×10^{-7} F) in the supporting electrolyte.

Figure 26 is a polarogram of a multicomponent system using rapid sweep techniques. The indium and cadmium waves are separated for approximately ten percent of their total height. This is an improvement over normal square-wave polarography where no separation was obtained at these concentrations. Resolution of the indium-cadmium wave was slightly

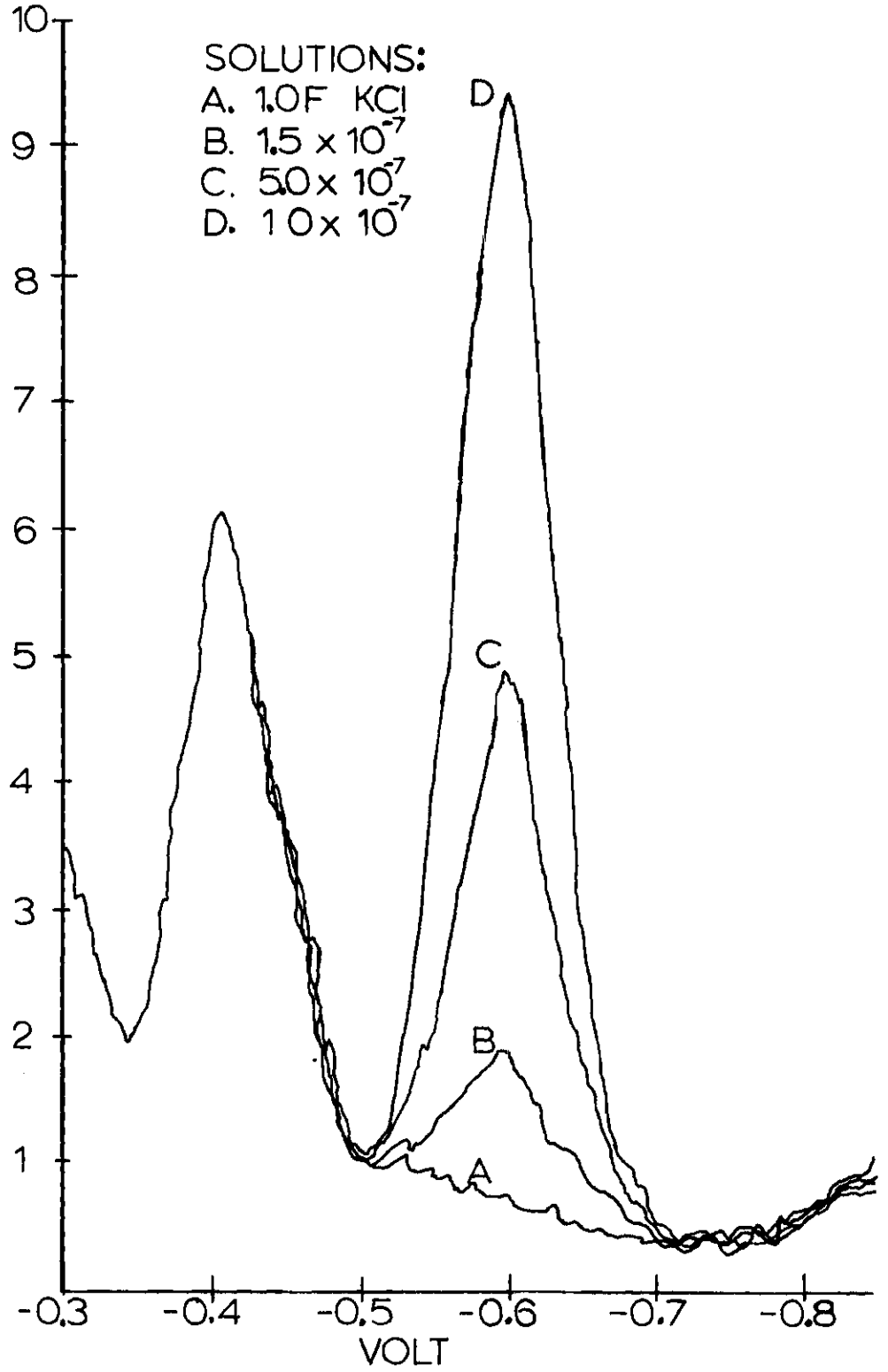

Figure 24. Rapid-Sweep Square-Wave Polarogram of the Cadmium Ion in Potassium Chloride Solution (sweep-rate -0.02v sec^{-1}; square-wave 30 mv)

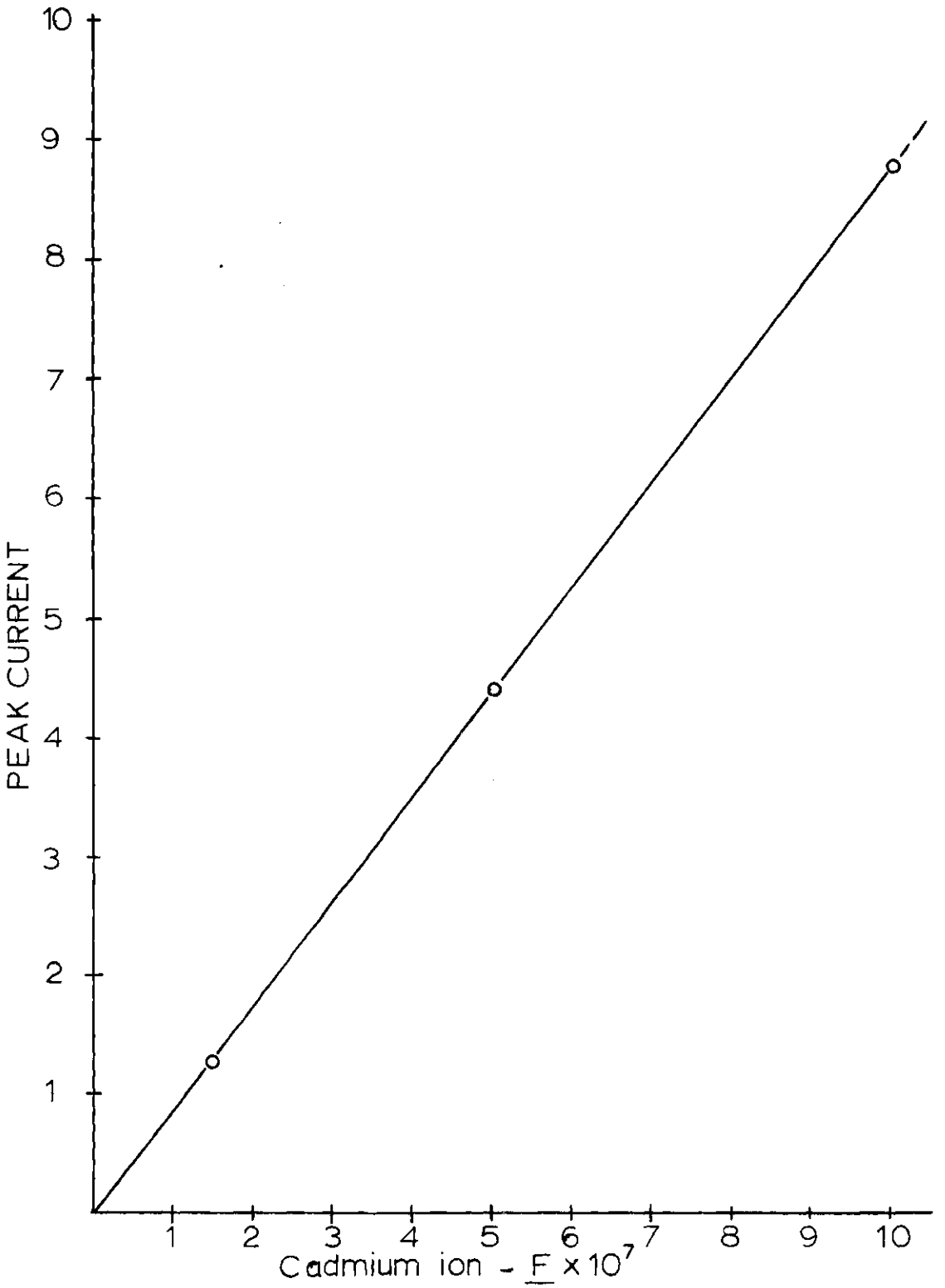

Figure 25. Peak Current Versus Concentration of Cadmium

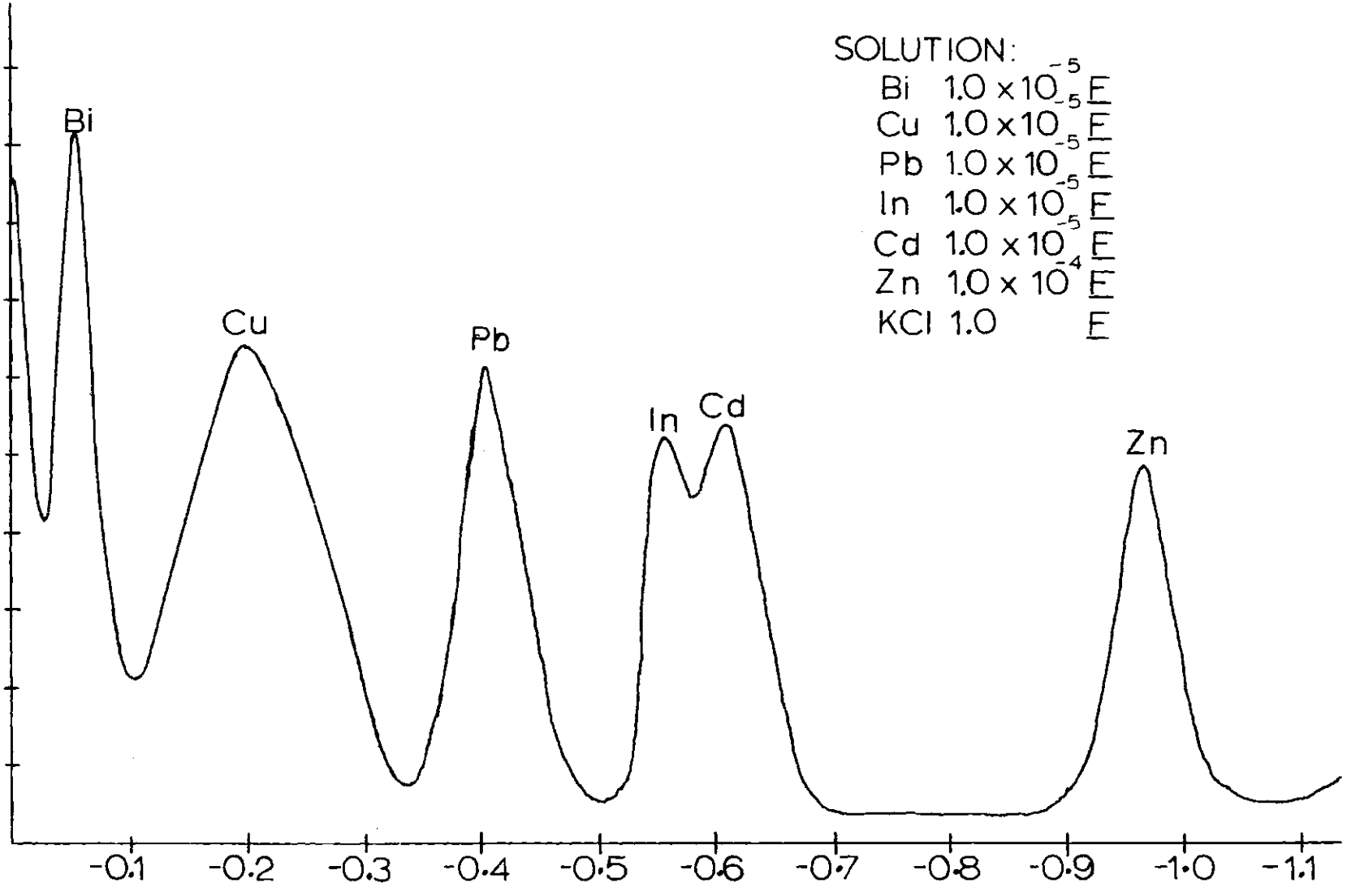

Figure 26. Rapid-Sweep Square-Wave Polarogram of a Multicomponent System

improved by slowing the sweep rate to 0.01 volt per second.

An additional advantage of rapid-sweep square-wave polarography is applicability in anodic stripping techniques. Cadmium ions at a concentration of 1×10^{-8} F were easily detected in some preliminary studies, but no extensive work was done to determine the lower detection limits of cations.

Differential Pulse Polarography

The data obtained from the differential pulse polarography studies with our instrument were disappointing. The current readout was very erratic at high gain positions of the current amplifier due to a deficiency in the basic design of the current monitoring circuits. The slew rate of the track and hold units, even after being modified as discussed in Chapter III, was too fast. The units tracked the high frequency noise instead of monitoring the average faradaic current flow during the time when the sample gate was open. Secondly, the time parameters of the potential pulse, sample delay time, etc. were not synchronized with sixty cycle noise to help eliminate its effects.

The lower detection limits for highly reversible cations, such as Pb (II) or Cd (II), in single component systems were about 1×10^{-6} F. Symmetrical waves with width at half-height of 45 mv were obtained for cadmium (II) ion in 1 F potassium nitrate. In a multicomponent system of lead and cadmium, the latter at 5×10^{-6} F was detected in the presence of 1×10^{-4} F lead. The potential pulse was 25 mv, and had a half-wave length of 2 msec. A sample delay time of 0.7 msec and a sample gate width of 0.2 msec were used. The drop life was set at 4.2 sec.

Square-Wave Polarography versus Differential Pulse Polarography

The relative sensitivities of the various potential step techniques have been a much debated topic in recent years. It has been accepted generally that pulse techniques are more sensitive than square-wave polarography. This became especially true with the advent of computer controlled experiments and the use of ensemble averaging to reduce the inherent noise problem of pulse methods. The above conclusion seems to be based on the assumption that, in square-wave polarography, the concentration of the electroactive species is decreased by the continuous square-wave signal, thereby reducing the faradaic current obtained for any one given potential step. A study of the relative sensitivities of differential pulse and square-wave polarography by chronocoulometric techniques was made. A reversible reduction (Cd^{2+}) and an irreversible reduction (Zn^{2+}) were studied.

Results obtained from the cadmium and zinc systems are shown in Table 4. Solutions used for the study were 1 F in potassium nitrate as supporting electrolyte and 1×10^{-3} F in cadmium or 1×10^{-3} F in zinc. A drop life time of 4.4 sec and a delay time (age of drop when pulse is applied) of 4.2 sec were used in the pulse method.

The oscilloscope was triggered at 4.2 sec into the drop life for both techniques. The initial potential was set at $E_{\frac{1}{2}}$ for each trial. Chronocoulograms for one full cycle of the square-wave signal were displayed on the oscilloscope. After correcting for double-layer charging current, the algebraic difference of the cathodic and anodic faradaic currents was calculated.

Table 4. Chronocoulometric Results from the Comparative Study of Square-Wave and Pulse Polarography

Metal Ion	Pulse Length (msec)	Continuous Square-Wave (Q in μC)	Single Pulse Per Drop (Q in μC)
Cd^{2+}	0.47	0.14	0.15
Zn^{2+}	0.47	7.3×10^{-3}	5.6×10^{-3}
Cd^{2+}	15.0	1.14	1.14
Zn^{2+}	15.0	0.18	0.17

It is evident from the data in Table 4 that, for the reversible system, there is no appreciable difference in the total faradaic current flow for the two techniques. In square-wave polarography, the depletion of the oxidized form is counter balanced by the increase in concentration of reduced form. The length of the pulse has little or no effect on the ratio of the two total currents.

For systems exhibiting some irreversibility, the results indicate that, for relatively short pulses (0.5 msec) square-wave polarography has a slightly larger faradaic current flowing. As the pulse length is increased, the total current flow of the system approaches that of the completely reversible system with no appreciable difference in total current.

Chronocoulometry

The chromium tris(2,2'bipyridine) $[Cr(BiPy)_3^{+3}]$ complex is not well-characterized polarographically. Above pH 2.8 three waves with $E_{\frac{1}{2}}$ potentials of -0.46, -0.76, and 0.97 volt are obtained using classical

dc polarography. The drop action of the current is very erratic throughout the polarogram. The first two waves appear to be irreversible due to their low slopes. The diffusion limited current for the first wave is twice that obtained for the second wave. The third wave, however, has a very steep slope and could be termed quasi-reversible. The value of the third diffusion current is not an even multiple of the second wave value. Specific adsorption of the reactants and/or the products could be responsible for the unusual polarographic characteristics.

In Chapter II it was shown that the surface excess of reactants or products can be measured by double step chronocoulometry. A solution 1×10^{-3} F $Cr(BiPy)_3(ClO_4)_3$ and 0.5 F in potassium chloride was used in the study. The pH of the solution was adjusted to 2.90 with dilute hydrochloric acid. The initial potential of the working electrode was set to -0.40 volt where there is no faradaic reaction occurring. The potential was stepped negatively 0.20 volt to the first diffusion current plateau and then back to -0.40 volt.

The relationships, Q versus $t^{\frac{1}{2}}$ and Q_A versus $[\tau^{\frac{1}{2}} + (t-\tau)^{\frac{1}{2}} - t^{\frac{1}{2}}]$ are plotted in Figure 27. Values of Q and Q_A at f(t) = 0 were 0.67 and 1.10 C, respectively. A linear least squares program written for a Model 362K Wang Electronic Calculator was used to extrapolate the data to f(t) = 0.

The double-layer capacity of mercury electrodes in potassium chloride media in the vicinity of -0.4 volt is about 40 $\mu F\ cm^{-2}$ (45). Correcting the zero time intercept values of Q and Q_A for the double-layer charging current, the coulometric results correspond to surface excesses

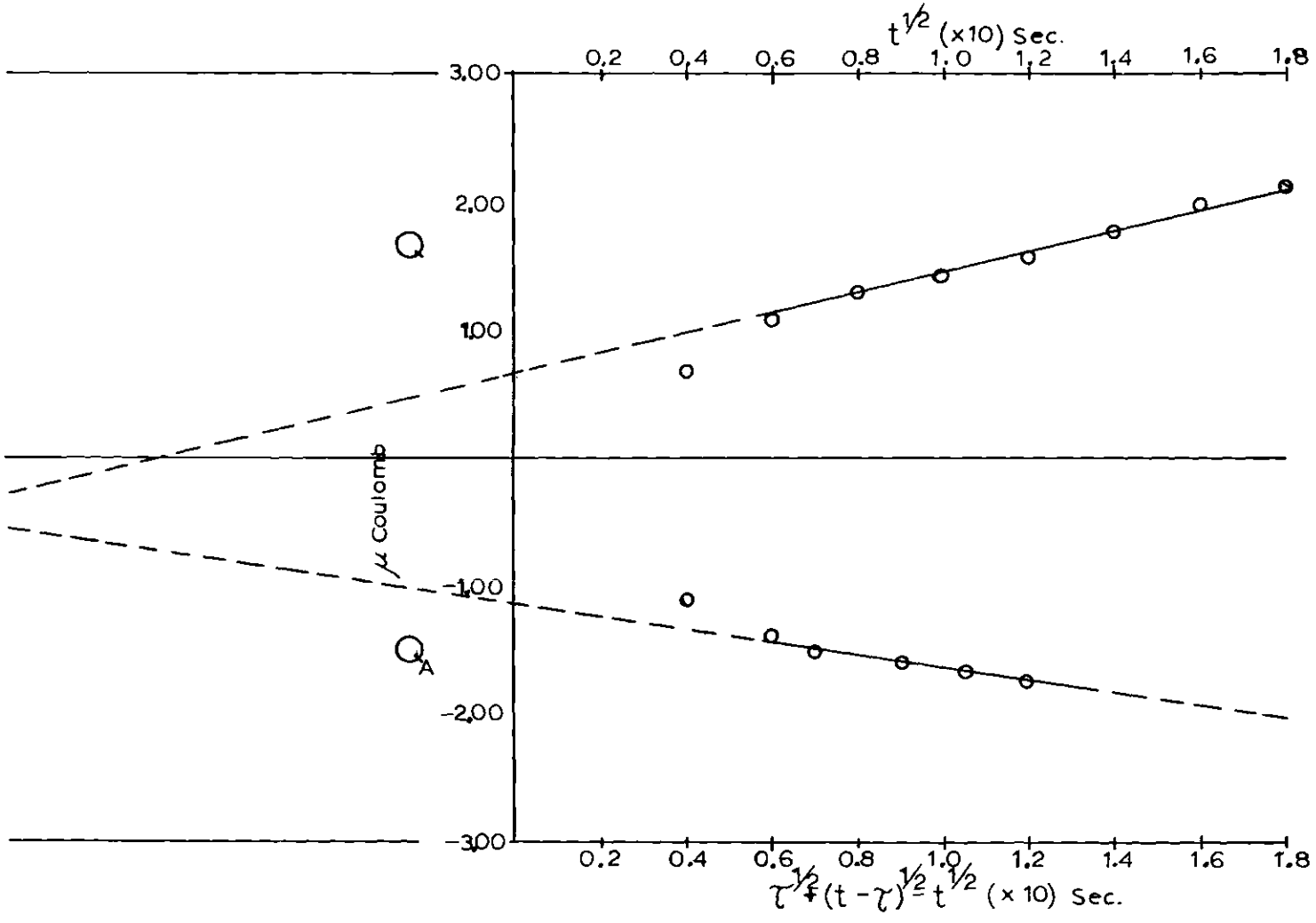

Figure 27. Chronocoulogram from the Chromium Tris BiPyridine Complex in a Perchlorate Medium

of 1.1×10^{-10} moles cm^{-2} of reactants and 1.9×10^{-10} cm^{-2} of products. Albrecht (46) determined the molecular structure of $Cr(BiPy)_3$(III) complex. Using his values for the lattice parameters, a molecular unit area of 1.54×10^{-14} cm^2 was calculated. Making the following two assumptions: (1) monomolecular layers of the species are adsorbed and (2) species are in the closest packing type of arrangement (90 percent of the total volume is occupied by the molecules), the surface excess values are equivalent to electrode surface coverages by adsorption of 111 percent by the reactants and 195 percent by the products.

The polarographic characteristics of cadmium (II)-ethylene bis-(oxyethylenenitrilo) N,N,N',N' tetraacetic acid (EGTA) was the subject of a recent study (47). Above pH 2.5 two waves are obtained. Both waves are irreversible and are highly pH dependent. Above pH 2.5 the current for the first wave never reaches the diffusion-limited value of that attained by aquo-cadmium ion. The diffusion limited current for a solution 4.2×10^{-3} F in Cd (II) and 4.4×10^{-3} F in EGTA decreases from about 24 μA at pH 2.50 to approximately 1 μA at pH 4.60 ($A_{max} = 2.2 \times 10^{-2}$ cm^2). The half-wave potentials shift from 0.60 volt to 0.75 volt over the 2.5 to 4.6 pH range. The specific adsorption of EGTA could cause this type of polarographic behavior of the cadmium-EGTA complex. Double-step chronocoulometry was utilized to evaluate the surface activity of the various reactants and electrode reaction products.

Test solutions 4.2×10^{-3} F in cadmium and 4.3×10^{-3} F in EGTA and 0.114 F in tetramethyl-ammonium nitrate as supporting electrolyte were used. Chronocoulograms for the above solutions at pH values of 2.60,

3.20, 3.80, and 4.60 were obtained. Chronocoulograms for solutions at the same concentration of cadmium ion and tetramethyl-ammonium nitrate, but with no EGTA present, were also obtained for comparison.

The values of Q and Q_A at f(t) = 0 exhibited by the first polarographic wave of the various solutions, both with and without EGTA, were all equal to or less than the calculated double-layer charging current. This indicates no specific adsorption of cadmium ion or cadmium-EGTA complexes in the cadmium-EGTA system in the pH range of 2.5 to 4.6.

Results are presented in Table 5. The values are the average of two determinations. The calculated double-layer charging current was 0.10 μC, and the precision of the technique using our instrument is about ± 0.10 μC. The factors causing the negative values of Q are unknown. It is postulated that the unusual values may result from the specific adsorption of EGTA, thereby reducing the effective area of the mercury electrode. The concentration of the uncharged EGTA would decrease with increased pH of the solution because of two effects: (a) increased deprotonation of the chelate and (b) decrease in the faradaic reaction that would release the EGTA from the cadmium-EGTA complex.

Table 5. Results from Chronocoulograms of the Cadmium-EGTA System

pH	Q(μC)	Q_A(μC)
2.60	-1.48	0.17
3.20	-0.85	0.14
3.80	-0.15	0.19
4.60	0.02	0.10
Cd (II) (No EGTA)	0.19	0.11

CHAPTER VI

ELECTRODE KINETICS OF ZINC BY POTENTIAL STEP METHOD

Introduction

The electrode reaction of zinc (II) has been studied by many investigators by several methods (2,3,48,49,50,6). Both single step and two consecutive-step mechanisms have been proposed. Heyrovsky (2), on the basis of oscillographic measurements of the reduction of zinc (II) in a sodium perchlorate medium, was the first to postulate the consecutive-step mechanism for this reaction. Hush and Blackledge (3), using impedance and dc measurements, also concluded the consecutive-step mechanism for the zinc (II) reduction in a perchlorate medium. Opposing these findings are Timmer, Sluyters-Rehbach, and Sluyters (47), who, based on ac measurements, proposed the one-step electrode reaction.

In Chapter II it was shown that the kinetics parameters of fast consecutive-step electrochemical reactions can be measured by potential step techniques. Careful evaluation of potential step data can be used to prove or disprove the existence of two consecutive steps in the zinc (II) reduction. Examination of the equation for the current-time function leads to the following three conclusions, which may be used as criteria for the existence of consecutive-steps in the mechanism:

1. Since α_a will not generally be equal to α_b, the slopes of the anodic and cathodic Tafel region will not add up to unity, as they must for a single transfer step $[\alpha + (1-\alpha) = 1]$.

2. Extrapolation of the Tafel region to $\eta=0$ will give two values of exchange currents.

3. If either exchange current equals to infinity, the Tafel region extrapolates to the exchange current characteristic of the slower step, but the slopes add up to 2 instead of 1.

Tafel Plots

In Chapter V it was observed that the reversibility of the electrochemical reaction of zinc (II) in potassium nitrate medium decreased with increasing electrolyte concentration. To study this phenomenon and the basic mechanism of the reaction, potential step experiments were performed with the $Zn(II)_{aqu}/Zn(Hg)$ exchange reaction in potassium nitrate solutions.

For each series of tests the concentrations of the zinc (II) in solution and the zinc metal in the amalgamated electrode were held constant while the concentration of potassium nitrate was varied. The potential of the working electrode was set at E_e and a cathodic or an anodic potential step of given magnitude was applied to the dropping amalgam electrode (DAE) at a predetermined point in the drop life. The magnitude of the potential step was varied from 2 to 300 mv. Plots of the transit current versus the square root of time were obtained and extrapolated to $t^{\frac{1}{2}}=0$. The zero-time intercept, i_o, (corrected by the Oldham-Osteryoung approach) was then used in connection with equations (2-24) and (2-25) to graphically determine the apparent exchange current densities, i_a^o and i_b^o, and the transfer coefficients, α_a and α_b, for the two consecutive steps (if two steps occur) of the electrode reaction.

A major difficulty in the evaluation of the i versus $t^{\frac{1}{2}}$ curves was

the determination of the time delay bracket for the extrapolation to $t^{\frac{1}{2}}=0$. The simple application of the Oldham-Osteryoung theories was not sufficient to insure the acquisition of accurate values of i_o.

To define the time delay to be utilized in the zinc study, tangents were drawn to i versus $t^{\frac{1}{2}}$ curves at time delays from 30 μsec to 100 msec and the i/i_x values determined. It was found that, for values of η of 10 to 200 mv (both cathodic and anodic), i/i_x increases to a maximum value, then remains almost constant for a period of time, and then begins to slightly decrease. The period of time for which the ratio remains almost constant is dependent of the concentration of the supporting electrolyte and magnitude of the potential step. For the concentration range of 0.02 to 2.0 F potassium nitrate and potential step size of 2 to 200 mv, the ratio remains constant from 80 μsec to about 200 μsec. Based on this information, a time delay bracket of 110 to 140 μsec was chosen as the ordinate value to which the tangent is drawn and extrapolated to $t^{\frac{1}{2}}=0$. This time bracket is well within the period where i/i_x is constant for all values of η and potassium nitrate concentrations and was used to evaluate all i versus $t^{\frac{1}{2}}$ plots. Very short times are excluded because of the double-layer charging interference and very long times were affected by the decrease in the amount of kinetic information in the current data.

In Chapter II it was stated that the flow of capacitance current, i_c, is given by equation (2-23)

$$i_c = (\Delta E/R)\exp(-t/RC)$$

The time required for the charging or discharging of the double layer is dependent of the RC time constant and η ($\eta = \Delta E$). The time constant, in

sec, is equal to the product of the solution resistance, in ohms, times the double-layer capacitance, in farads.

Payne (51) found that, at a potential of about -1.0 volt, the double-layer capacitance is virtually independent of the nitrate ion concentration. The capacitance varies from 16.5 $\mu F/cm^2$ to 17.5 $\mu F/cm^2$ over the concentration range of zero to 0.2 F nitrate ion. Using Payne's value for C, the solution resistance was calculated from experimentally obtained RC values. The effective resistance was reduced to approximately 20 to 30 ohms for the various concentrations of potassium nitrate by carefully adjusting the positive feedback. Substituting the values of 0.4 μF for C and 30 ohms for R into equation (2-23), i_c, at a time delay of 125 μsec was calculated for various values of η. The results are given in Table 6. Also presented are the experimental values of the total current at a time delay of 125 μsec for a 1.0×10^{-3} F solution of zinc.

Table 6. Theoretical Capacitance Current Content of the Total Measured Current (units = amp)

η	$i_c(\times 10^6)$	$i(\times 10^4)$	$i_c/i(\times 10^3)$
10	0.13	0.60	2.2
50	0.65	2.0	3.2
100	1.3	4.0	3.2
125	1.6	5.2	3.1
150	1.9	6.4	3.0
175	2.2	7.3	3.0

The data in Table 6 indicate that the total current at the time delay of 125 μsec consists of approximately 0.3 percent capacitance current and 99.7 percent faradaic current. Longer time delay would reduce the relative amount of capacitance current but the amount of kinetically controlled faradaic current would also be reduced.

Shown in Figure 28 is an example of the Tafel plots obtained in the zinc study. The linear regions of the curves between 0.1 volt and 0.2 volt, both cathodic and anodic, were used in all plots for the determination of kinetic parameters. The use of large values of η was prevented by limiting factors for both cathodic and anodic potential steps. The magnitude of the cathodic potential step was limited to approximately 300 mv by the reduction of hydrogen. It was observed that, for anodic potential steps greater than 250 to 300 mv, the i versus $t^{\frac{1}{2}}$ curves coincided at times greater than approximately 110 μsec. It is postulated that this deviation from the theoretical curve is caused by a rapid increase in the $Zn^{+} + e \rightleftarrows Zn^{o}$ electrode reaction as the potential is stepped more and more anodically. The rate of the reaction increases until the current is almost completely controlled by the diffusion processes.

Also plotted in Figure 28 is a theoretical curve obtained by substituting into equation (2-23) the values of i_a^o, i_b^o, α_a, and α_b obtained from the Tafel region of the experimental curves and then varying the value of η and calculating log i_o. The Tafel relationship is not valid for values of η less than 100 mv; however, equation (2-23) should hold true for all values of η. Therefore, the excellent correlation between the two curves in the small η region adds validity to the value of the exchange currents and transfer coefficients obtained in the study.

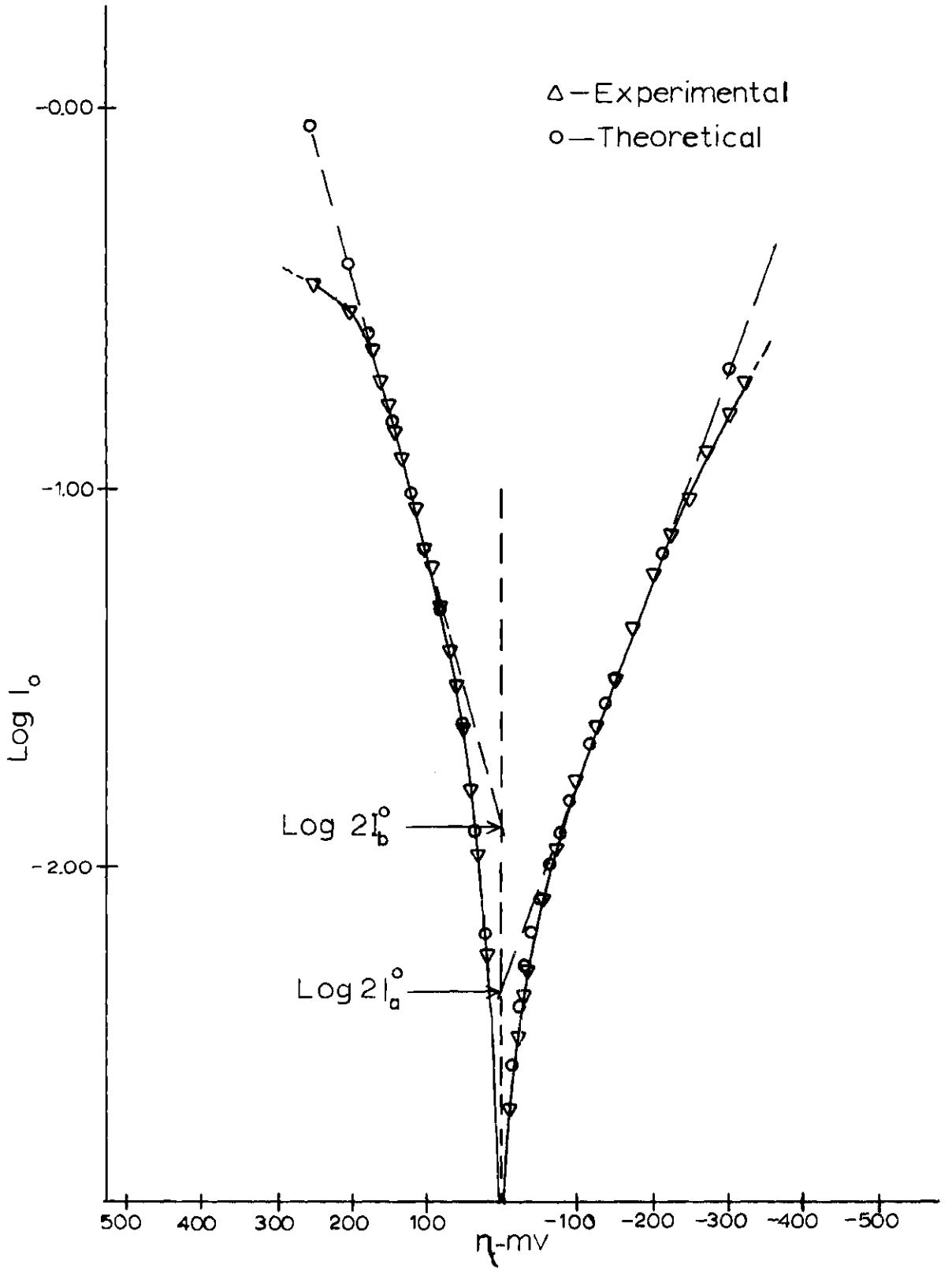

Figure 28. Experimental and Theoretical Tafel Plots (Solution 1.0 F in Potassium Nitrate)

The values of the kinetic parameters obtained for the zinc system are presented in Table 7. The dependence of the parameters on the concentration of the supporting electrolyte is clearly seen in these results. The values, $\alpha_a = 0.34$ and $\alpha_b = 0.56$, for a solution 1.0 F in potassium nitrate agree very well with the values, $\alpha_a = 0.31$ and $\alpha_b = 0.52$, obtained by Hush and Blackledge (3) for a solution 1.0 F in potassium chloride. Hush and Blackledge used impedance and dc measurements in their investigation. Plots of i_a^o, i_b^o, α_a, and α_b against the concentration of potassium nitrate are given in Figures 29 and 30.

A qualitative evaluation of the values of the apparent current indicates that, at moderately high ionic strengths, a two step reaction occurs in which the rate is predominantly controlled by the step, $Zn^{2+} + e \rightleftarrows Zn^{+}$, the apparent activation barrier for the second step, $Zn^{+} + e \rightleftarrows Zn(Hg)$ being smaller. As the ionic strength decreases, i_a^o is decreasing more rapidly than i_b^o, until complete mixed rate control by both steps is achieved.

The direction of the above trend would be consistent with the Frumkin theory (ref. 52, Ch. 7) of salt effects. According to this theory, the potential drop between the electrode surface

$$\Phi = \psi_o + \Phi' \qquad (6\text{-}1)$$

where Φ' is the potential drop between the electrode surface and the outer Helmholz plane and ψ_o is the potential drop between the outer Helmholz plane and the bulk of the solution. Since electrode reactions are believed to occur at the outer Helmholz plane, Φ' may be considered the

Table 7. Results Obtained for the Electrokinetic Parameters of the Zn(II)/Zn(Hg) Reaction in Potassium Nitrate Solutions

KNO_3	Zn^o	Zn(II)	i_a^o	i_b^o	α_a	α_b
F	($\times 10^3$)	($\times 10^3$)	($\times 10^3$)	($\times 10^3$)		
0.05	5.92	5.0	8.5	8.5	0.25	0.74
0.10	5.92	5.0	8.0	8.9	0.26	0.71
0.50	5.92	5.0	3.5	6.0	0.36	0.52
1.00	5.92	5.0	2.5	5.7	0.34	0.56
1.50	5.92	5.0	2.3	5.3	0.33	0.53
2.00	5.92	5.0	1.8	5.1	0.36	0.53
2.68	5.92	5.0	1.8	5.3	0.34	0.53
0.05	5.62	5.0	8.6	7.4	0.22	0.71
0.10	5.62	5.0	7.5	7.3	0.27	0.69
0.20	5.62	5.0	5.6	7.7	0.30	0.63
0.30	5.62	5.0	4.2	6.5	0.35	0.58
0.41	5.62	5.0	3.2	6.7	0.37	0.55
0.50	5.62	5.0	2.8	6.4	0.37	0.52

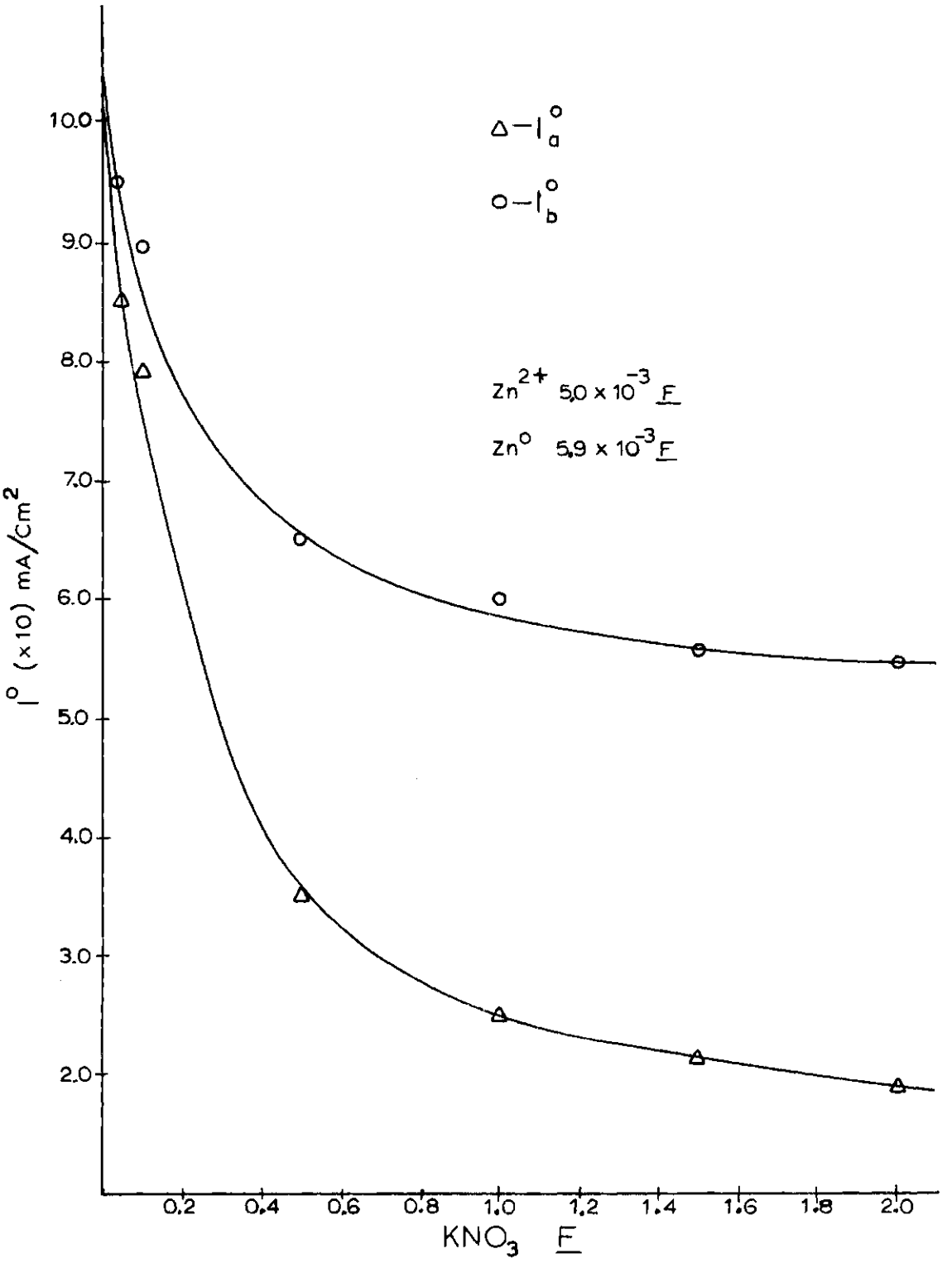

Figure 29. Exchange Current Densities (i_a^o and i_b^o) Versus Supporting Electrolyte Concentration (KNO_3)

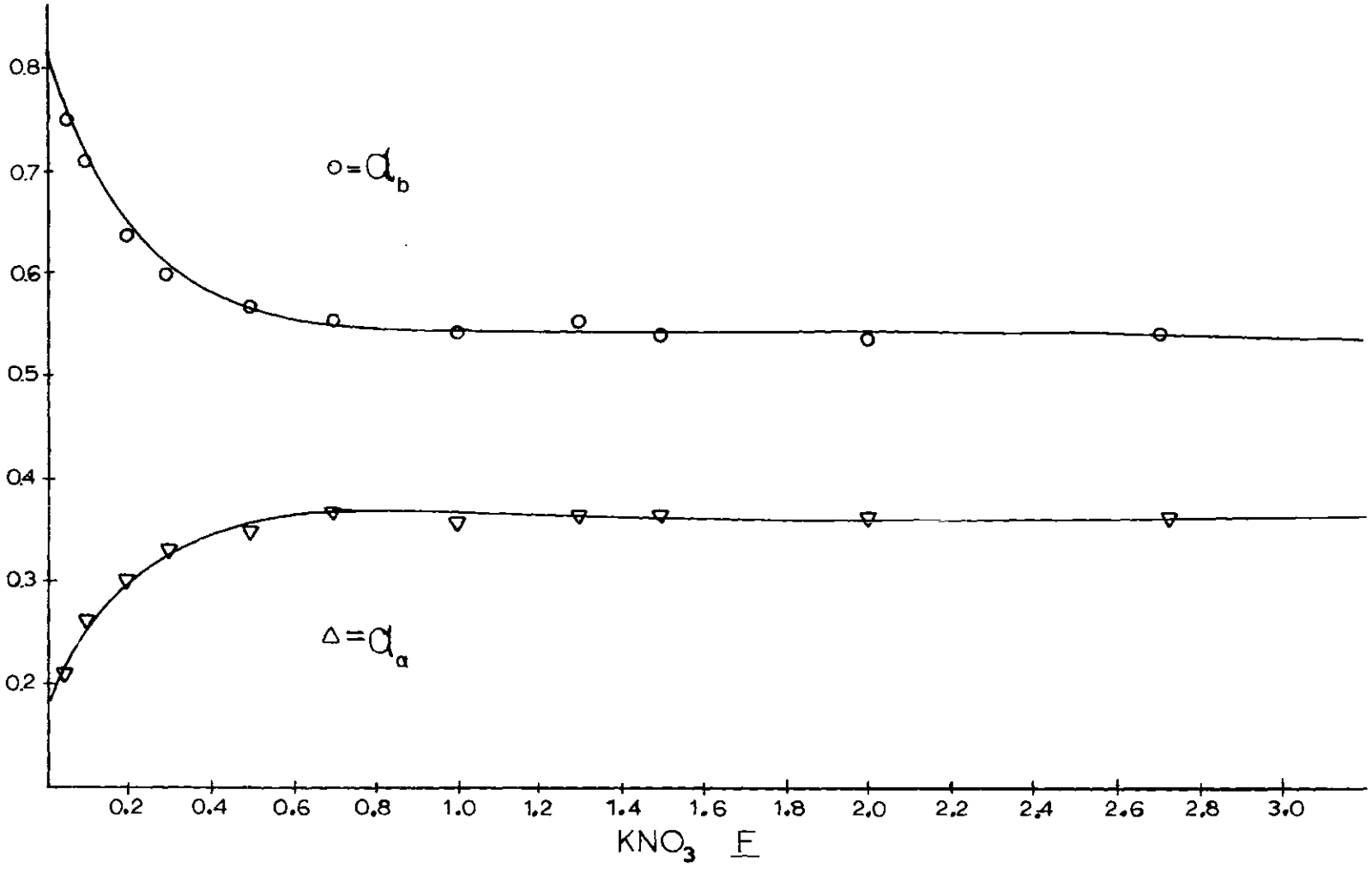

Figure 30. Transfer Coefficients (α_a and α_b) Versus Supporting Electrolyte Concentration (KNO_3)

driving force for the reaction. As the concentration of the supporting electrolyte decreases, the value of ψ_o becomes more negative. The apparent exchange current i^o is related to the true exchange current i_t^o by

$$i^o = i_t^o \, e^{(\alpha n - z) f \, \psi_o} \tag{6-2}$$

where z is the charge on the electroactive species. Since $(\alpha n - z) < 1$, i^o must increase as ψ_o becomes more negative in order to maintain a constant value for i_t^o.

The relative rate of change between the two apparent exchange currents can also be explained in terms of the Frumkin theory if we assume a two-step mechanism. On the basis of the two-step mechanism, we have, according to Frumkin theory,

$$\left(\frac{\partial \ln k_a}{\partial \psi_o}\right) = - 2f(1-\alpha_a) \tag{6-3}$$

$$\left(\frac{\partial \ln k_b}{\partial \psi_o}\right) = - 2f(1-\alpha_b) \tag{6-4}$$

where k_a and k_b are the standard rate constants for the first and second steps, respectively. The values of these rate constants are directly proportional to the size of the apparent exchange currents. An approximate relationship between ψ_o and the supporting electrolyte concentration can be obtained by using the Gouy-Chapman theory, as modified by Stern (52). For a 1:1 electrolyte in the absence of specific adsorption, one obtains

$$\psi_o = \text{const.} + 1/f \ln \mu \qquad (6\text{-}5)$$

where μ is the ionic strength of the solution. For ionic strengths for which equation (6-5) is valid, the following relationships will hold (3)

$$\left(\frac{\partial \ln k_a}{\partial \ln \mu}\right)_T = -2(1-\alpha_a) \qquad (6\text{-}6)$$

$$\left(\frac{\partial \ln k_b}{\partial \ln \mu}\right)_T = -2(1-\alpha_b) \qquad (6\text{-}7)$$

Because of $\alpha_a \leqq \frac{1}{2}$ and $\alpha_b \geqq \frac{1}{2}$, k_a will increase more rapidly than k_b as μ is lowered, so that a transition from rate control by $Zn^{2+} + e \rightleftarrows Zn^{+}$ to mixed control, or even to control by $Zn^{+} + e \rightleftarrows Zn(Hg)$ might be observed at low ionic strengths.

The observed increase in α_b at the lower ionic strengths would be consistent with the reasoning presented in the preceding paragraph; however, the factors causing the reverse trend in α_a are unknown. This trend was observed regardless of the zinc ion concentration in solution or the zinc metal concentration in the amalgam.

Small Step Techniques

As was indicated in Chapter II, the determination of the charge-transfer resistance at low overvoltages provides a way of verifying the value of i_a^o and i_b^o determined from Tafel plots. Presented in Table 8 are the data obtained from a series of experiments in which the zinc ion and zinc metal concentrations were held constant at 5.0×10^{-3} F and 5.5×10^{-3} F, respectively, and the potassium nitrate concentration varied from

0.05 F to 1.00 F. As can be seen in Table 8, the correlation between the values for the charge transfer resistance obtained by the two techniques was good. The variation between the two $(\partial\eta/\partial i)_{i\to o}$ values was found to be less than 10 percent of the Tafel plot value for all trials. These findings add confidence in the validity of the values of the kinetic parameters obtained by the extrapolation of the Tafel plots.

Table 8. Results for Small and Large (Tafel) Potential Steps

Curve	KNO_3 conc	α_a	α_b	i_a^o ($\times 10^3$)	i_b^o ($\times 10^3$)	Small $(\partial\eta/\partial i)_{i\to o}$	Tafel $(\partial\eta/\partial i)_{i\to o}$
A	0.05	0.23	0.73	7.69	8.18	1.49	1.59
B	0.10	0.23	0.74	7.78	7.78	1.77	1.62
C	0.50	0.31	0.59	4.25	7.30	2.56	2.35
D	1.00	0.32	0.56	2.28	6.05	3.94	3.82

Theoretical plots calculated from equation (2-23) in the low overvoltage regions (+20 to -20 mv) show that the curves pass through the origin at slopes predicted by equation (2-24). It was found that variations in α values tend to spread the curves apart somewhat in the $\pm$ 10 to 20 mv region and that the i_a^o to i_b^o ratio controlled the curvature of the plots about the origin. Figure 31 shows plots of $i_a^o = i_b^o = 1 \times 10^{-3}$ amp/cm^2 with two different combinations of α_a and α_b, and also of $i_a^o = 10^{-4}$, $i_b^o = 10^{-3}$ amp/cm^2 with the same two combinations of α_a and α_b.

Comparison of experimental and theoretical overvoltage curves (Figure 32) reveals the following points. The curves for 0.05 F and 0.1 F

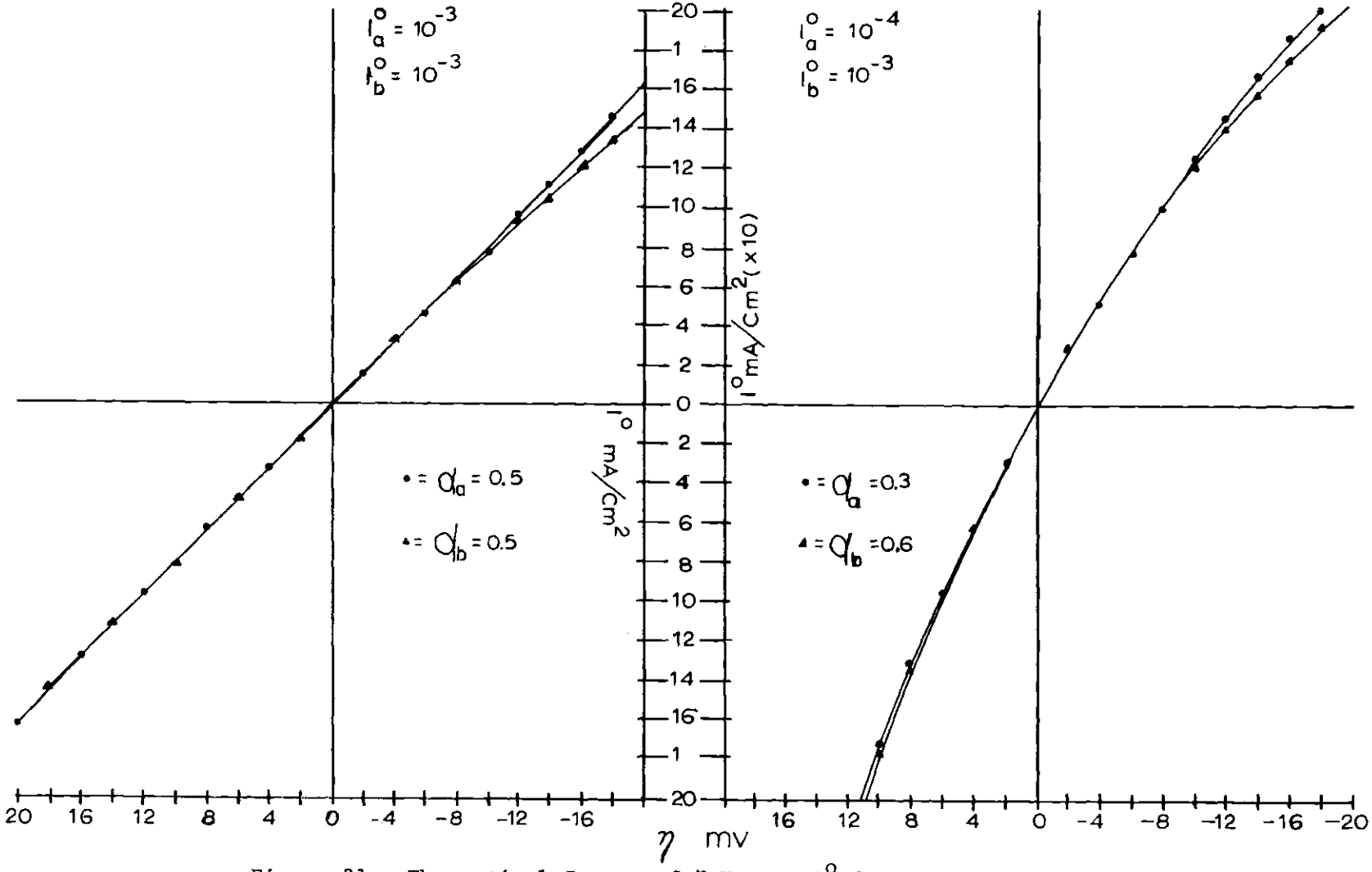

Figure 31. Theoretical Curves of η Versus i^o for Small Potential Steps

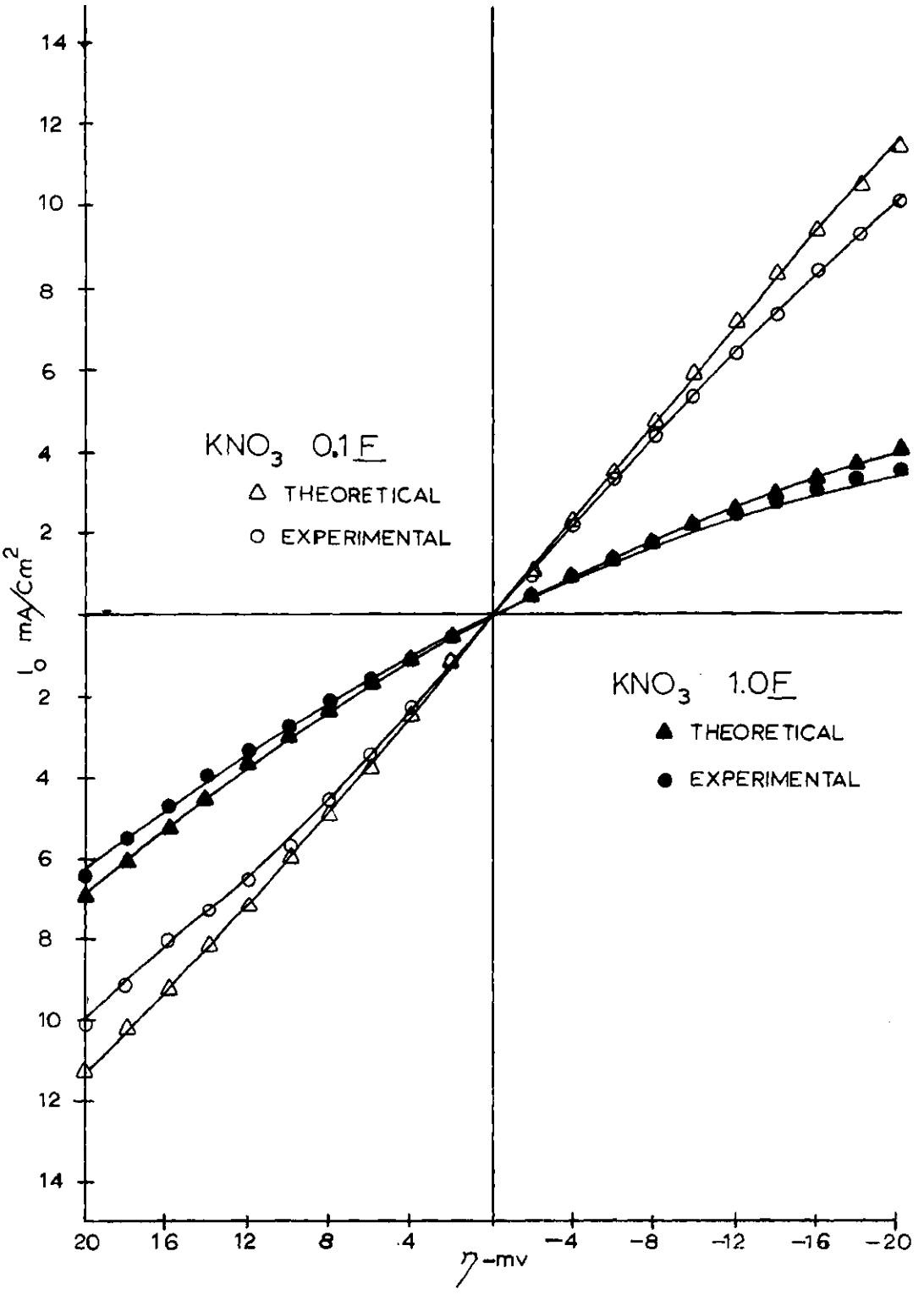

Figure 32. Experimental and Theoretical Curves for the Small Potential Step Technique

potassium nitrate possess little or no curvature in the ± 10 to 20 mv region, indicating i_a^o and i_b^o being approximately equal in value. The 0.5 F and 1.0 F experimental curves exhibit definite curvature and essentially coincide with the theoretical curves.

Reaction Orders

The determination of reaction orders is a very useful tool for the elucidation of reaction mechanisms. For electrochemical systems, the reaction order for a particular species is determined from the variation of the exchange current with the concentration of the species, all other concentrations remaining constant. Delahay (48) has shown that, for single charge-transfer reactions, the following relationship holds:

$$\left(\frac{\partial \ln i^o}{\partial \ln a_o}\right)_{a_R} = p^1 - \alpha p \qquad (6\text{-}8)$$

$$\left(\frac{\partial \ln i^o}{\partial \ln a_R}\right)_{a_o} = s^1 - (1-\alpha)s \qquad (6\text{-}9)$$

where p^1 and s^1 are the reaction orders for the oxidized and reduced forms, respectively, and p and s are the coefficients for the two forms in a balanced equation.

Tafel plots were obtained for two series of solutions (Figures 33 and 34). In one series the concentration of zinc metal in the amalgam electrode was held constant at 5.5×1.0^{-3} F and the zinc ion concentration varied for 1.0×10^{-4} F to 5×10^{-2} F. In other series, the zinc concentration in solution held constant at 5.0×10^{-3} F and zinc concentration in the amalgam is varied. Assuming a single-step reaction for

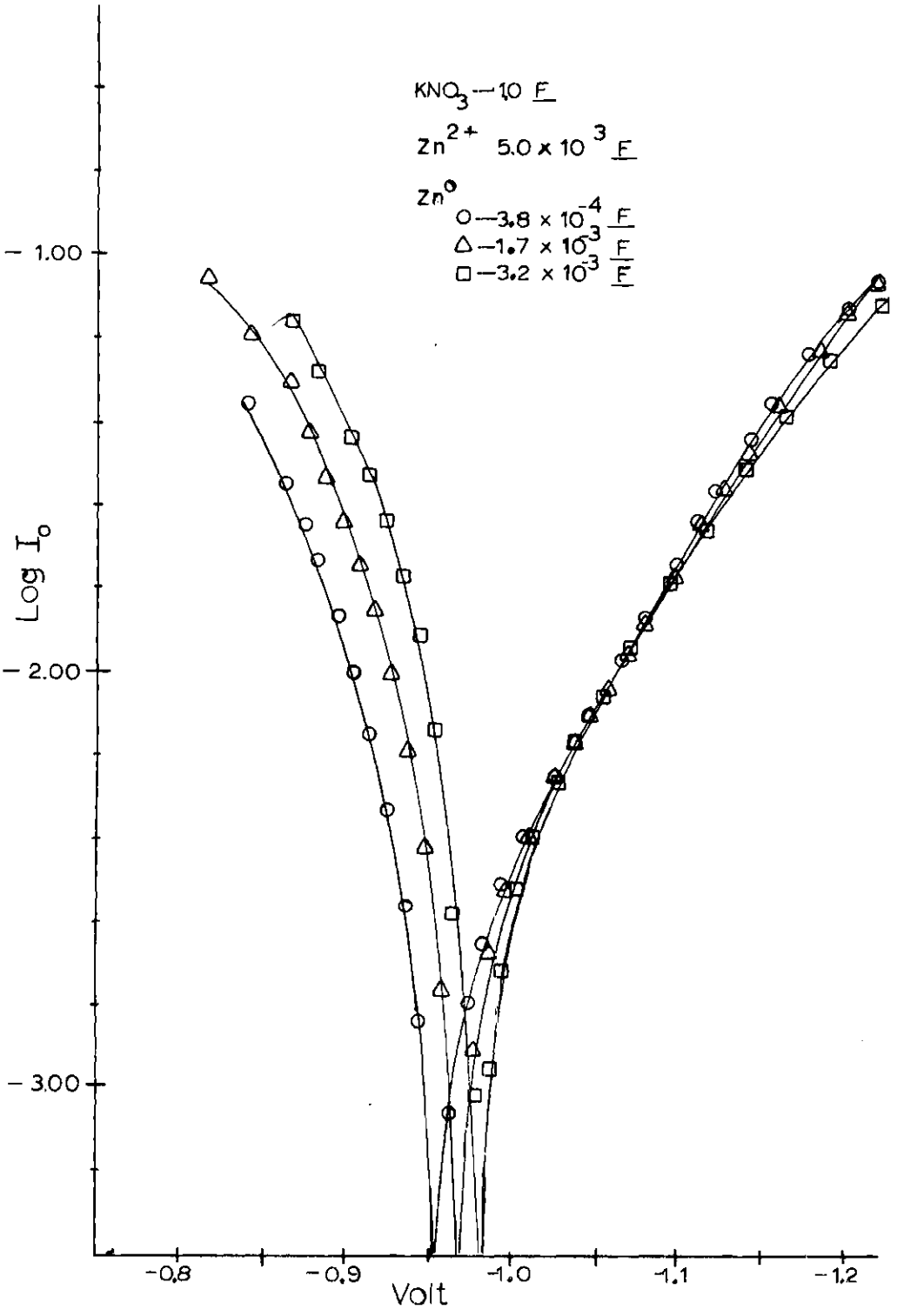

Figure 33. Tafel Plots for the Determination of the Reaction Order of Zinc Metal

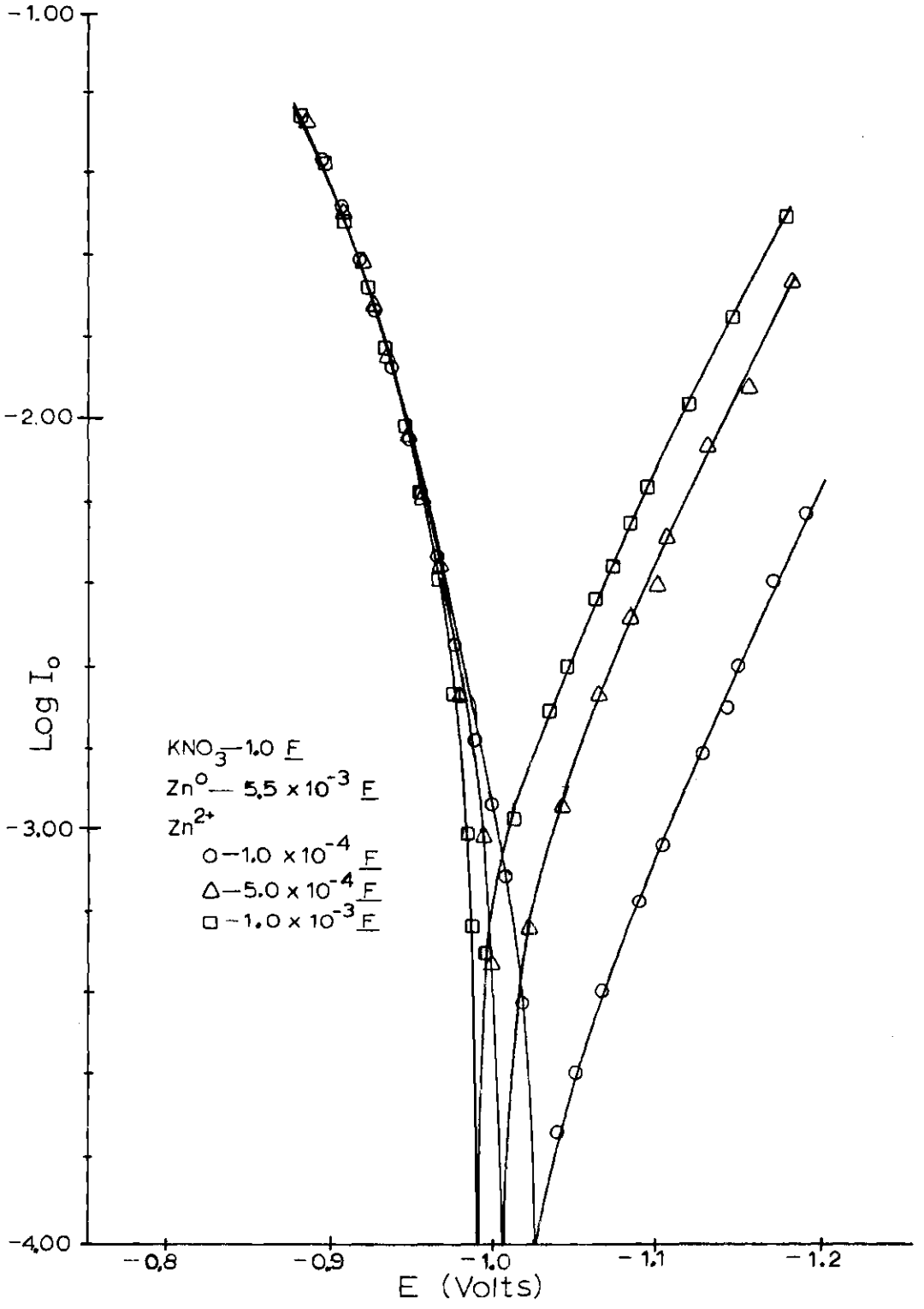

Figure 34. Tafel Plots for the Determination of the Reaction Order of Zinc Ion

the zinc system, and from the slopes of log i_a^o versus log $C_{Zn^{2+}}$ and log i_b^o versus log C_{Zn} plots, reaction orders of 1.02 for the zinc ion and 0.94 for zinc metal were calculated.

It was shown earlier that, for two-step reactions, the Tafel plots at large cathodic overvoltages have a slope of $-\alpha_a f$ and an intercept of $2i_a^o$ at $\eta=0$. Hence, for a first order reaction with respect to zinc (II), the current at large cathodic overvoltages should be proportional to the concentration of the zinc ion. Conversely, for first order with respect to Zn metal, the current at large anodic overvoltage should be proportional to the concentration of the zinc in the amalgam. These criteria are observed for the Zn (II)/Zn^o(Hg) couple, and it is concluded that the reduction and oxidation are of the first order with respect to both Zn (II) and Zn^o.

The results obtained in the determination of reaction orders can be interpreted either in terms of a single two-electron transfer (or two undiscernible one-electron transfers) or a two consecutive one-electron transfers. The former mechanism is ruled out by two other features of the Tafel plots. The exchange current obtained by extrapolation to $\eta=0$ for cathodic and anodic potential steps were different (except for very low ionic strengths); also, the sum of α_a and α_b did not equal unity.

Conclusions

Based on the experimental results obtained in this study, it is concluded that the charge-transfer reaction of zinc in nitrate media is via a consecutive step mechanism.

$$Zn^{2+} + e \rightleftarrows Zn^{+}$$

$$Zn^{+} + e \rightleftarrows Zn(Hg)$$

with the first step rate-determining at moderately high ionic strengths. As the ionic strength is lowered ($\mu < 1.0$), mixed rate control between the two steps is observed. It is also concluded that the electrochemical reactions of the zinc system in nitrate media are of the first order with respect to Zn(II) and Zn^{o}.

APPENDIX I

LIST OF SYMBOLS AND ABBREVIATIONS

Latin

a	an activity
A	the electrode surface area
A_{max}	maximum surface area of electrode
C	formal concentration
C^*	double-layer capacitance
D	a diffusion coefficient
E	a potential
E_e	formal equilibrium electrode potential versus any reference, determined by the particular concentrations of the two species of the electrochemical couple
E_{max}	potential of zero electrode charge
erfc	defined as 1-erf, where erf = $\int_o^{\sim y} \exp(-z^2)dz$
ΔE	magnitude of square-wave
f	the ratio F/RT
F	Faraday constant
I	current, amperes
i_c	double-layer charging current
i_f	faradaic current
i_x, i_y	invalid zero-time intercept of an i versus f(t) plot
i_a^o	apparent exchange current density for first step of an electrode reaction

i_b^o apparent exchange current density for second step of an electrode reaction

m flow rate of mercury, milligrams per second

n the number of electrons involved in an electrochemical reaction

o electro-reducible species

P $\exp(E-E_{\frac{1}{2}})nf$

p_i reaction order of the i^{th} species

q the charge density, Q/A

Q electrode charge, coulombs

r electrode drop radius

R gas constant

R resistance (Chapter III)

R_f negative feedback loop resistance

R_i internal resistance

R_e external resistance

t a time

T absolute temperature

V volume of electrode drop

x distance from electrode surface

y argument of the function $\exp y^2 \operatorname{erfc} y$, defined as $y = \lambda t^{\frac{1}{2}}$

z the charge on any species

Greek

α a cathodic transfer coefficient

β the ratio t/τ

Γ surface excess, moles cm^{-2}

η overvoltage in volts, defined as $\eta = E-E_c$

θ function of time, defined by $\theta = [\tau^{\frac{1}{2}} + (t-\tau)^{\frac{1}{2}} - t^{\frac{1}{2}}]$, seconds$^{\frac{1}{2}}$

λ parameter containing kinetic terms, used in $y = \lambda t^{\frac{1}{2}}$, seconds$^{-\frac{1}{2}}$

μ_i chemical potential of the i^{th} species

τ the step reversal time of the potential step

Φ the rational potential

Φ' the potential across the compact double layer

ψ_o the potential across the diffuse double layer

Units of Measure

cm centimeters

cm^2 square centimeters

mA milliamperes

ml milliliters

ms milliseconds

mv millivolts

sec seconds

μA microamperes

μC microcoulombs

μF microfarads

μsec microseconds

APPENDIX II

SCHEMATICS OF CIRCUITS

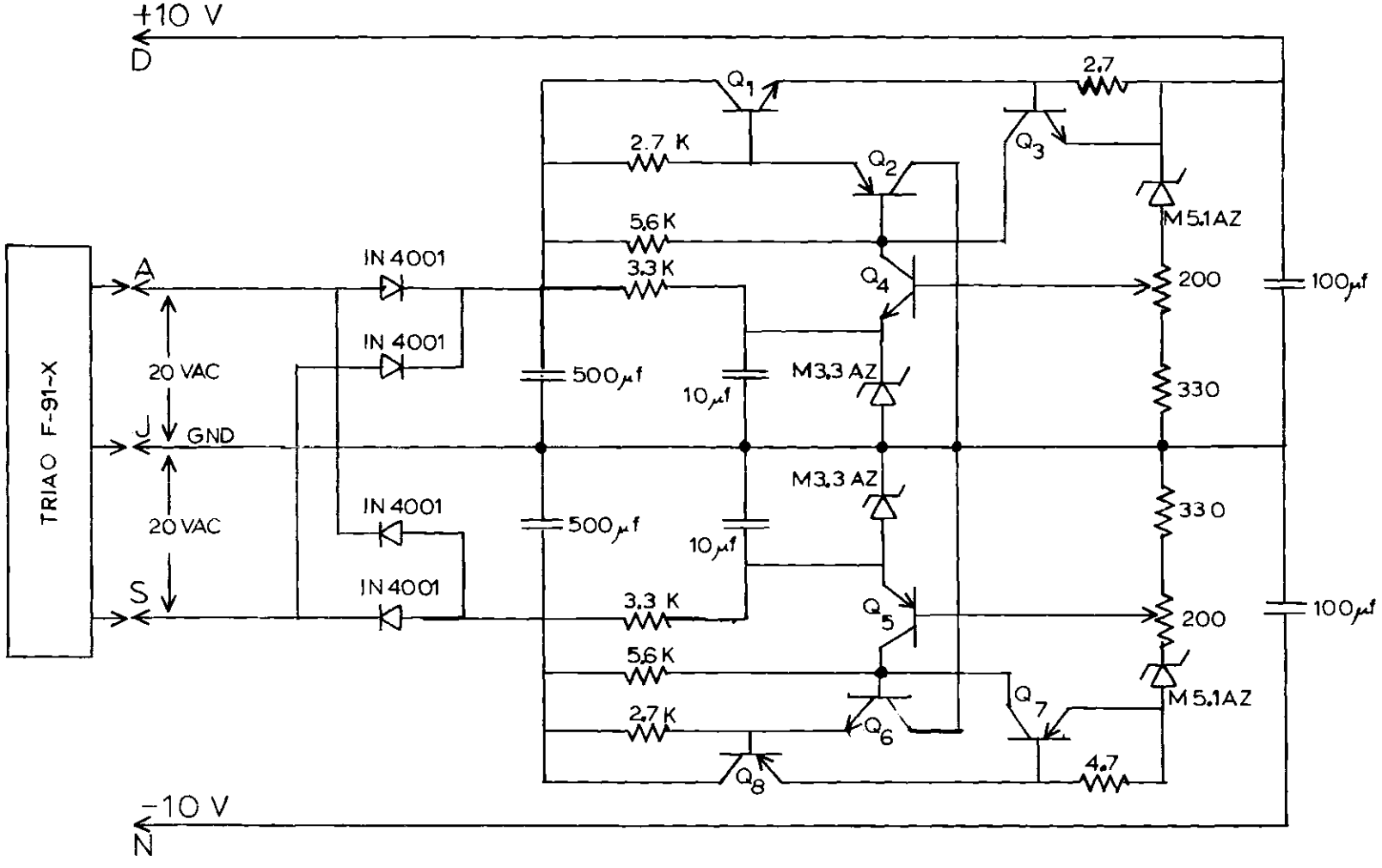

Figure 35. Detailed Schematic of the ± 10 Volt Power Supply

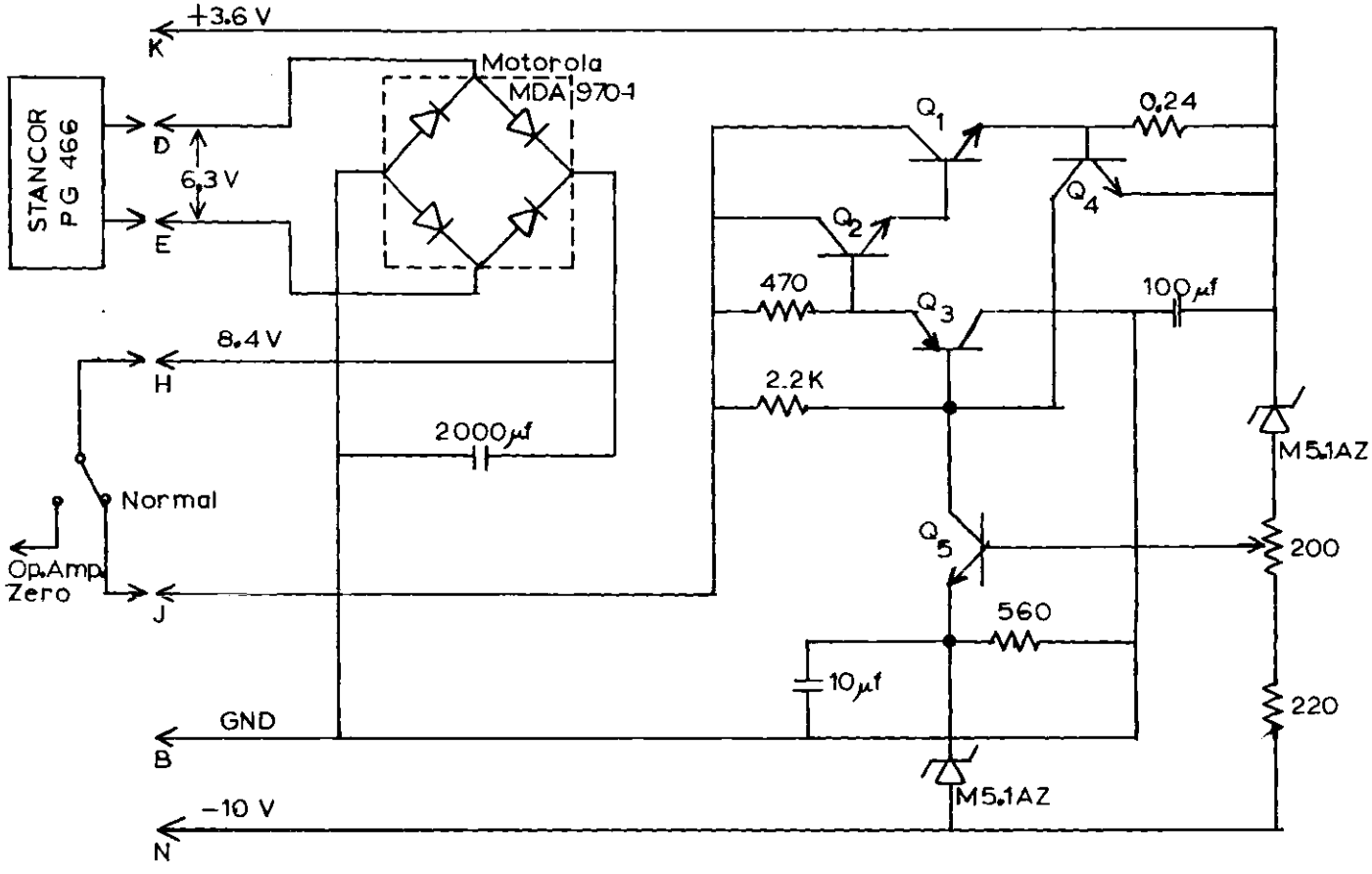

Figure 36. Detailed Schematic of the + 3.6 Volt Power Supply

BIBLIOGRAPHY*

1. R. L. Poole, Dissertation, Georgia Institute of Technology, Atlanta, Georgia, 1970.

2. J. Heyrovsky, Discussions Faraday Soc., 1, 212 (1947).

3. N. S. Hush and J. Blackledge, J. Electroanal. Chem., 5, 420 (1963).

4. L. Gaiser and K. Heusler, Electrochim. Acta, 6, 67 (1962).

5. N. Tanaka, Y. Aoki, and A. Yamada, Electrochim. Acta, 14, 1155 (1969).

6. B. Timmer, M. Sluyters-Rehbach, and J. H. Sluyters, J. Electroanal. Chem., 14, 181 (1967).

7. J. Koryta, Electrochim. Acta, 6, 67 (1962).

8. H. Gerischer and N. Vielstich, Z. Physik. Chem (Frankfurt), 3, 16 (1955).

9. P. Delahay, Advances in Electrochemistry and Electrochemical Engineering, edited by P. Delahay, Interscience, New York, 1961, pp. 247-251.

10. L. Meites, Polarographic Techniques, p. 210, Interscience, New York, 1955.

11. K. B. Oldham and R. A. Osteryoung, J. Electroanal. Chem., 11, 397 (1966).

12. H. Gerischer, Z. Electrokhem., 64, 29 (1960.

13. J. A. V. Butler, Trans. Faraday Soc., 28, 379 (1932).

14. K. J. Vetter, Z. Physik. Chem., 194, 284 (1950).

15. K. J. Vetter, Z. Elektrochem., 56, 931 (1952).

16. J. Tafel, Z. Physik. Chem., 50, 641 (1905).

*Journal title abbreviations used are those listed in "Index of Periodicals," Chemical Abstracts, 1961.

17. K. J. Vetter, Z. Naturforsch., 7a, 328 (1952).

18. R. M. Hurd, J. Electrochem. Soc., 109, 327 (1962).

19. F. C. Anson, Anal. Chem., 38, 54 (1966).

20. F. C. Anson, Anal. Chem., 36, 932 (1964).

21. J. Christie, G. Lauer, R. A. Osteryoung, and F. C. Anson, Anal. Chem., 35, 1979 (1963).

22. J. Christie, G. Lauer, and R. A. Osteryoung, J. Electroanal. Chem., 7, 60 (1964).

23. P. J. Lingane and J. H. Christie, J. Electroanal. Chem., 10, 284 (1965).

24. I. Shain and W. M. Schwarz, J. Phys. Chem., 70, 845 (1966).

25. D. Ilkovic, Collection Czechoslov. Chem. Communs., 6, 498 (1934).

26. A. Bresle, Acta Chem. Scand., 10, 947 (1956).

27. P. O. Kane, J. Polarog. Soc., 1, 10-19 (1962).

28. H. B. Mark and C. N. Reilley, J. Electroanal. Chem., 3, 54 (1962).

29. P. E. Sturrock, Private communication, July 1971.

30. G. C. Barker and I. L. Jenkins, Analyst, 77, 685 (1952).

31. G. C. Barker, Anal. Chim. Acta, 18, 118 (1958).

32. H. V. Malmsladt and C. G. Enke, Digital Electronics for Scientists, W. A. Benjamin, Inc., New York, 1969, p. 115.

33. Philbrick Researches, Inc., Bulletin AC 650 January, 1967.

34. G. L. Booman, Anal. Chem., 29, 213 (1957).

35. D. D. Deford, Division of Analytical Chemistry, 133rd Meeting, ACS, San Francisco, Calif., April, 1958.

36. M. T. Kelley, D. J. Fisher, and H. C. Jones, Division of Analytical Chemistry, 144th Meeting, ACS, Los Angeles, Calif., April, 1963.

37. W. L. Underkofler and I. Shain, Anal. Chem., 35, 1779 (1963).

38. G. L. Booman and W. B. Holbrook, Anal. Chem., 35, 1793 (1963).

39. L. Nemec, J. Electroanal. Chem., 8, 166 (1964).

40. G. Lauer and R. A. Osteryoung, Anal. Chem., 38, 1106 (1966).

41. H. B. Mark and C. N. Reilley, J. Electroanal. Chem., 3, 54 (1962).

42. G. W. C. Milner, Congr. on Anal. Chem. in Industry, St. Andrews, June (1957).

43. R. Poole, Dissertation, Georgia Institute of Technology, Atlanta, Georgia, 1969.

44. I. M. Kolthoff and J. J. Lingane, Polarography, Interscience, New York, 1952, p. 545.

45. B. E. Conway, Electrochemical Data, Elsevier, New York, 1952, p. 231.

46. Guenter Albrecht, Z. Chem., 3(5), 182 (1963).

47. W. M. Shackelford, Dissertation, Georgia Institute of Technology, Atlanta, Georgia, 1971.

48. A. Armata and P. Delahay, J. Phys. Chem., 68, 880 (1964).

49. J. H. Christie, E. P. Parry, and R. A. Osteryoung, Electrochim. Acta, 11, 1525 (1966).

50. M. Caselli, G. Ottombrini, and P. Paroff, Electrochim. Acta, 13, 241 (1968).

51. R. Payne, J. Electrochem. Soc., 113, 999 (1966).

52. P. Delahay, Double Layer and Electrode Kinetics, Interscience, New York, 1966, p. 204.

53. Ibid., p. 184.

VITA

John Anderson Liddle was born to Alexander Barthwick and Margret Jennings Liddle on April 21, 1940, in Nashville, Tennessee. He attended Donelson High School in Donelson, Tennessee, and graduated in June, 1958. He received a Bachelor of Science degree from Middle Tennessee State College in January of 1963.

In June, 1963, he married Glenda Jean Thornton. They are the parents of two boys, Harold David and Glenn Barthwick.

From March 18, 1963, to March 18, 1965, he served as an officer in the United States Army. He was employed with the Monsanto Company in Anniston, Alabama, as a chemist from June, 1965, to September, 1967.

In September of 1967, he entered the Graduate Division of the Georgia Institute of Technology in the School of Chemistry and was awarded a teaching assistantship. In March, 1970, he was granted a National Defense Education Act Fellowship.

In July of 1971 he was employed by the National Center for Disease Control in Atlanta, Georgia.